



Size and Spatial Distributions of Sub-km Main-belt Asteroids

吉田, 二美

(Degree)

博士 (理学)

(Date of Degree)

2002-03-31

(Date of Publication)

2009-06-16

(Resource Type)

doctoral thesis

(Report Number)

甲2566

(URL)

<https://hdl.handle.net/20.500.14094/D1002566>

※ 当コンテンツは神戸大学の学術成果です。無断複製・不正使用等を禁じます。著作権法で認められている範囲内で、適切にご利用ください。



博士論文

Size and Spatial Distributions of Sub-km Main-Belt Asteroids

(小惑星帯における微小小惑星のサイズ・空間分布)

平成 14 年 1 月
神戸大学大学院自然科学研究科

吉田二美

Contents

| | |
|---|-----------|
| Abstract..... | 1 |
| 1 Introduction..... | 3 |
| 1.1 Historical aspects of asteroid surveys | 4 |
| 1.2 Size and spatial distributions of known MBAs..... | 6 |
| 1.3 Size and spatial distributions of known NEAs..... | 14 |
| 1.4 Purposes of this study..... | 19 |
| 2 Statistical method to derive size and spatial distributions of sub-km MBAs..... | 21 |
| 2.1 Method for deriving their semi-major axis and inclination from sky motion vector of each asteroid..... | 22 |
| 2.2 The accuracy of a and I estimated from sky motion vector of each asteroid..... | 25 |
| 2.3 Estimation of size distribution based on a' from sky motion vector of each asteroid..... | 30 |
| 2.3.1 Translation from a' to absolute magnitude or size..... | 30 |
| 2.3.2 Error estimation of the slope of the CSD obtained from the a' | 31 |
| 3 Survey Observations and Results..... | 39 |
| 3.1 Preliminary survey..... | 39 |
| 3.1.1 Observations and data reduction..... | 40 |
| 3.1.2 Daily motion and photometry..... | 42 |

| | |
|---|------------|
| 3.1.3 Results..... | 44 |
| 3.2 Sub-km Main-Belt Asteroids Survey (SMBAS)..... | 49 |
| 3.2.1 Description of SMBAS..... | 49 |
| 3.2.2 Data reduction..... | 52 |
| 3.2.2 (a) Procedure of the standard image reduction..... | 53 |
| 3.2.2 (b) Detection of moving objects..... | 54 |
| 3.2.2 (c) Number of detected moving objects..... | 57 |
| 3.2.3 Photometry..... | 59 |
| 3.2.3 (a) Measurement of brightness..... | 59 |
| 3.2.3 (b) Correction of sensitivity among nine CCD chips..... | 62 |
| 3.2.3 (c) Correction of airmass..... | 62 |
| 3.2.4 Measurements of positions and velocities of moving objects..... | 64 |
| 3.2.5 Calculation of ecliptic components of object's motions..... | 65 |
| 3.2.6 Observational bias corrections..... | 69 |
| 3.2.7 Results..... | 72 |
| 3.2.7 (a) Overview of results..... | 72 |
| 3.2.7 (b) Size distribution in the whole main-belt..... | 83 |
| 3.2.7 (c) Size distribution in three regions of the main-belt..... | 85 |
| 3.2.7 (d) Spatial distribution in the whole main-belt..... | 89 |
| 4 Discussion..... | 93 |
| 4.1 Size distribution of sub-km MBAs..... | 91 |
| 4.2 Spatial distribution of sub-km MBAs..... | 102 |
| 5 Conclusions and future prospect..... | 103 |
| 5.1 Summary and conclusions..... | 103 |
| 5.2 Future prospect..... | 104 |

| | |
|-------------------------------|-----|
| Acknowledgements | 107 |
|-------------------------------|-----|

Bibliography

Appendix 1

Proc. of 33rd ISAS Lunar and Planetary Sympo., 21-24.

SUBARU Sub-km Main Belt Asteroids Survey Plan –Statistical Estimation of Size Distribution–

Fumi Yoshida and Tsuko Nakamura

Appendix 2

Proceedings of the 33rd symposium on Celestial Mechanics (in press).

Sub-km Main Belt Asteroids Survey (SMBAS) using SUBARU telescope -The Estimation Methods of Size Distributions-

Fumi Yoshida and Tsuko Nakamura

Appendix 3

Pub. Astron. Soc. Japan Letter, **53**, L13-L16.

First Subaru Observations of Sub-km Main Belt Asteroids

Fumi Yoshida, Tsuko Nakamura, Tetsuharu Fuse, Yutaka Komiyama,
Masafumi Yagi, Satoshi Miyazaki, Sadanori Okamura, Masami Ouchi,

and

Masayuki Miyazaki

Abstract

This thesis is the results of the first systematic investigation of very small Main-belt Asteroids (sub-km MBAs) using the 8.2m Subaru telescope ; we call this survey SMBAS (Sub-km Main-belt Asteroid Survey). Asteroids belonging to this size region in the main-belt has never been explored before, due to their faintness.

Recent theoretical works and laboratory experiments on collisional evolution of asteroids highlight the importance of sub-km MBAs from the two viewpoints : 1) the majority ($\sim 70-80\%$) of the near earth asteroids (NEAs) are sub-km-sized and are supposed to be originated from the main-belt, and 2) this size region lies near the border-line size separating the two catastrophic impact mechanisms, namely those in the strength regime and the gravity regime. Therefore, the research of the sub-km MBAs contributes to the estimation of the production rate of NEAs in the main-belt, and furthermore would give us clues on the mechanism of the collision evolution among the small bodies.

For the analysis of this survey, we developed a method to derive the size distribution of sub-km MBAs, based on *statistical* estimates of the semi-major axis (a) and inclination (I) for each detected asteroid, because the traditional determinations of orbits for sub-km MBAs by follow-up observations are practically impossible owing to strict telescope-time of the Subaru telescope or other 8–10m large telescopes. Hence, our SMBAS cannot determine other orbital elements except the a and I . In addition, we cannot avoid some errors in our a - and I -estimates, caused by the lack of information on eccentricity (e).

ABSTRACT

Therefore, we evaluated those errors from Monte Carlo simulations by adopting Bowell's equations which assume $e = 0$. We confirmed that these errors could vary the slope of Cumulative Size Distributions (hereafter CSD) for the main-belt asteroids (MBAs) detected from the SMBAS within the range of only ± 0.1 . It is found that the slope of the CSD from our statistical method (see Chapter 2) has a precision comparable to that from the past MBAs survey observation. Then we applied the above estimation of errors to analyze our SMBAS data, which were taken in February 2001.

The main results of the survey observations are summarized as follows :

- (1) The sky number density of MBAs is found to be ~ 260 per deg^2 down to $R \sim 26$ mag near opposition and the ecliptic.
- (2) The slope of the CSD for small MBAs ranging from a few km to sub-km seems to be fairly shallower ($\sim 0.8 - 1.2$, depending upon locations in the main-belt) than that for large MBAs obtained from the past asteroid surveys (~ 1.8). This means that the number of sub-km MBAs is much more depleted than a result extrapolated from the size distribution for large asteroids.
- (3) The spatial distribution of sub-km MBAs resembles that of larger MBAs. The I -distribution of sub-km MBAs suggests that a larger number of small asteroids with high inclination may exist compared with that of larger MBAs.

Finally, the implication for depletion of sub-km MBAs is discussed in relation to collisional mechanisms such as the formation of rubble pile asteroids.

Chapter 1

Introduction

The current size, spatial and compositional distributions of the main-belt asteroids (MBAs) have been believed to reflect long-term history of collisional evolution (e.g., Wetherill, 1989). Generally the size distribution of asteroids is represented in the form of a cumulative size distribution, (hereafter, we abbreviate it as CSD). A high resolution analysis of the main-belt CSD will bring about an insight into the interrelation between different objects, in terms of the production rate of meteoroids and near-earth asteroids (NEAs), the cratering rate on the inner planets, and the early accretion processes in the main-belt region of our solar system. It may also be able to estimate the impact risk to interplanetary spacecraft, the original mass in main-belt and the impact strengths of the asteroids (e.g. Kuiper *et al*, 1958, Anders, 1965, Jedicke & MetCalfel, 1998). From such motivations, some systematic survey observations of MBAs have so far been done and the CSDs for MBAs have been revealed down to a few km in diameter.

However recently, the importance of the study of sub-km MBAs has been pointed out mainly from two viewpoints : 1) majority ($\sim 70-80\%$) of NEAs are sub-km-sized and are supposed to be originated from sub-km MBAs (<http://cfa-www.harvard.edu/iau/mpc.html>), and 2) this size region lies near the border-line size separating two catastrophic impact mechanisms, namely those in the strength regime and the gravity regime (e.g., Melosh & Ryan, 1997, Durda *et al.*, 1998).

Concerning the first point, it is generally accepted that NEAs originated from MBAs through collision processes among asteroids and subsequent gravitational perturbations associated with the Kirkwood gaps (e.g., Wisdom, 1983, Morbidelli & Moons, 1995). Hence, the study for the CSD of sub-km MBAs may shed light on a physical relation between NEAs and sub-km MBAs.

If the second point above is correct, the possible difference between the CSD slope for sub-km MBAs obtained from SMBAS and that for known MBAs larger than a few km in diameter may be interpreted as the difference in collisional nature between the strength regime and the gravity regime. In other words, we may give a clue (or an answer) to the question of whether sub-km MBAs are rubble piles (aggregates of impact fragments) or monolith-like bodies. For these reasons, we consider that the observational study of sub-km MBAs is very important.

In this chapter, we first review the history of the past asteroids surveys and discuss their size and spatial distributions of known MBAs and NEAs. Then we mention the purpose of this study.

1.1 Historical aspects of asteroid surveys

Four previous asteroid surveys are described in this section. They are also listed in **table 1-1**.

- 1) The Yerkes-McDonald survey (YMS) is the first systematic photographic asteroid survey. It was carried out in 1950—1952 and detected 1,550 asteroids for $14,400 \text{ deg}^2$ within $\pm 20^\circ$ of the ecliptic. The survey was complete down to the photographic magnitude (V_p) 16.5 (Kuiper *et al.*, 1958).
- 2) The Palomar-Leiden survey (PLS) in 1960s is also a photographic survey. It discovered more than 2,000 asteroids for 216 deg^2 area of the sky centered on

opposition at the vernal equinox. Orbits for about 1,800 objects were determined and their magnitude-frequency distribution up to a photographic magnitude of about 20 mag (corresponding to a few km in diameter of asteroids) was estimated (van Houten *et al.*, 1970).

- 3) The Spacewatch survey during 1992–1995 found out as many as 59,226 asteroids for $3,740 \text{ deg}^2$ with the limiting magnitude $V < \sim 21$ (Jedicke & Metcalfe, 1998). Since this survey is the program specially designed for the automated search and study of NEAs, the duration of each observation was too small to determine the orbit of each MBA. So their orbital elements needed for estimating their absolute magnitude (H) were obtained from a statistical method. For the purpose of translation from H to size of each asteroid, they used relative numbers of existing asteroids for various taxonomic types and the corresponding typical albedos among MBAs (Ivanov *et al.*, 2001).

Table 1-1

The previous asteroid surveys and SMBAS

| Survey | Observation time | Telescope size(m) | Limiting magnitude | Sky coverage (deg ²) | Number of detected asteroids |
|--------------------------|---------------------|----------------------|-----------------------|-------------------------------------|---------------------------------|
| Yerkes-McDonald | 1950-52 | 0.25 | $V_p < 14-16$ | 14,400 | 1,550 |
| Palomar-Leiden | 1960 | 1.25 | $V_p < 20-21$ | 216 | > 2,000 |
| Spacewatch | 1992-95 | 0.90 | $V < 21$ | 3,740 | 59,226 |
| Sloan Digital Sky survey | 1998-2000 | 2.5 | $r^* < 21.5$ | 500 | ~13,000 |
| Our SMBAS | 2001 | 8.2 | $R \sim 26$ | 3.26 | 1,111 |

V_p : photographic magnitude

r^* : R-band (the effective wavelengths is 6280 Å) in SDSS

4) The Sloan Digital Sky Survey (SDSS) also contributed to studies of asteroid size distribution, though it is basically designed for systematic survey observations of galaxies and quasars (Gunn *et al.* 1998, York *et al.*, 2000, Ivezić *et al.* 2001). This survey found 10,000 asteroids, and estimated that the main-belt contains about 700,000 asteroids larger than 1 km in diameter. Moreover, the SDSS could distinguish between carbonaceous asteroids (C-type) and rocky asteroids (S-type), because it observed in five bands. Since the albedos between the S-type asteroids and the C-type asteroids are different, the C-type asteroids are twice times larger than the S-type ones for the same apparent magnitude. The size of each asteroid was estimated more correctly, because its type could be identified in SDSS.

1.2 Size and spatial distributions of known MBAs

We describe here the size distribution of known MBAs obtained from the above surveys, in comparison with theoretical works. First we discuss theoretical results. The first theoretical work on the size distribution of asteroids was started by Dohnanyi (1969). For a simplified system of asteroids in equilibrium in which a self-similar collision cascade occurs, Dohnanyi (1969, 1971, 1972) and Hellyer (1970, 1971) predicted that a power-law CSD was expected to take place over a wide range of sizes.

From observations, however, for large asteroids with D (diameter) $> \sim 100$ km, it is known that the CSD is not a power-law. This is usually interpreted as remnants of the primordial size distribution near the main-belt location in our solar system. For small asteroids, on the other hand, one usually supposes that asteroids obey a power-law CSD, which it can be represented with the following relation,

$$N(>D) \propto D^{-b}, \quad (1.1)$$

where $N(>D)$ is the total number of asteroids with diameters larger than D km. Dohnanyi (1969) found that the typical value of b is equal to 2.5.

Next we discuss the observed CSDs for the surveys mentioned above. When we talk about the size of asteroids, we must be careful about that there are two kinds of diameters. They are the diameter estimated from infrared observations (represented by the IRAS data) and the one obtained by optical observations with some assumption for albedos. Though the estimation of albedos needs both infrared and optical observations, albedo's data allow us more precise determination of the diameter of each asteroid. However, since all surveys listed in **Table 1-1** are optical observations, when a diameter of each detected object is estimated, an typical albedo would be assumed. Although the infrared diameter is important, we do not discuss here about it in detail, since we are mainly interested in the comparison of the results for optical surveys.

Kuiper *et al.* (1958) found from YMS that the CSD appears to consist of two parts, separated by the asteroid size near 30 km in diameter. They suggested that the discontinuities of the CSD possibly reflected the division of condensation by accretion and fragments by collisional breakup. They also estimated that the value of b is 2.40 ± 0.12 in the absolute photographic magnitude range of 6 to 11. One can see that the value of b in YMS is consistent with the Dohnanyi model (**Figure 1-1 (a)**).

Van Houten *et al.* (1970) obtained from PLS that the b is equal to 1.75 in the photographic magnitude up to about 20 (**Figure 1-1 (a)**). Cellino *et al.* (1991) found from the IRAS data that the CSD of MBAs larger than 20–40 km in diameter cannot be fit to a single power-law.

Jedicke & Metcalfe (1998) found that the variation of power-law index from 1.23 to 2.79 for MBAs larger than 2 km in diameter, depending upon locations in the main-belt and the size. They stated that it is impossible to represent the CSD of MBAs by a single power-law. Since they gave only differential size distributions, we did not cite their figures. According to Jedicke & Metcalfe (1998), the power-law index varies over the H range of 8.0 to 17 for the whole

main-belt region. Moreover the value of b seemed likely to vary greatly for $H \sim 13$.

In SDSS (**Figure 1-1 (b)**), the power-law index is 3 for $D > 5$ km and 1.3 for $D < 5$ km, respectively. Ivezić *et al.* (2001) said that the number of smaller asteroids extrapolated from previous studies using the data for $D > 5$ km was an overestimate. That is, it seems that the small asteroids were not as plentiful as had been expected from observations of larger ones. This result is consistent with our result from SMBAS, as will be mentioned in Chapter 3.

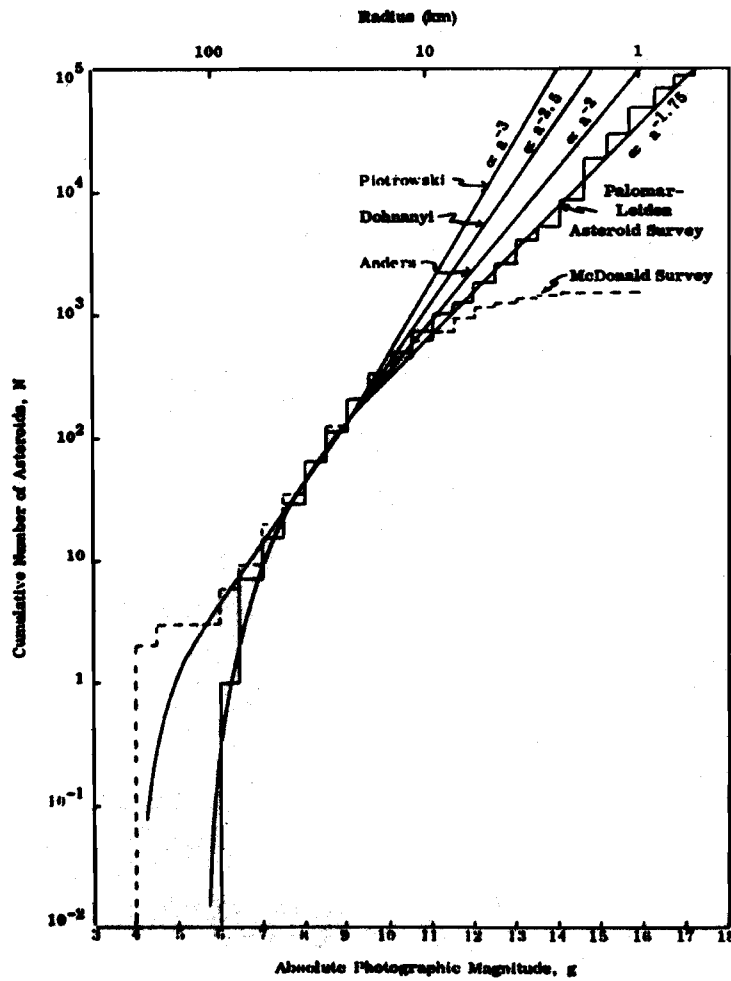


Figure 1-1 (a)

The CSDs for the Yerks-McDonald survey (1950—1952) and the Palomar-Leiden survey (1960s)

This figure was taken from Soberman (1971). The histograms are for YMS and PLS. For comparison, distributions are shown also for power-law indexes of -3 (Piotrowski 1953), -2.5 (Dohnanyi, 1969), -2 (Anders, 1965), and -1.75 (PLS).

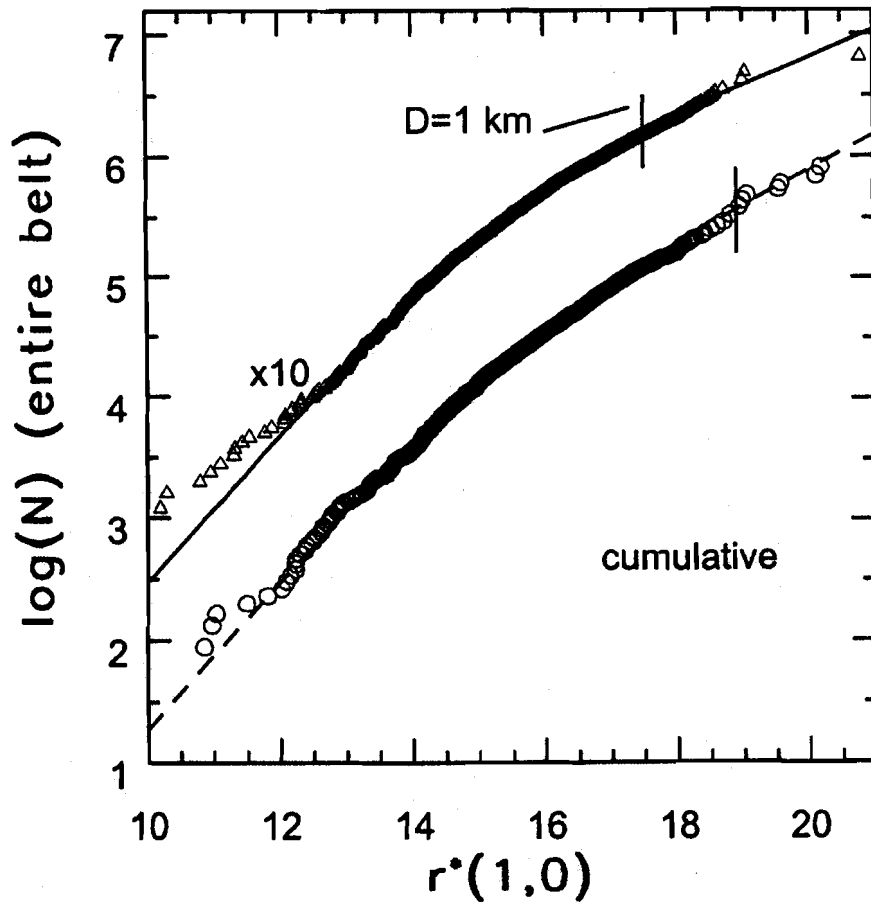


Figure 1-1 (b)

The CSD of entire main-belt for the Sloan Digital Sky Survey (1998-2000)

$r^*(1,0)$ is “uncorrected” absolute magnitude, which is defined by $r^*(1,0) = r^* - 5 \log(R\rho)$, where R is the heliocentric distance, ρ is the earth-asteroid distance, and $\rho = -\cos(\phi) + [\cos(\phi) + R^2 - 1]^{1/2}$, where ϕ is the phase angle. The symbols (circles, likely C-type asteroid ; triangles, likely S-type asteroids) show the nonparametric estimates. The lines are analytic fits to these estimates (Ivezić *et al.*, 2001).

Next, we describe the spatial distribution of known MBAs. The data are taken from September 2001 version of Lowell Observatory asteroid-orbit database (<ftp://ftp.lowell.edu/pub/elgb/astorb.html>). Their diameters were calculated

from H -mag by assuming appropriate albedos. In this paper, we define the region within 2.0–3.5 AU as the main-belt. And also we define the asteroids which have the a s of this region as MBAs. We divided here known MBAs into four groups with respect to the diameter as: $D \text{ (km)} > 100$, $10 < D < 100$, $1 < D < 10$, and $D < 1$.

Figure 1-2 (a)—(c) show their a , I , and e distributions, respectively. From **Figure 1-2 (a)**, we see that the a -distribution is roughly uniform over the main-belt except asteroids with $D < 1 \text{ km}$ (namely sub-km asteroids). We also notice that the number of asteroids decreases rapidly in the locations corresponding position to the Kirkwood gaps in every size region. There are many sub-km MBAs in the inner main-belt. However, this is likely to be affected by the observational bias rather than their intrinsic distribution, because of their faintness.

Figure 1-2 (b) shows that the e -distribution of large MBAs has a peak near 0.2. On the other hand, the eccentricity range of sub-km MBAs is seen to be wider than that of other MBA groups. **Figure 2 (c)** shows that the inclination range of MBAs is within ~ 50 degree.

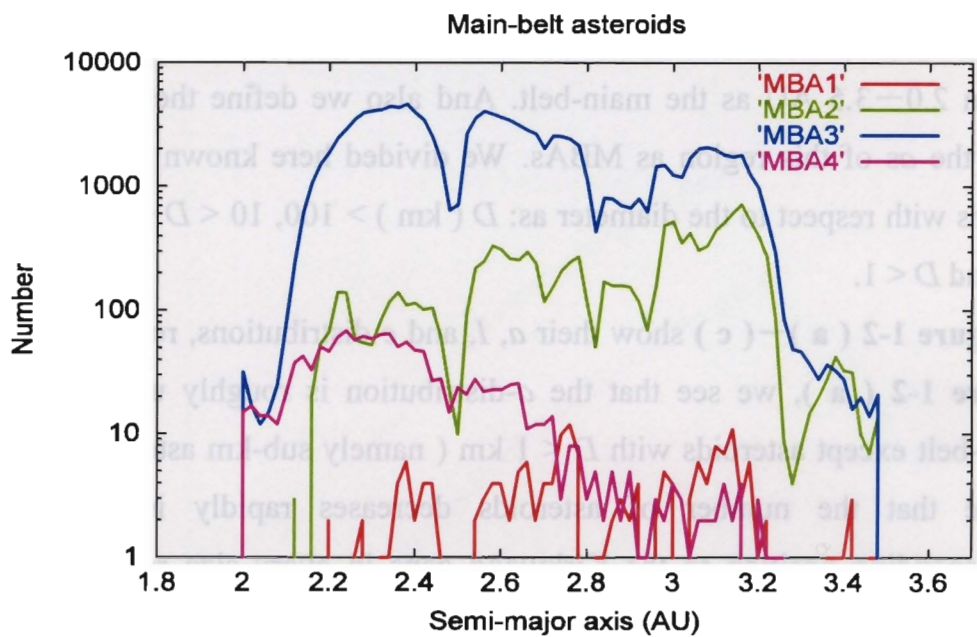


Figure 1-2 (a)
The a -distribution for known MBAs.

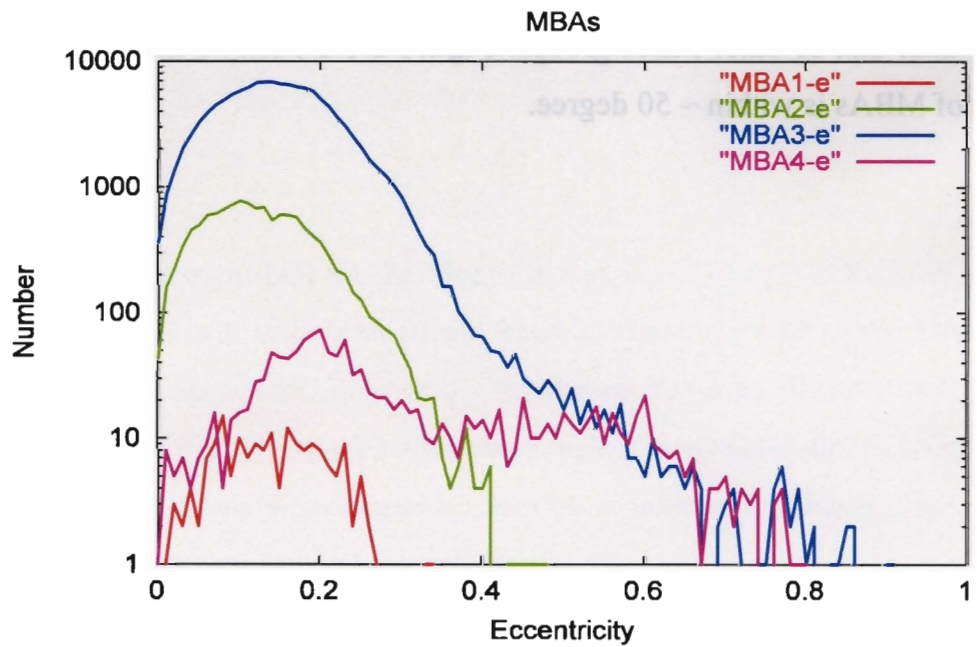


Figure 1-2 (b)
The e -distribution for known MBAs.

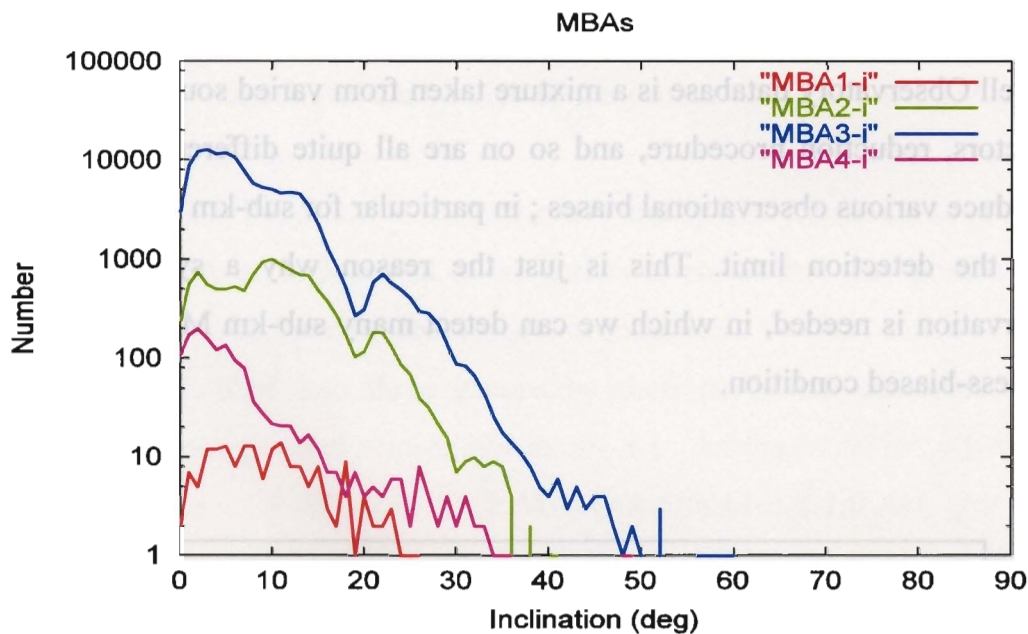


Figure 1-2 (c)

The I -distribution for known MBAs.

The size range indicated by each line is as follows : MBA1 : $D \text{ (km)} > 100$; MBA2 : $10 < D < 100$; MBA3 : $1 < D < 10$; MBA4 : $D < 1$.

Now we discuss the spatial distribution of asteroids as far as beyond the orbit of Jupiter, in the (a, I) plane. This allows us to grasp the three-dimensional spatial distribution of asteroids. The situation is indicated in **Figure 1-3**. The swarm near 4 AU is the Hilda group, and that of near 5.2 AU is the Trojan group. It is well known that the two dense groups with high I near 2 AU are the groups divided by three kinds of secular resonance and one mean motion resonance. Though arguments about the resonance in the main-belt are important in the orbital evolution of MBAs, we avoid here a detailed explanation about it because it exceeds the scope of this thesis. One can see that the I -distribution of asteroids in the inner-planet regions is extended up to $I = 70^\circ$, and the orbital distribution of such asteroids is almost uniform in the whole sky when viewed from the earth. This is one reason why the systematic survey of NEAs is not easy.

It is likely that those distributions discussed above reflect more or less the true

nature of special distributions of asteroids as a whole. But we must notice that the Lowell Observatory database is a mixture taken from varied sources. Telescopes, detectors, reduction procedure, and so on are all quite different. Those factors introduce various observational biases ; in particular for sub-km MBAs which are near the detection limit. This is just the reason why a systematic survey observation is needed, in which we can detect many sub-km MBAs in a unified and less-biased condition.

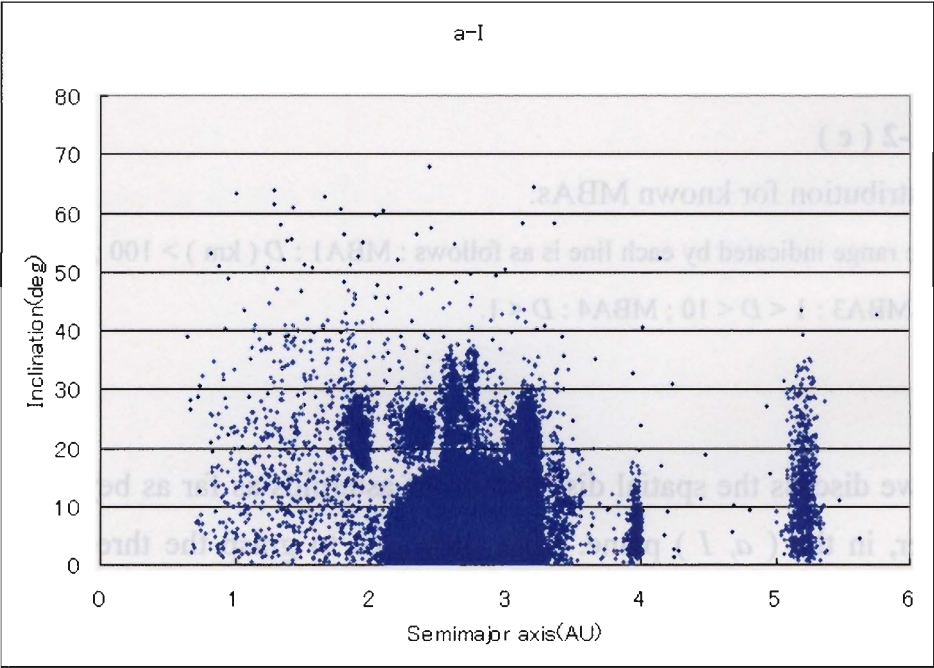


Figure 1-3
The (a, I) spatial distribution of asteroids within the orbit of Jupiter.
The data are from the Lowell Observatory asteroid-orbit database.

1.3 Size and Spatial distributions of known NEAs

Since it is generally believed that NEAs come from the main asteroid belt, it is necessary to examine the distributions of NEAs as well, in relation to the Subaru

survey of sub-km MBAs. Scientifically, orbital and taxonomic distributions of NEAs are greatly meaningful for studies of the orbital evolution of MBAs, their material property, and so on.

Socially, it is also important to study the size and spatial distributions of NEAs in order to estimate an impact risk of dangerous asteroids that may bombard the earth. For the purpose, Space Guard Project is underway.

NEAs are classified into three groups by their perihelion distances (q), aphelion distances (Q) and semi-major axes (a): Amors ($1.017 < q \text{ (AU)} < 1.3$), Apollos, ($a < 1.0 \text{ AU}$, $q < 1.017 \text{ AU}$) and Atens ($a < 1.0 \text{ AU}$, $Q > 0.983 \text{ AU}$). **Figure 1-4** shows their absolute magnitude distributions. Each group has a peak of histogram near 19–20 mag, which is corresponding to sub-km in diameter. Their size range just matches the size range that we would investigate for MBAs. Their CSDs are indicated by curves of dots. The slopes of the CSD for Amors, Apollos, and Atens are 1.60, 1.86, and 1.46, respectively. Their slopes are roughly comparable with the value of PLS (1.75).

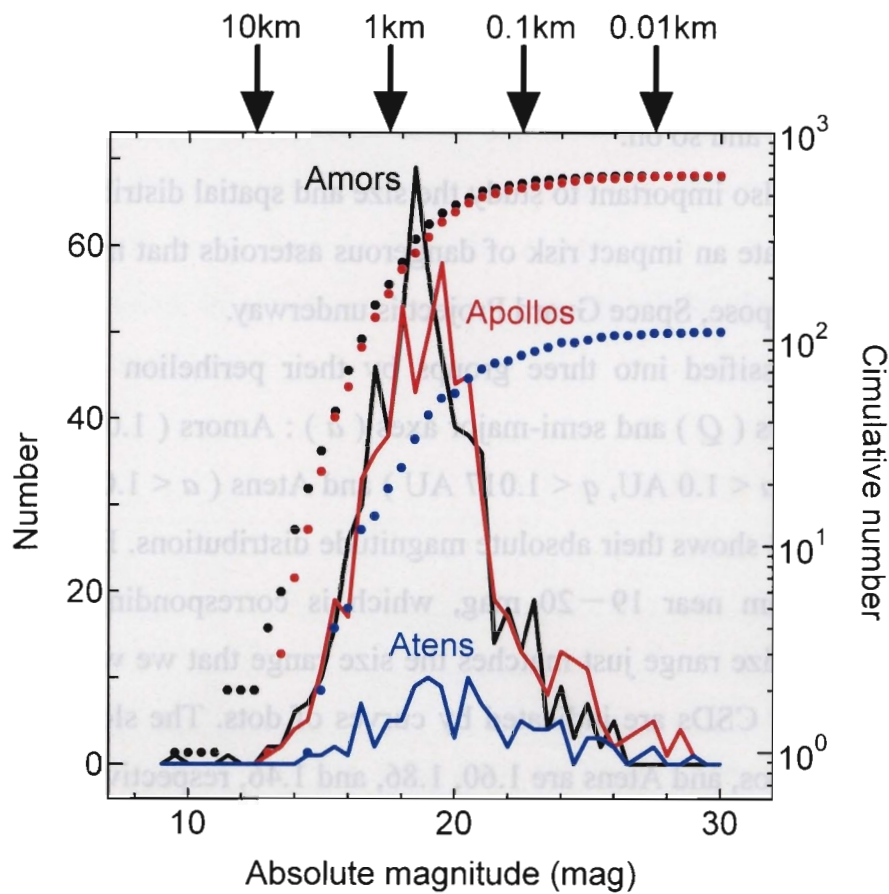


Figure 1-4
The differential and cumulative absolute-magnitude distributions of NEAs.

The black, red, and blue lines for Amors, Apollos, and Atens, respectively. Their cumulative H -distributions are indicated by dots. Diameters corresponding to the H are shown on the top of figure. The data are from Lists of known NEOs of MPC (Minor Planet Center) : <http://cfa-www.harvard.edu/iau/NEO/ThenEOPage.html>).

From **Figure 1-3**, it seems that the orbital distribution of NEAs is almost uniform in the whole sky with respect to a and I . So one may think that a -distribution seems non-biased. However, when they are classified by the size, one can see that there are many large NEAs near the inner main-belt and they are not in the neighborhood of the earth. Small NEAs ($D < 1$ km) are distributed uniformly from near-earth orbits to the inner main-belt (see **Figure 1-5 (a)**). The

classification of the size is the same as that for MBAs in the former section.). From the **Figure 1-5 (a)**, one can find that asteroids which are larger than 10 km in diameter and have orbits similar to the earth's orbit have been never discovered so far.

Figure 1-5 (b) shows the e -distribution of NEAs. The e -range of NEAs with $D < 10$ km is spread up to 0.8. This trend is also seen for MBAs with $D < 10$ km (see **Figure 1-2 (b)**). The peak position of the e -distribution of NEAs shows a slightly smaller value than that of MBAs of the same size region (see **Figure 1-2 (b)** and **1-5 (b)**). Though it seems that NEAs are the asteroids that have been thrown out the main-belt and the e of those asteroids should have undergone such large orbital evolutions, it is interesting to note that the e of large NEAs is smaller than that of large MBAs.

From **Figure 1-5 (c)**, it is seen that the I -distribution of small NEAs ($D < 1$ km) is analogous to that of MBAs for all size range. Namely, asteroids with larger I is scarce. For large NEAs, it seems that there are ten times more asteroids with $I = 20^\circ$ than asteroids with other I . These facts may express the characteristics of orbit evolution of NEAs which are presumably originated from the area of MBAs.

Although we believe that at least the overall characteristics of orbits and size for NEAs explained so far are real, it is certain the well-known NEAs list of MPC which we investigated here contains the observational bias as well as that of well-known MBAs. In near future, the systematized survey by the Space Guard Program may give an unbiased view of NEAs.

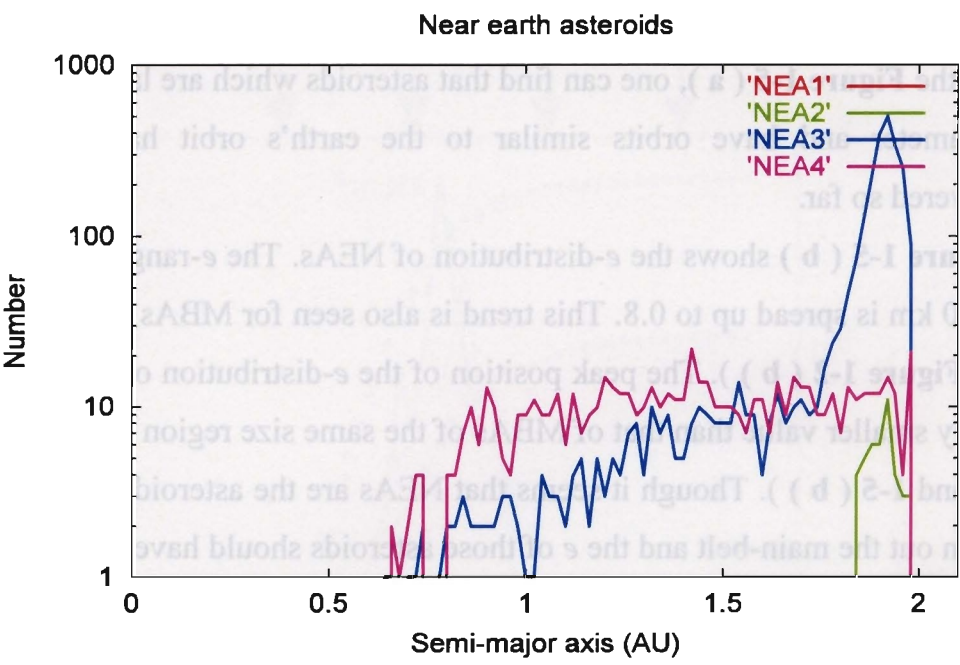


Figure 1-5 (a)
The a -distribution for known NEAs.

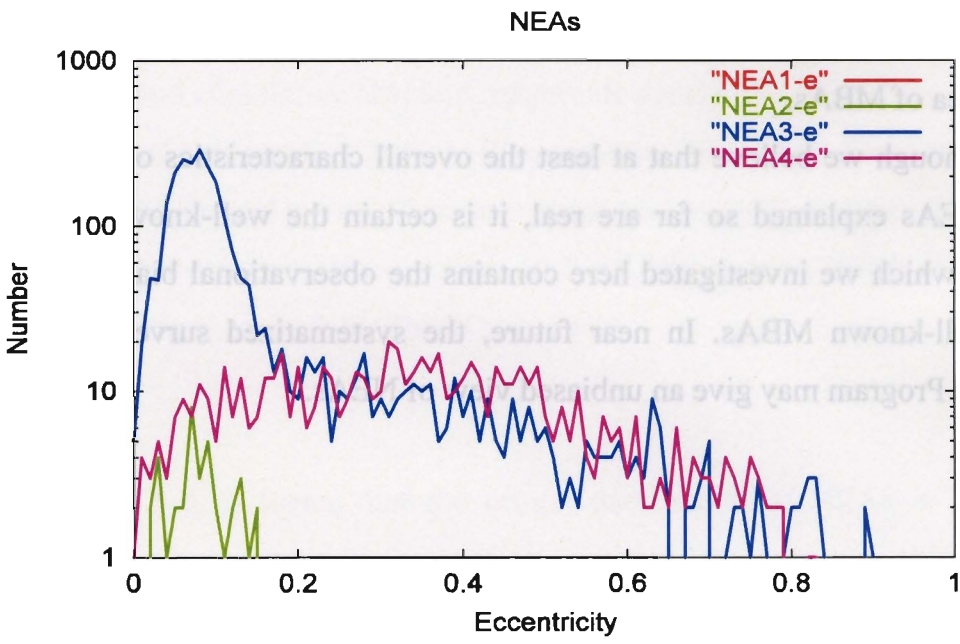


Figure 1-5 (b)
The e -distribution for known NEAs.

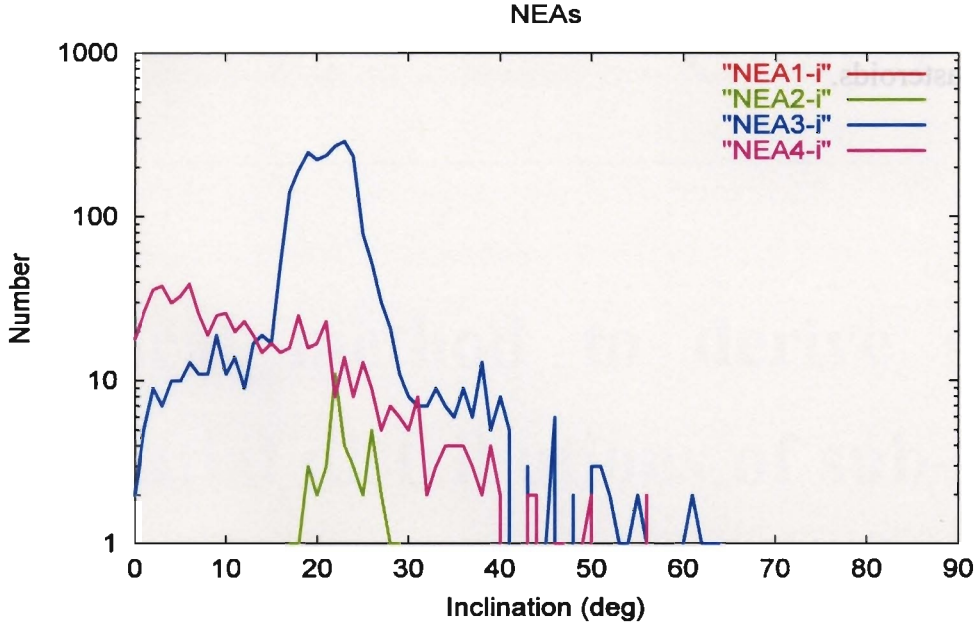


Figure 1-5 (c)

The I -distribution for known NEAs.

The size range indicated by each line is as follows : NEA1 : $D \text{ (km)} > 100$; NEA2 : $10 < D < 100$; NEA3 : $1 < D < 10$; NEA4 : $D < 1$.

1.4 Purposes of this study

As we mentioned before, the orbit distribution of asteroids has the size dependence. All asteroids near the earth's orbit are small-sized ones. As for the observations made so far, the systematic observation of small asteroids has never been done because of the limitation of the performance of the telescope. In particular, the sub-km asteroids in the main-belt have never been investigated.

For these reasons, the purpose of this thesis study is focused on the systematic investigations of the size and spatial distributions of sub-km MBAs. In particular, we want to know how the size distributions of sub-km MBAs depend upon locations in the main-belt. We are also interested in whether the I -distribution of sub-km MBAs is different or not from that for large MBAs. With these results, we expect that we can give a contribution for understanding the relation between

CHAPTER 1 INTRODUATION

sub-km MBAs and NEAs, and impact mechanism and collisional evolution of small asteroids.

Chapter 2

Statistical method to derive size and spatial distributions of sub-km MBAs

Even if the motion of an asteroid was observed for only one night, the orbit can be determined at least in principle from three measured positions. However, the orbit determined with this method can include large errors. The International Astronomical Union (IAU) has adopted currently the rule that if a new asteroid was observed at more than three nights, the asteroid is given a temporary designation. And then after more follow-up observations are made at a few other oppositions, it acquires a permanent number when its orbit becomes definitely reliable.

However, the above procedure is true only for bright asteroids that medium-sized telescopes can observe. Practically, it is impossible to make follow-up observations of faint asteroids discovered by the Subaru telescope or with other 8—10 m class large telescopes, because of the severe restriction of the allocated telescope times. So it is probably hard to determine the precise orbital elements for those faint asteroids using traditional astrometric means.

Instead, we noticed that, for asteroids near the ecliptic and opposition, an approximate semi-major axis (a) and inclination (I) of a MBA can be statistically estimated from its sky motion vector without follow-up observations

(Nakamura, 1997, Yoshida and Nakamura, 1999a, 1999b, 吉田, 1999), thanks to the special geometry in near-opposition observations. Moreover, if the a s and I s are calculated for many asteroids by the statistical method, we can estimate the mean errors of the a and I for those asteroids. This approach is appropriate for our purpose, since it is expected for us to detect a large number of sub-km MBAs in SMBAS using the Subaru telescope (Yoshida *et al.*, 2001b). Similar methods in order to estimate the orbits of asteroids were also adopted in the Spacewatch survey and SDSS. We describe in this chapter a method of statistical estimates of orbits and their errors of MBAs detected in our SMBAS.

2.1 Method for deriving their semi-major axis and inclination from sky motion vector of each asteroid

In the Subaru survey, the observed data in hand are only the apparent daily motion and its position angle for each asteroid. Thus, we must infer some of orbital elements of asteroids from those data only.

Figure 2-1 represents a correlation diagram between the a s and the daily motions for existing asteroids observed in a near-opposition window. Similarly, **Figure 2-2** shows a correlation between the I s and the position angles of their sky motion vectors for the same asteroids. From these figures, it is understood that approximate a and I for each asteroid can be obtained from only its apparent sky motion without making exact orbit determinations. However, for quantitative analysis, we need a more refined mathematical procedure, because possible correlations between a and I are not taken into account in **Figure 2-1** and **2-2**.

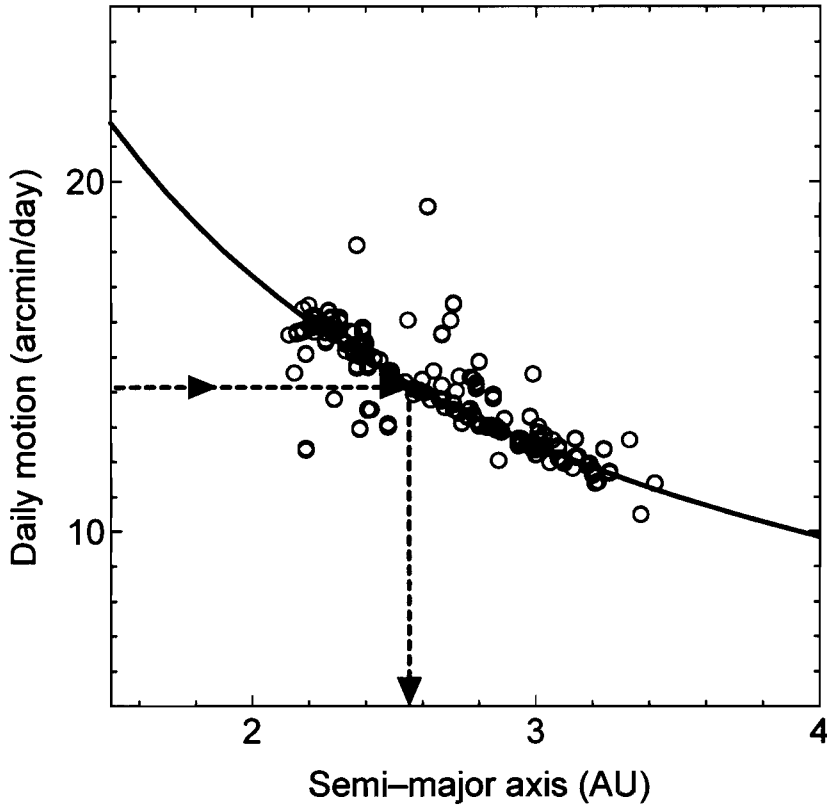


Figure 2-1

a vs. daily motion correlation for known asteroids.

Calculations were made for an assumed opposition window ($4^\circ \times 5^\circ$: near the vernal equinox) on September 23, 1999 for about 40,000 asteroids (<ftp://ftp.lowell.edu/pub/elgb/astorb.html>) which were available as of September 1999. The solid curve is for circular ecliptic orbits. This relationship means that the value of *a* can be approximately determined from the observed daily motion of each asteroid.

In 1990, *Bowell et al.* proposed a method to derive approximate *a* and *I* from the sky motion vector, based on geometrical and kinematical relations of the two-body problem. They showed that if the eccentricity (*e*) of an asteroid's orbit is zero, its semi-major axis (*a'*) and inclination (*I'*) of the asteroid which are near opposition on the ecliptic are represented by the next equations using the apparent motion vector of the asteroid: (*Bowell et al.*, 1990, Nakamura & Yoshida, 2001),

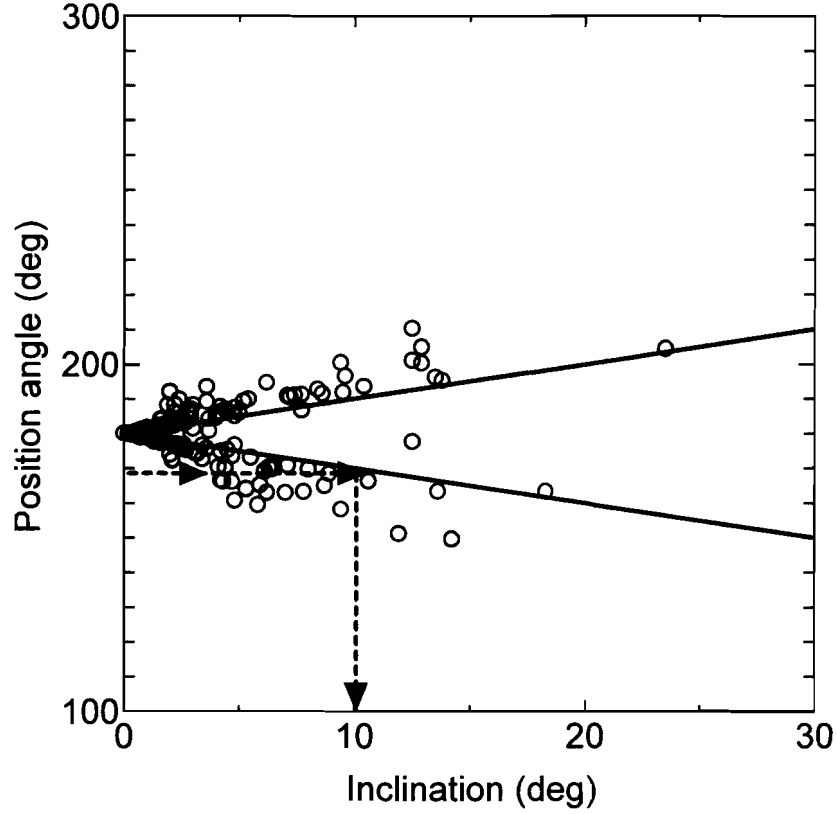


Figure 2-2

I vs. position angle of motion correlation for known asteroids.

The data used are the same as in **Figure 2-1**. The solid line correspond to the motions whose position angle motions are $180^\circ \pm I$. Based on this relation, it is expected that the value of *I* can roughly be inferred from the observed position angle of each asteroid.

$$a' = \frac{1}{2\gamma} \left(\gamma - 2k\lambda \pm \sqrt{|\kappa|} \right) \quad (2.1)$$

$$\tan I' = \frac{|\beta|}{\lambda + \frac{k}{a'-1}} \quad (2.2)$$

$$\gamma = \lambda^2 + \beta^2 \quad (2.3)$$

$$\kappa = \gamma^2 - 4k\lambda\gamma - 4k^2\beta^2, \quad (2.4)$$

where λ is the component in longitude of the motion vector, β is the latitude component and k is Gauss constant. In **Equation (2.1)**, the last term of the

second member should be added if $\kappa < 0$ in **Equation (2.4)**, and be subtracted if $\kappa > 0$. Note that these equations are valid only for near-opposition and near-ecliptic observations. For convenience, we call **Equations (2.1)—(2.4)** “Bowell’s equations” and use them throughout this paper. In order to distinguish the semi-major axis and inclination calculated using the above equations from the ones obtained by the traditional follow-up observations (in other words, true orbital elements), we hereafter write the former as a' and I' and the latter as a and I .

2.2 The accuracy of a and I estimated from sky motion vector of each asteroid

The most important point in applying **Equations (2.1)—(2.4)** to the Subaru observations is to confirm whether the calculated a' and I' should have no systematic deviations from the true a and I of each asteroid in a *statistical sense* ; stochastic random deviations are out of our control. To check the above systematic deviations, we made some Monte Carlo simulations as follows, rather than using the data of existing asteroids. The reason why we had to perform the simulation was that the number of actual asteroids in our specified window was too small for statistical analysis, as seen in **Figure 2-1, 2-2**.

First, we generated many hypothetical asteroids with various orbital elements with the Monte Carlo simulations and picked up 5,000 asteroids in our specified window. The orbital element ranges of the generated asteroids and the assumed observational windows are listed in **Table 2-1**. The sampled number 5,000 of hypothetical asteroids and the observational window size in **Table 2-1** may need explanations. The window size is comparable with that for our SMBAS. As for the sample number, the more the smaller random error we have (the relative error is 1 % for 10,000, for instance). However, the available telescope time for the Subaru is probably 3—4 nights at most and an expected number of detectable

sub-km MBAs per night was 1,000–1,500 from our past experience (Yoshida *et al.*, 2001a). So, the number 5,000 is a result of compromise between statistical accuracy and available resources.

Next, we calculated their daily motions at opposition using a two-body ephemeris generator. We then compared the a and I for each hypothetical asteroid with the a' and I' calculated from its motion vector. Here in the statistics we removed unusual asteroids of about 1 % whose orbits became out of the asteroid belt. Such a result seems to be an inevitable drawback of the estimation from Bowell's equations. However, this removal did not affect the statistical result, because of the small number. **Figure 2-3** shows the a and a' calculated by above simulation. From **Figure 2-3** it seems that there is no systematic difference between the a and the a' , though the scattering is roughly equal to 0.1 AU. Also **Figure 2-4** shows the I and I' calculated by above simulation. From **Figure 2-4**, one can see that the difference between the I and the I' is considerably large, especially for $I > 10$ deg. In **Table 2-2** and **2-3**, we listed more quantitative results for the systematic difference between the true orbital elements and ones calculated by Bowell's equations which were shown in the **Figure 2-3** and **2-4**.

From these tables, we see that, if the systematic deviation in the a , that is, mean ($a - a'$) in **Table 2-2** is corrected, we can estimate the a for individual asteroids to the error level (i.e., SD) of 0.13 ~ 0.15 AU. Though such errors are rather larger than the width of the Kirkwood gaps, they are enough for our survey purpose because we are mainly interested in an overall structure of sub-km MBAs.

As for inclination, on the other hand, the estimations by Bowell's equations are not good. In particular, the errors for medium- and high-inclination orbits are fairly large (~ 6 deg). This seems to be a drawback inherent to Bowell's equations, since Bowell *et al.* (1990) also reported a similar tendency. Fortunately, however, the inclination errors do not affect the estimation of size distribution for sub-km MBAs, in which we are most interested. Moreover, since sub-km MBAs are distributed up to the inclination of ~ 30 deg (see Chapter 3),

with even an error of $I \sim 6$ deg, we will be able to grasp the global 3-dim structure of the sub-km size region of the main-belt.

Table 2-1
The orbital-element ranges of the generated asteroids and the assumed observational window.

| | |
|----------------------|----------------------------|
| a (AU) | 2.75 ± 0.75 |
| I (deg) | 15 ± 15 |
| e | 0.2 ± 0.2 |
| Angular elements | uniform over $0-360^\circ$ |
| Observational window | $2^\circ \times 2^\circ$ |

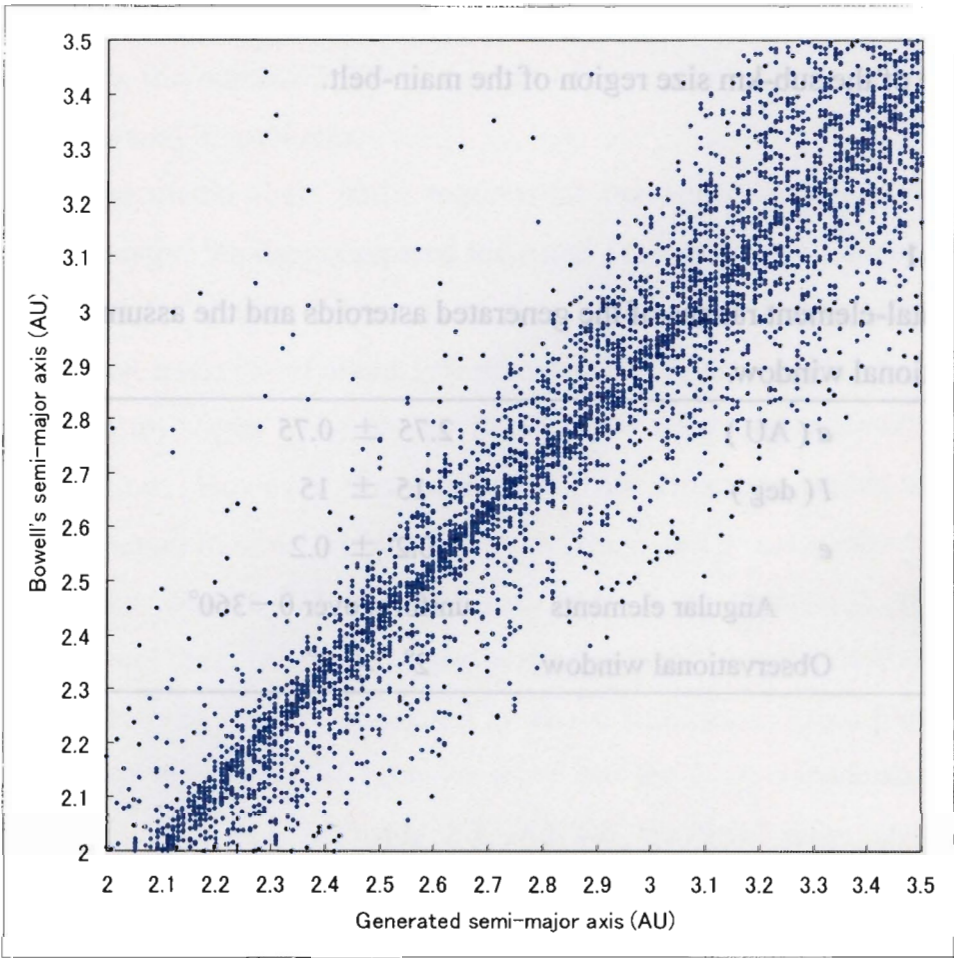


Figure 2-3
Generated a vs. Bowell's a' plot.

The horizontal axis : the value of a generated in a computer run. The vertical axis: the value of a' from Bowell's equations. The input parameters are from **Table 2-1**.

Table 2-2
Errors of semi-major axis obtained from Bowell's orbit.

| Zone | range (AU) | mean($a - a'$) | SD ($a - a'$) |
|------------|-----------------|------------------|-----------------|
| Inner-belt | $2.0 < a < 2.6$ | 0.075 | 0.14 |
| Mid-belt | $2.6 < a < 3.0$ | 0.070 | 0.13 |
| Outer-belt | $3.0 < a < 3.5$ | 0.083 | 0.15 |

SD : the standard deviation

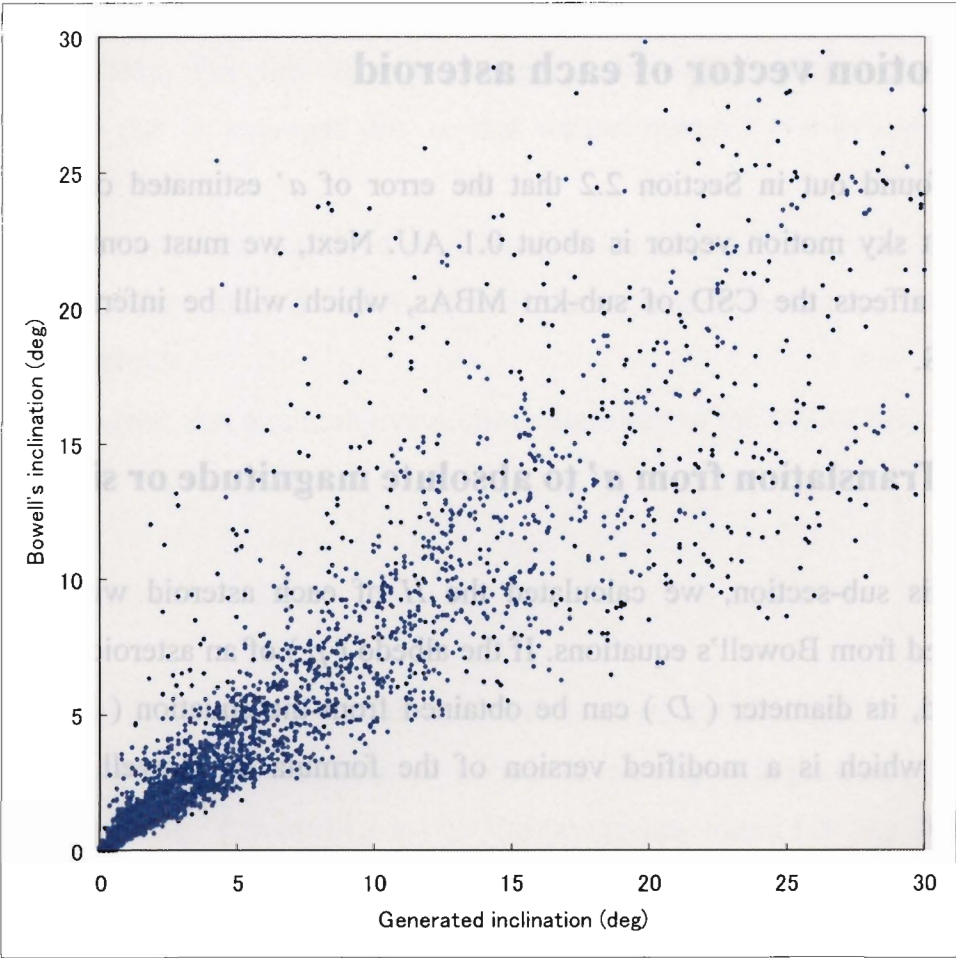


Figure 2-4
Generated I vs. Bowell's I' plot.

The horizontal axis: the value of I generated in a computer run. The vertical axis: the value of I' from Bowell's equations. The input parameters are from **Table 2-1**.

Table 2-3
Errors of inclination obtained form Bowell's orbit.

| Zone | range(deg) | mean($I-I'$) | SD($I-I'$) |
|--------------|---------------|----------------|--------------|
| Low-incl. | $0 < I < 10$ | 0.27 | 1.5 |
| Medium-incl. | $10 < I < 20$ | 2.35 | 4.4 |
| High-incl. | $20 < I < 30$ | 6.37 | 5.8 |

SD : the standard deviations

2.3 Estimation of size distribution based on a' from sky motion vector of each asteroid

We found out in Section 2.2 that the error of a' estimated only from the apparent sky motion vector is about 0.1 AU. Next, we must confirm how the a -error affects the CSD of sub-km MBAs, which will be inferred from our SMBAS.

2.3.1 Translation from a' to absolute magnitude or size

In this sub-section, we calculated the H of each asteroid with a' and I' estimated from Bowell's equations. If the albedo (p) of an asteroid is known or assumed, its diameter (D) can be obtained from the equation (Bowell *et al.* 1989) which is a modified version of the formula by Bowell and Lumme (1979):

$$\log D = 3.1295 - 0.5 \log p - 0.2 H. \quad (2.5)$$

The H of an asteroid near opposition and near the ecliptic is given by

$$H = V - 5 \log r (r - 1) - \delta V, \quad (2.6)$$

where V and δV stand for the apparent magnitude and light variation in V -band, respectively, and r is the heliocentric distance. We need the heliocentric distance r of this asteroid to calculate H -magnitude. But, because of $r = a (1 - e^2) / (1 + e \cos \omega)$ near the ecliptic, its r can never be estimated without knowledge of this asteroid's e and ω (argument of perihelion), whose determination is impossible from only a few observations. For the known MBAs, we know that their es are near zero and the values of the ω seem to be distributed uniformly. Thus, by averaging r over various $e \cos \omega$ for many asteroids, the mean r is

expected to near a . So we assumed here from the beginning that $r \sim a'$ (or $e \sim 0$) for each asteroid. For this sample-averaging; the light variation (δV) of asteroids will also be averaged out, so that we put here $\delta V = 0$ in applying the **Equation (2-6)**.

Since we cannot measure albedos of asteroids in SMBAS, we must assume a certain albedo for detected MBAs in calculating the D based on the H for individual asteroids.

It is well known that a cumulative number distribution for MBAs brighter than magnitude H is expressed as

$$\log N(<H) = C + \alpha H. \quad (2.7)$$

where α and C are constants. The value of α corresponds to the slope for $\log N$ vs. H plot. If we rewrite **Equation (2.7)** with the help of **Equation (2.5)**, the result is equal to the **Equation (1.1)**. The power-law index (b) in **Equation (1.1)**, which corresponds to the slope for $\log N$ vs. $\log D$ plot, is connected to α by $b = 5 \alpha$.

2.3.2 Error estimation of the slope of the CSD obtained from the a'

Using the semi-major axis (a') calculated from the motion vector of hypothetical asteroids obtained from a few nights observations, Nakamura & Yoshida (2001) obtained the CSD for the population of the asteroids and evaluated its relating error. In this sub-section, their evaluation process is reviewed shortly.

As mentioned above, the a' and I' obtained from a few nights observations contain the uncertainty of both e and ω for individual asteroids. So we examined how this uncertainty will influence the power-law index b . This is needed for the estimate of the error in the b that we get from the SMBAS

observations. We performed the following simulation and compared the original slope of the CSD with the slope estimated from a' .

The step-by-step procedure was:

1. Generate likely orbit distributions of asteroids with Monte Carlo simulations.

The produced parent populations have various a , I , and e within the ranges designated in **Table 2-4**. Since we have no information at all on the orbital distribution for the sub-km MBAs, we assumed, as commented at the footnote of **Table 2-4**, that the orbital distributions for sub-km MBAs are similar to those for currently known MBAs. The slope of CSD for generated population is taken to be equal to 1.75, which is the value from PLS.

2. Pick up 5,000 asteroids in an observational window assumed $(4^\circ \times 5^\circ)$, for each distribution in **table 2-4**. Because a very long computation time was required for a narrow window, we had to take this observational window which is larger than that for SMBAS (about $2^\circ \times 2^\circ$).

Generally, since a larger observational window includes asteroids that have more various orbits, the values of the SD ($a - a'$) and the SD ($I - I'$) in the **table 2-2** and **2-3** become larger than ones for a narrower window. Thus we expect that the result from SMBAS will give a better agreement between the original slope and the one obtained from Bowell's equations than the results from this simulation, because a narrower window reduces the fraction of the orbits with unusual a' and I' .

The reason that we pick up 5,000 asteroids is same as that mentioned in the simulation of Section 2.2

3. Calculate apparent motion velocities in longitude and in latitude, with a two-body ephemeris generator, for each picked-up asteroid.

4. Calculate a' and I' of each asteroid using Bowell's equations (2.1)–(2.4)

from its apparent motion vector.

5. Assume that $r = a'$, and calculate the H' of the asteroid with **Equation (2.6)**
6. Assume typical albedo among known MBAs because we also have no information at all on the albedos for the sub-km MBAs, translate the H' to D of the asteroid with **Equation (2.5)**.
7. Produce the size distribution from various D s of picked 5,000 asteroids for every population and get the slope (b') of the cumulative size distribution by a least squares method.
8. Compare the original slope (b) of the generated population with the b' estimated from a' .

Figure 2-5 (a)–(c) show $\log N$ vs. H plot for the three cases (A, B and C in **Table 2-4**) with $b = 1.75$. N is the cumulative number of asteroids as a function of their H . In **Figure 2-5 (a)–(c)**, straight lines stand for the slope for $\alpha = 0.35$ ($b = 1.75$). Open circles show the original cumulative H -distribution generated as input data. We regard this distribution as the true CSD of sub-km MBAs. Filled circles represent the cumulative H -distribution obtained from a' calculated using **Bowell's equations** for the asteroids that lie within the observational window. What we obtain from our SMBAS is this distribution. The open circles and filled circles are linearly fitted by a least squares method, respectively.

One can see from **Figure 2-5 (a)–(c)** that agreement between the input H -distribution and the one obtained from **Bowell's equations** is fairly good for all of the three model populations for hypothetical sub-km MBAs. The obtained b 's for each case are listed in **Table 2-5**, along with α 's. The original slopes α (G)

in **Table 2-5** were not exactly equal to 0.35, due to the statistics of a finite sample number (5,000). If we could do simulations without computer limitations, α (G) should tend to 0.35.

Table 2-4

Orbital-element ranges for three model populations of sub-km MBAs

| | case-A | case-B | case-C |
|-----------|---------------|---------------|------------------|
| a (AU) | 2.6 ± 0.5 | 2.7 ± 0.6 | 2.6 ± 0.6 |
| I (deg) | 10 ± 10 | 15 ± 15 | 7.5 ± 5 |
| e | 0.2 ± 0.1 | 0.2 ± 0.2 | 0.175 ± 0.08 |

A : most similar to the orbital distribution of currently known MBAs.

B : slightly wider in range than the orbital distribution of currently known MBAs.

C : corresponds to the FWHM of the orbital distribution for currently known MBAs.

Table 2-5

Generated and Bowell's slopes for three model population of sub-km MBAs.

| | case-A | case-B | case-C |
|-------------------------------|--------|--------|--------|
| α (G) | 0.335 | 0.352 | 0.352 |
| α' (B) | 0.343 | 0.329 | 0.349 |
| b (G) | 1.675 | 1.760 | 1.760 |
| b' (G) | 1.715 | 1.645 | 1.745 |
| $\Delta b = b - b'$ | -0.040 | 0.115 | 0.015 |
| $\Delta b - \ll \Delta b \gg$ | -0.070 | 0.085 | -0.015 |

α (G) : the H -slope for open circles, α' (B) : the one for filled circles.

$\ll \Delta b \gg$ represents the mean of Δb , namely 0.030.

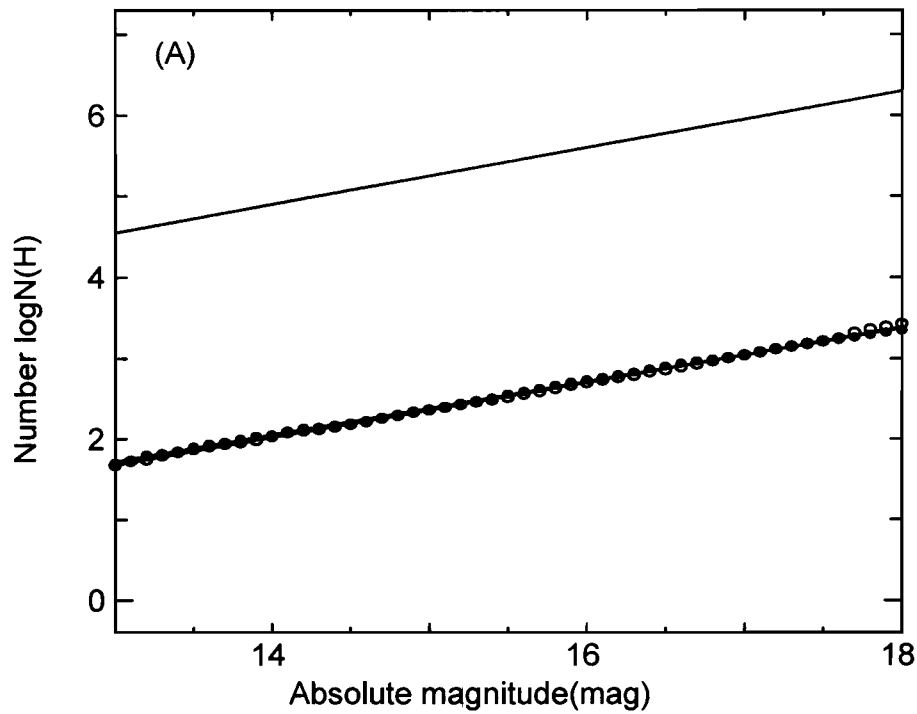


Figure2-5 (a)

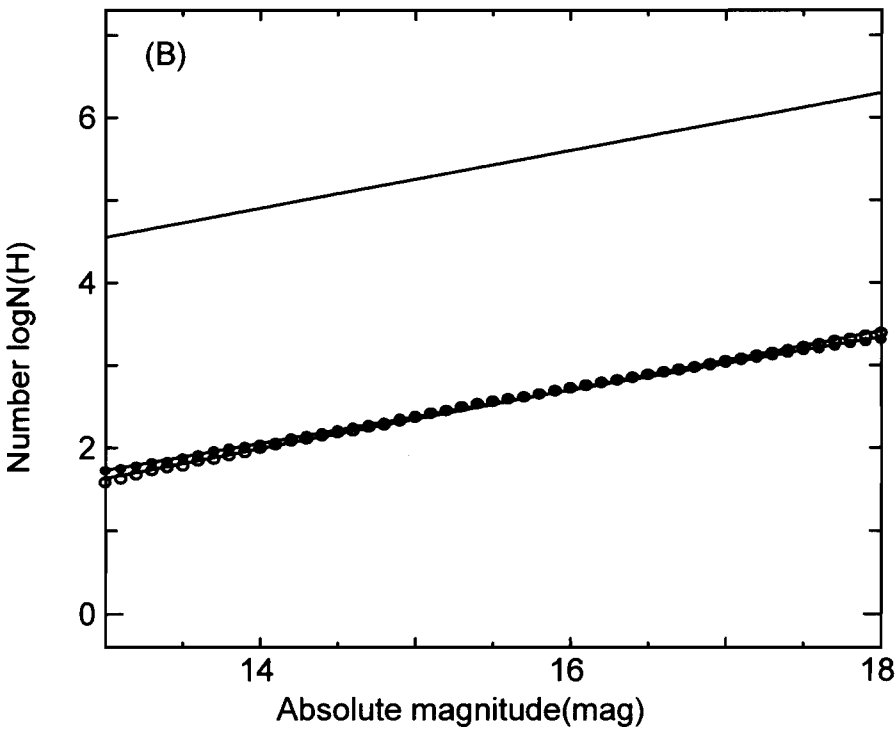


Figure 2-5 (b)

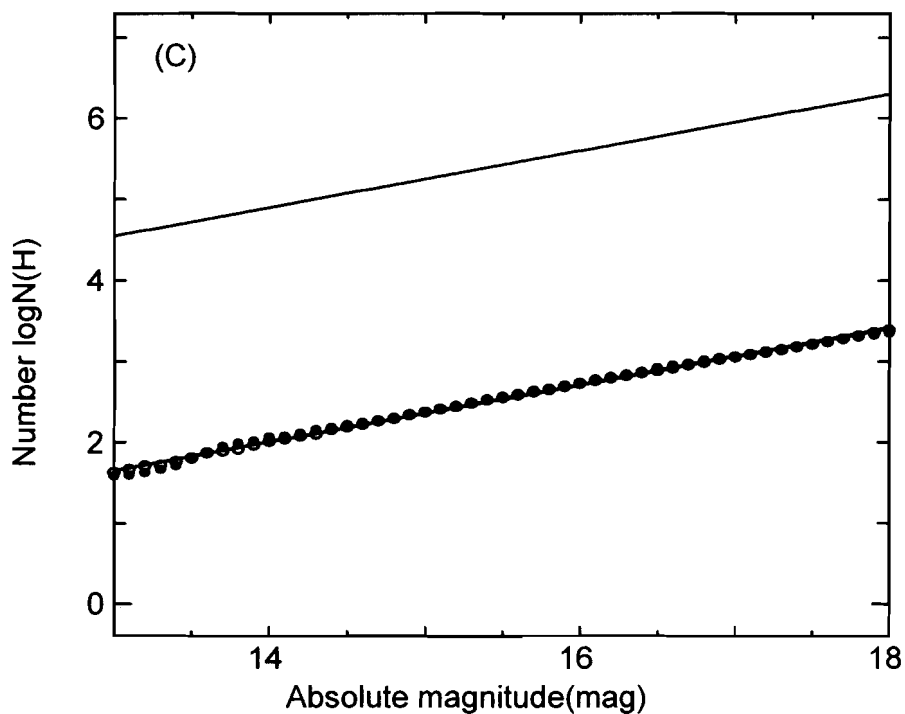


Figure 2-5 (c)
 Comparison of simulation-generated H -distributions with those estimated by Powell's equations.
 The former and the latter distributions are expressed by open and filled circle, respectively. A straight line in each graph shows the slope of $\alpha = 0.35$. **Figure 2-5 (a)—(c)** correspond to case-A—C in **Table 2-4**.

In the previous discussion, we assumed the slope of the CSD for the original populations is $\alpha = 0.35$ ($b = 1.75$). However, in the actual SMBAS, we do not know the true b of the CSD for sub-km MBAs. What we have from the SMBAS observations is only the b' estimated from Powell's equations. Therefore, we must investigate here by simulations like **Figure 2-5 (a)—(c)** how the b' is related to the b , for a wide range of observed b' . So, we determined the correction value for the b' by calculating the difference between b' and b for various model populations.

We adopted here the nine kinds of $b = 1.0, 1.5, 1.6, 1.7, 1.75, 1.8, 1.9, 2.0$ and

2.5, for each original orbital distribution shown **Table 2-4**. Therefore, we made 27 orbital distributions in total. **Figure 2-6** shows the correction values calculated for each parent orbital distribution with the various b 's. For the data points on this graph, we draw a straight line coming as close as possible to all the data points in a least-squares sense. The error bars for each data point correspond to the standard deviation of the b' (error bar of x-component) and that of the $b - b'$ (error bar of y-component). Both of which were derived from the variation for the three parent orbital distributions. Note that the errors of all the correction values are less than ± 0.1 in all cases. This means that if there is a difference of slope larger than 0.1 between the size distribution for sub-km MBAs and that for km-sized MBAs, the statistical method mentioned above can easily distinguish the difference. When the correction value $b - b'$ is applied to the CSD derived from observed a 's, we will obtain the true CSD of the sub-km MBAs.

A simplified analysis of only several tens of sub-km MBAs observed with the Subaru on June 12, 2000 suggests that the CSD for sub-km MBAs is likely to be appreciably different from that for larger ones (Yoshida *et al.* 2001a). This result is encouraging, since it implies that even if that the method developed in this chapter has an error of ~ 0.1 in the estimate of the CSD slope, our method still gives a sufficiently meaningful result.

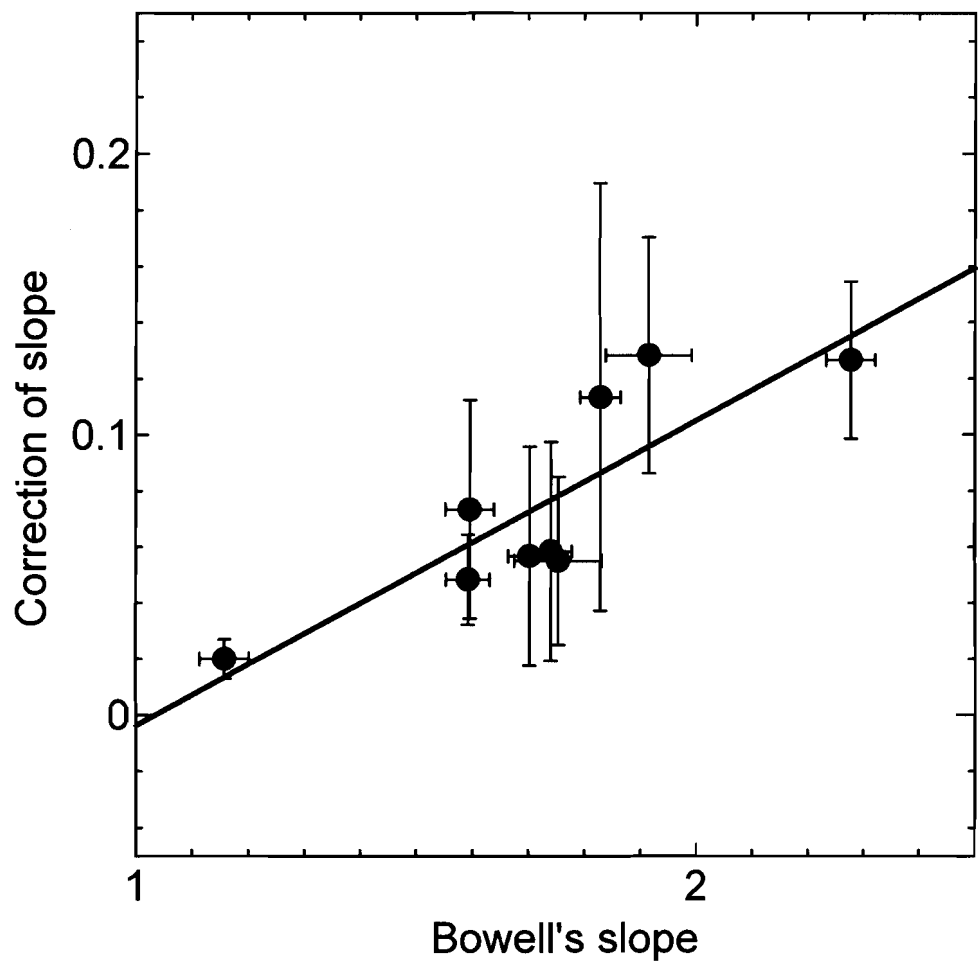


Figure 2-6
Correction to be applied to the slope (b') calculated by **Bowell's** equation, as a function of b' .
The straight line is a least-squares-fitted curve to each data point. The error bars for each data point correspond to the standard deviation arising from variations among the three cases in **Table 2-4**.

Chapter 3

Survey Observations and Results

In this chapter, we describe the two systematic survey observations of sub-km MBAs which we conducted using the Subaru telescope for exploring their size and spatial distribution. The first preliminary survey has a small sample number, because the survey was a part of the test runs for the camera performance and did not satisfy the observational conditions which we would intend as described in Section 3.1. The second main survey which we call SMBAS has enough number of sub-km MBAs as described in Section 3.2. The size distributions for sub-km MBAs obtained from both surveys showed the same trend.

3.1 Preliminary survey

We report here first observations of sub-km MBAs obtained with the prime-focus mosaic CCD camera for the Subaru telescope. We have detected 27 moving objects in a single image of the sky (field of view : $27' \times 27'$), whose location was 41° off opposition. From their positions and projected motions on the sky, all the detected objects were found to be new and consistent with the characteristics of MBAs. The V -magnitudes of the discovered asteroids range approximately from 19 to 24. Under some simple but reasonable assumptions, we estimated the CSD for the asteroids. This is a report on the first attempt to obtain the CSD of sub-km MBAs (the minimum diameter corresponds to about 0.6

km) by a statistical analysis of their Subaru images. In the following, we describe the image reduction method, the resulting CSD, a preliminary comparison of it with the CSD for asteroids larger than a few kilometers deduced from the past survey observations, and discuss implications for our obtained CSD.

3.1.1 Observations and data reduction

Observations were made at 14^h 26^m UT of June 12, 2000 at the prime focus of the 8.2m Subaru telescope atop Mauna Kea, Hawaii. We used the wide-field mosaic camera called the Subaru Prime-Focus Camera (Suprime-Cam) (Komiyama *et al.*, 2000), which covers the field of view of 27' \times 27' at the prime focus (F/1.9) with eight chips (2048 \times 4096 pixels each, the pixel size is 0.2''). The narrow gaps exist between the exposure areas, namely eight chips. Each CCD has an overscan region.

Since our observations were performed as a part of a Suprime-Cam testing run, we could not help pointing the telescope to the sky with the elongation angle (Sun-Earth-object angle) of 139° off opposition (RA = 20^h 10.0^m and Dec = -16° 45') near the ecliptic plane, to avoid both the moon and the Milky Way. The exposure time was 5 min with *V*-filter. We took two images of the same field in succession with a time interval of 9 min, to detect moving objects. The mean seeing sizes for the two images were 0.8'' and 0.9'', respectively.

Image reduction was carried out using IRAF on a chip-by-chip basis. First, the overscan region was trimmed, and then an average dark level corresponding to each chip was subtracted. In order to correct the difference in pixel sensitivity, the flat-field calibration must be done. For this purpose, we took several images of the twilight sky with the field-center offset slightly each other. And from them a median flat-field image was constructed, with which each observed image was divided. Finally, a cosmic-ray removal procedure was applied for each chip.

Because of the short exposure time and the not-so-good seeing, asteroids could

not be identified in a single image. So, we subtracted the second image from the first one, in an attempt to easily recognize moving objects. **Figure 3-1** shows a part of the differenced image, where one can see moving objects as pairs of separated black-and-white dots. By careful eye-inspection of segmented and enlarged images, we could eventually detect 27 moving objects in total over all the eight chips.

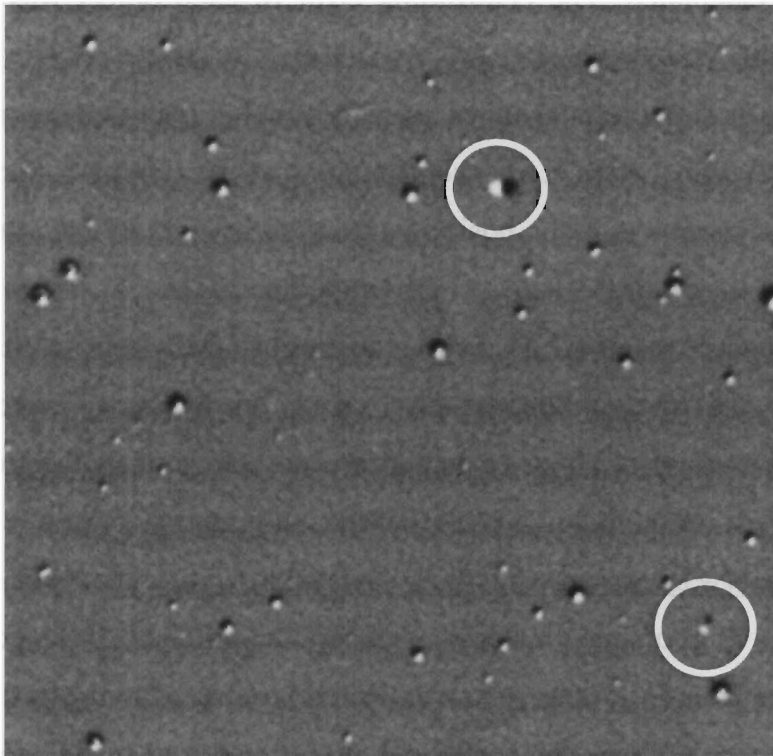


Figure 3-1

Two detected asteroids from Subaru Suprime-cam observations.

Moving objects appear as pairs of black-and-whites dots, since the second image was subtracted from the first one. A black rim attached to each star was caused by the telescope guiding error and the change of the seeing during the two exposures. The field-of-view of this figure is $2.5' \times 2.5'$.

3.1.2 Daily motion and photometry

To estimate daily motions of the detected moving objects, we picked up from each chip about 10 stars that have entry in the USNO-A2 catalog (<http://tdc-www.harvard.edu/software/catalogs/ua2.html>). The positional measurements of those stars were made with the APPHOT task in IRAF. The position for each moving object was also measured relative to the catalog stars for both the first image and the second one, and the apparent velocity for the object was calculated. The centroiding error of each object was much smaller than the seeing size.

We made a simulation using a two-body ephemeris generator, to deduce a statistical relation between the semi-major axis (a) of asteroids and their apparent daily motions in the position of this observational window. It was found that the motions of all the detected moving objects were consistent with those for MBAs, though it was difficult to surely distinguish MBAs from NEAs. However, considering that the number of discovered yet MBAs (approximately one hundred thousand) is almost a hundred times larger than the total number of other small bodies including NEAs (nearly a thousand) (<http://cfa-www.harvard.edu/iau/lists/Unusual.html>), it is very unlikely that our detected moving objects include considerable number of objects other than MBAs by chance. In fact, given an expected number of non-MBA objects in our observations ($\sim 27 / 100 = 0.27$), the Poisson statistics teaches us that probabilities for our result to include one or two of non-MBAs by chance respectively are 0.20 or 0.03. This means that 27 objects detected in this observation are substantially all MBAs. We have also confirmed that those moving objects are all new by referring to the asteroid database of the CBAT's Miner Planet Service.

Then, we describe here photometric reduction of our observations. Again APPHOT in IRAF was used to do aperture photometric measurements. For some reasons, we needed to follow the reduction procedures mentioned below. First,

we could not have chances to observe photometric standard stars separately but instead had to use background stars in the asteroid images for photometric calibration, because the observations were performed as a part of a Suprime-Cam test run. For the magnitude range of the detected asteroids ($V \sim 19-24$ mag), the only available star catalog was USNO-A2. Moreover, this catalog gives B - and R -magnitudes only, whereas our observations were made with V -band. Because of this band mismatch, we assumed, as an inevitable compromise, an average ($V-R$) for the background stars, whose average value was derived from populations of stars with known spectral types. Namely, we adopted an averaged value ($V-R$) $\sim +0.37$, which was calculated from the color frequency distribution for photometric standard stars observed over the whole sky (Landolt, 1983, Mermilliod & Mermilliod, 1994). By applying this color correction, we suppose that the observed V -mag for each asteroid can be tied to the R -mag of USNO-A2 catalog at least approximately. In this way, the magnitudes of the detected asteroids were found to range from 18.8 through 23.8 in V -band (see **Table 3-1**). It is inferred that thus obtained V -magnitudes of the asteroids can bear an error (σ_c) of ~ 0.27 , which is the standard deviation of ($V-R$) s for various spectral types from the above mean ($V-R$). In addition, the USNO-A2 catalog notifies us that each catalog star has a magnitude error (σ_m) of 0.25 on the average.

Next, we make estimation of absolute magnitudes (H) or equivalently the sizes for the observed asteroids. In order to calculate H -mag of an asteroid, we need to know its distances, since H -mag and the apparent V -mag are connected by the relation (Ephemerides of Minor Planets for 2001) :

$$H = V - 5 \log (\Delta \cdot r) - p (\alpha) - \delta V, \quad (3.1)$$

where Δ and r stand for the geocentric and heliocentric distances (in AU) respectively, $p (\alpha)$ is the phase function (α : phase angle, namely Earth-asteroid-Sun angle), and δV is the light variation.

To calculate r or Δ , we must know the semi-major axis (a) and eccentricity (e) of each asteroid. However, it is surely impossible to obtain e from such a short time arc as in this observation. As mentioned in Chapter 2, the a can be estimated with an error of ~ 0.1 AU from the apparent daily motions, if asteroids are near opposition (Nakamura and Yoshida 2001). It also mentioned there that the slope of the CSD can be determined with an error of 0.1 or so through extensive model calculations under the assumption of $e = 0$ (or $r = a$) for all the asteroids. Hence, the assumption of $r = a$ was also taken in this work. Practically, we hypothesized here as if all the detected asteroids were located in the middle of the main-belt (~ 2.7 AU). This is because, for our observations (41° off opposition), the correlation between the daily motion and a was not so good as near opposition. How this seemingly crude assumption placed here on the a of the observed asteroids affects the resulting CSD will be discussed later.

3.1.3 Results

Table 3-1 summarizes the measured daily motions, V -magnitudes and H -magnitudes of the 27 asteroids. In conversion of V -mag to H -mag using the **Equation (3.1)**, we adopted the phase function (with $\alpha = 14^\circ$ for the observation date) corresponding to the photometric slope parameter $G = 0.15$, which is the widely used value for the majority of asteroids (Ephemerides of Minor Planets for 2001). From these H -magnitudes, one can calculate the corresponding diameters by assuming an appropriate albedo. Before doing this, however, let us estimate the overall error (σ) contained in the H -magnitude. The σ consists of several component errors discussed in the previous Section 3.1.2 and other components, and the error breakdown will be expressed by the equation:

$$\sigma^2 = \sigma_o^2 + \sigma_c^2 + \sigma_m^2 + \sigma_v^2. \quad (3.2)$$

Table 3-1

Summary of asteroids detected in this observation.

| Asteroid number | chip No. | Apparent motion (arcmin/day) | Apparent magnitude (mag) | Absolute magnitude (mag) |
|--------------------|-------------|---------------------------------|--------------------------------|--------------------------------|
| 1 | 2 | 5.93 | 23.13 | 18.86 |
| 2 | 2 | 9.21 | 21.40 | 17.13 |
| 3 | 3 | (7.0) | (23.5) | (19.2) |
| 4 | 3 | 7.03 | 22.96 | 18.69 |
| 5 | 3 | 3.15 | 20.84 | 16.57 |
| 6 | 3 | 3.66 | 19.02 | 14.75 |
| 7 | 3 | 4.51 | 22.64 | 18.37 |
| 8 | 3 | 6.55 | 23.19 | 18.92 |
| 9 | 4 | 5.38 | 22.24 | 17.97 |
| 10 | 4 | 3.38 | 21.98 | 17.71 |
| 11 | 4 | (5.5) | 22.75 | 18.48 |
| 12 | 4 | (6.8) | (24.0) | (19.7) |
| 13 | 5 | 4.86 | 19.30 | 15.03 |
| 14 | 5 | 7.18 | 23.06 | 18.79 |
| 15 | 5 | 6.10 | 22.27 | 18.00 |
| 16 | 5 | 6.04 | 19.76 | 15.49 |
| 17 | 5 | 1.29 | 21.08 | 16.81 |
| 18 | 6 | 7.08 | 23.80 | 19.53 |
| 19 | 7 | 7.86 | 23.37 | 19.10 |
| 20 | 7 | 4.60 | 19.38 | 15.11 |
| 21 | 7 | 8.05 | 20.74 | 16.47 |
| 22 | 8 | 6.11 | 23.69 | 19.42 |
| 23 | 8 | 4.64 | 18.77 | 14.50 |
| 24 | 8 | 5.55 | 21.91 | 17.64 |
| 25 | 8 | (6.2) | 21.98 | 17.71 |
| 26 | 8 | (3.6) | 18.95 | 14.68 |
| 27 | 8 | 6.75 | 20.72 | 16.45 |

Note. The values in parentheses are low-accuracy data.

where σ_o is the error caused by the assumptions that $a = 2.7$ AU and $e = 0$ for all the observed asteroids. We found out $\sigma_o \sim 0.63$ by an orbital simulation as mentioned in Section 2.2 for an ensemble of the MBAs with realistic ranges of a and e . As for the light variation error (σ_v) caused by the rotation of asteroids, nothing can be known for our asteroids since the observation time was only 10 minutes. Therefore, we inferred it by regarding as σ_v a mode value for the distribution of the peak-to-bottom light variation amplitude of asteroids (吉田, 1999, Ephemerides of Minor Planets for 1998). The resulting σ_v is 0.25.

Since other errors like σ_c and σ_m have already been estimated in Section 3.1.2, we can obtain the σ from **Equation (3.1)** as $(0.63^2 + 0.27^2 + 0.25^2 + 0.25^2)^{1/2} = 0.77$. It is noted that the value is for a single asteroid. If there are n asteroids in a H -bin of **Figure 3-2**, the error for this bin should be σ / \sqrt{n} .

Figure 3-2 shows the differential (white-box histogram) and cumulative (black and white dots) H -mag distributions, drawn based on **Table 3-1**. The two asteroids whose measured magnitudes are fairly uncertain because of partial overlapping with stars in the asteroid of **Table 3-1** are omitted in **Figure 3-2**. The error bar attached to each dot is σ / \sqrt{n} for the above $\sigma = 0.77$. The diameter (D) scale in the upper abscissa was calculated from the lower H -mag scale for the averaged albedo of C- and S-type asteroids, that is, using an empirical formula $\log D = 3.65 - 0.2 H$. One can see from the formula that the faintest asteroid in **Table 3-1** corresponds to the diameter of about 550 m.

Next, we will examine the slope of the cumulative size distribution in **Figure 3-2**. Near the limiting magnitude, it is possible that some fraction of very faint asteroids escaped visual detection. To take into account this possible detection failure, a straight line slope was fitted by a least-squares method only for the asteroids indicated by filled (black) dots, which are at least 1.5 magnitude brighter than the detectable magnitude. The slope of the fitted line was then found to be 1.0.

Although the least-squares fitting error for the slope was calculated to be 0.1, this value should be taken as a formal error rather than a practical one, since the

H -mag error attached to each data point in **Figure 3-2** is as large as $0.40 - 0.77$ as a result from the assumption that all asteroids have $a = 2.7$ (AU). Hence, in order to estimate the realistic error of the slope, we produced in a computer a hundred sets of synthetic data points by generating random values that obey a Gaussian distribution with the standard deviation of σ / \sqrt{n} , and with them a hundred slopes were calculated. The mean deviation of these slopes from 1.0 was about 0.3. We consider, therefore, this value as a realistic error for our observed slope. Then the slope of CSD for MBAs from this observation is 1.0 ± 0.3 .

The dashed line in **Figure 3-2** represents the slope (~ 1.75) estimated from the Palomar-Leiden (Van Houten *et al.*, 1970) and Spacewatch (Jedicke and Metcalfe 1998) surveys, which covered the size range of $D >$ a few kilometers. As this line is intended to only show their slopes for comparison, the zero point is arbitrary. One can see from **Figure 3-2** that our slope for the size range of 6—1 km is much gentler than the Palomar-Leiden and Spacewatch slope. This suggests that, for a specified size range, the sky number density of sub-km MBAs is fairly more depleted than that extrapolated from the slope of the past surveys.

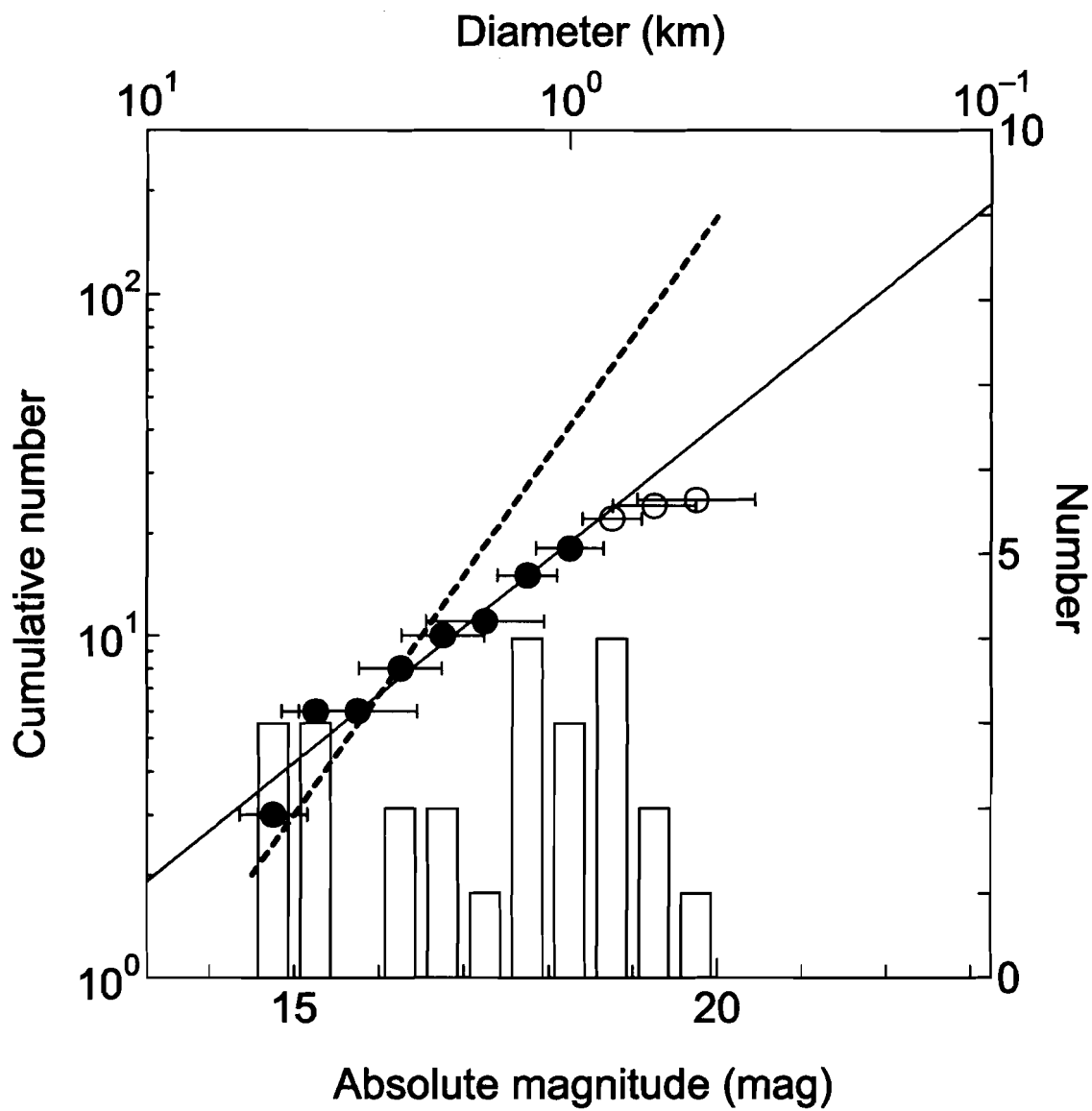


Figure 3-2 The differential (white-box histogram) and cumulative (black and white dots) H -mag distributions for our observed asteroids.

The diameter (logarithmic) scale in the upper abscissa is calculated from an empirical relation: $\log D = 3.65 - 0.2 H$. The solid line is least-squares-fitted to the black-dot points. As for the error bars, see text. The dashed line is drawn only to represent the slope for the past systematic surveys (the Palomar-Leiden and Spacewatch).

3.2 Sub-km Main-belt Asteroids Survey (SMBAS)

3.2.1 Description of SMBAS

To confirm the results of the preliminary survey mentioned in Section 3.1, the second observations were carried out on February 21 and 24, 2001 by the same instruments as in the preliminary observation. This survey is our main survey : Sub-km Main-belt Asteroids Survey (SUBAS). By this time, the Suprime-Cam has been improved, the number of CCD chips increased from eight to ten, and a field of view could cover the sky area of $34' \times 27'$. The ten CCD chips are arranged as in **Figure 3-3**. The lower-left CCD did not work in our observations. So we actually used nine CCD chips.

A large number of MBAs stay near the ecliptic plane and each asteroid is brightest near opposition because of the short distance between the earth and the asteroid. For these reasons, we pointed the telescope to near opposition with an elongation angle (Sun--Earth--object angle) of $\sim 180^\circ$ near the ecliptic plane. We selected seven observational fields shown in **Table 3-2** on Feb. 21. **Figure 3-4** shows our observational fields including the ecliptic, which they are near the base of the forefeet of the lion in the Leonis constellation. We observed the same seven fields also on Feb. 24. The total survey sky area is about 3.26 deg^2 . The *R*-band filter was used with 7 min exposure. The seeing size was $\sim 0.8 - 1.0$ arcsec on Feb. 21 and $\sim 0.7 - 0.9$ arcsec on Feb. 24. We performed two observational modes : 1) Wide Field (WF) survey mode and 2) Deep Field (DF) survey mode. In WF survey, we selected five observational fields shown in **Table 3-2** and in **Figure 3-4**. We took three images of the same field with a time interval of about 55 min. In DF survey, two fields shown in **Table 3-2** and in **Figure 3-4** were also selected, and eleven images of the same field were taken every 11 min in succession including the read out time of about 4 min. We also observed six photometric standard stars (see **Table 3-3**). The size of an image file is about 160 MB. So the total file size that we obtained is 23518.44 MB.

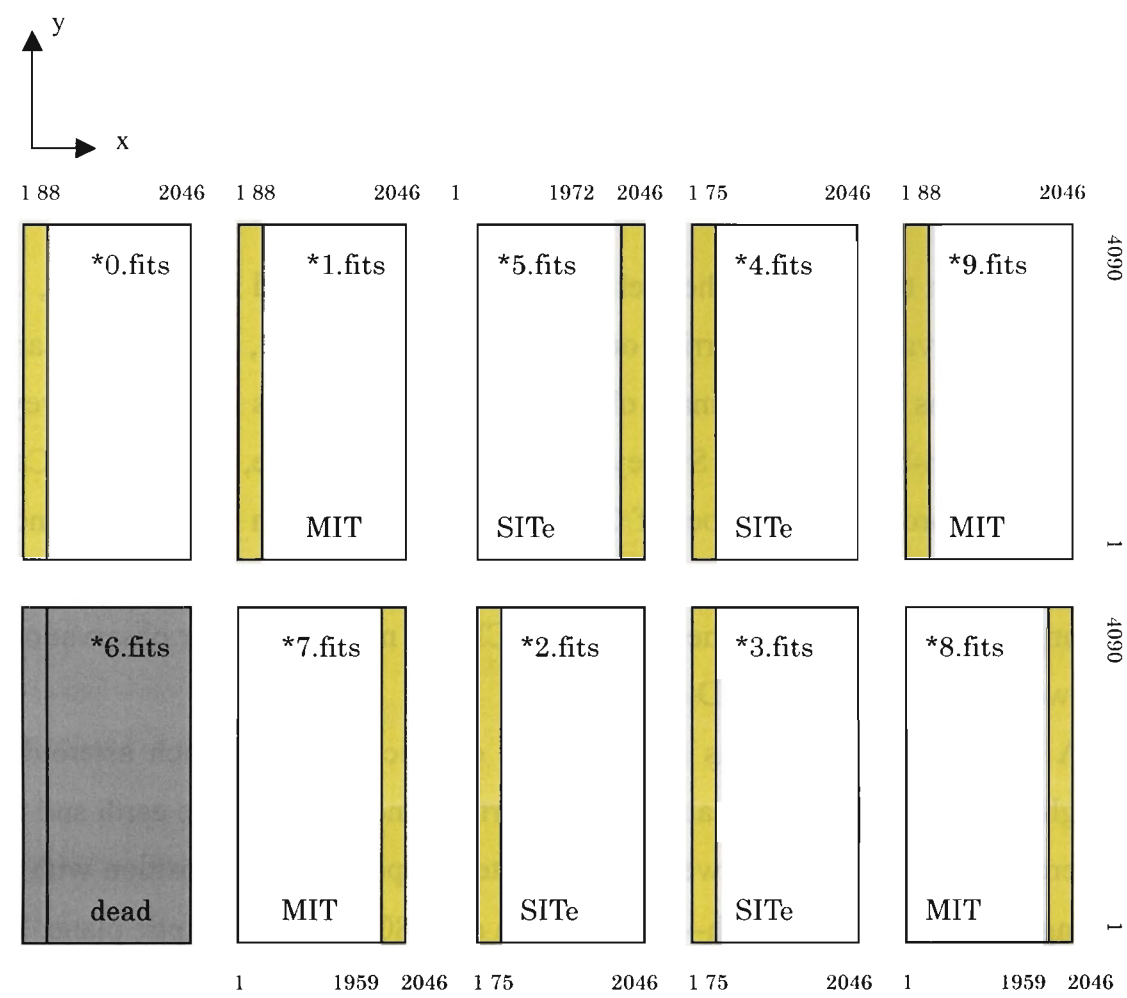


Figure 3-3
The CCD array of Suprime-Cam.

The MIT and SITe devices are used in mixture. The yellow region of each CCD is the overscan region. The top or bottom and right-hand numbers which attached to each CCD show effective areas. The leftmost CCD of the bottom was not available.

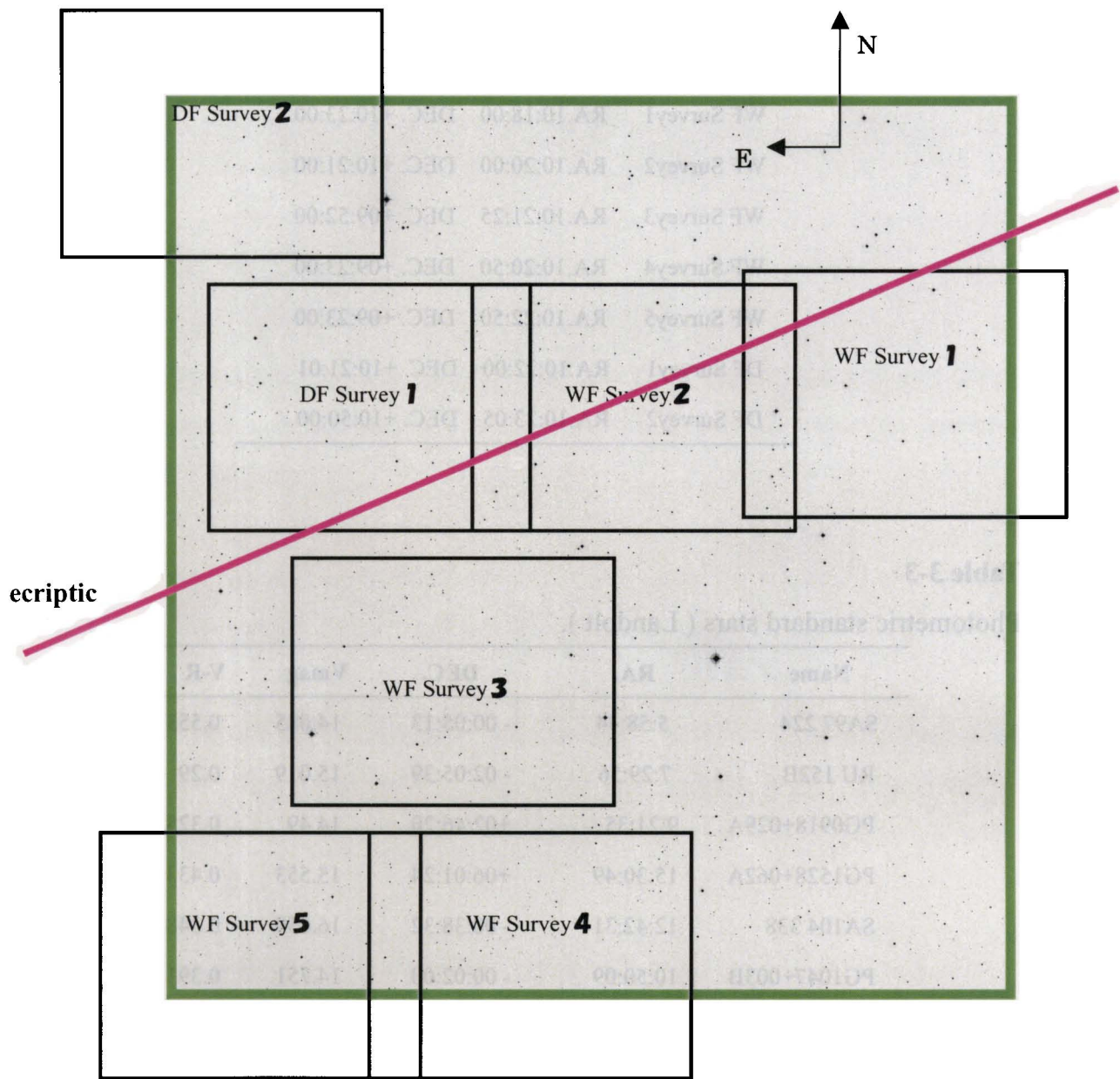


Figure 3-4
SMBAS observational fields and the ecliptic plane.

Table 3-2

The center coordinates (J2000.0) of the observational fields.

| | | |
|------------|-------------|----------------|
| WF Survey1 | RA.10:18:00 | DEC. +10:23:00 |
| WF Survey2 | RA.10:20:00 | DEC. +10:21:00 |
| WF Survey3 | RA.10:21:25 | DEC. +09:52:00 |
| WF Survey4 | RA.10:20:50 | DEC. +09:23:00 |
| WF Survey5 | RA.10:22:50 | DEC. +09:23:00 |
| DF Survey1 | RA.10:22:00 | DEC. +10:21:01 |
| DF Survey2 | RA.10:23:05 | DEC. +10:50:00 |

Table 3-3

Photometric standard stars (Landolt).

| Name | RA. | DEC. | Vmag | V-R |
|-------------|----------|------------|--------|-------|
| SA97 224 | 5:58:44 | - 00:05:13 | 14.085 | 0.553 |
| RU 152B | 7:29:56 | - 02:05:39 | 15.019 | 0.29 |
| PG0918+029A | 9:21:35 | +02:46:20 | 14.49 | 0.325 |
| PG1528+062A | 15:30:49 | +06:01:24 | 15.553 | 0.433 |
| SA104 338 | 12:42:31 | - 00:38:32 | 16.059 | 0.348 |
| PG1047+003B | 10:50:09 | - 00:02:00 | 14.751 | 0.391 |

3.2.2 Data reduction

Obtained images were divided into the three kinds of frames as follows: bias frames, sky-flat frames and object frames. A frame includes nine CCD-chip images taken during one exposure. Image reduction was carried out on a CCD-by-CCD basis in a standard method using NOAO IRAF, which we mention in the next section.

3.2.2 (a) Procedure of the standard image reduction

Here is the step-by-step reduction procedure:

1. The average value of the overscan region for each CCD was first subtracted from each CCD image.
2. The overscan region was trimmed and then the image which consists only of the effective area was made. The information of the area had been written in the image's header.

The first and second operations can be performed at the same time by using IRAF — noao — imred — bias — colbias (see **Figure 3-5**).

3. In order to correct two-dimensional bias pattern of each CCD, the bias image was subtracted from each CCD image. The bias image was made by averaging two raw bias frames which were taken every night.

This operation is effective to reduce the deviations (σ) of the sky.

4. In order to flatten any difference in pixel sensitivity within a CCD, a flat-field calibration must be done. For that purpose, we took several images of the twilight sky with the field-center offset slightly from each other. Then, a median flat-field image was constructed from them, by which each CCD image was divided.

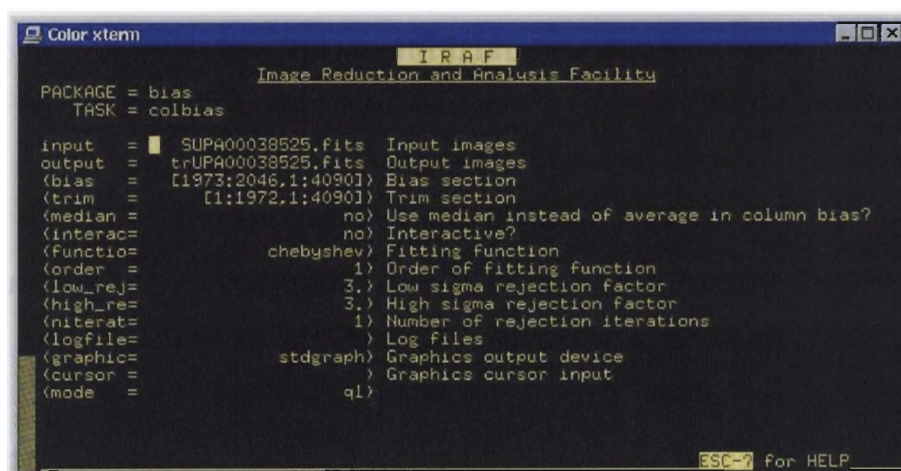


Figure 3-5

IRAF window: noao — imred — bias — colbias.

3.2.2 (b) Detection of moving objects

After we finished the above procedure for all the object frames, as the fifth operation, we finally subtracted the first image from the second one, and added it to the third image, in order to recognize easily moving objects in the WF survey. When multiple images are combined, their sky levels were adjusted to a certain level. This operation increases the dispersion of the sky level to some extent, if the number of combined images is small. However, the easy detectability of asteroids shown as trains of black and white dots is much more advantageous than some degradation of S/N. We also performed similar operations for sets of 11 images taken in the DF survey.

Figure 3-6 shows an example image for which the above operations were applied to a series of images obtained from the WF survey. One can see moving objects as trains of separated black-white-black dots. **Figure 3-7** shows one image for which the above operations were similarly performed for a series of images of the same CCD chip in the DF survey. One can see moving objects as a sequence of black-white-black-... dots.

This black-and-white image technique bears some other advantages as well.

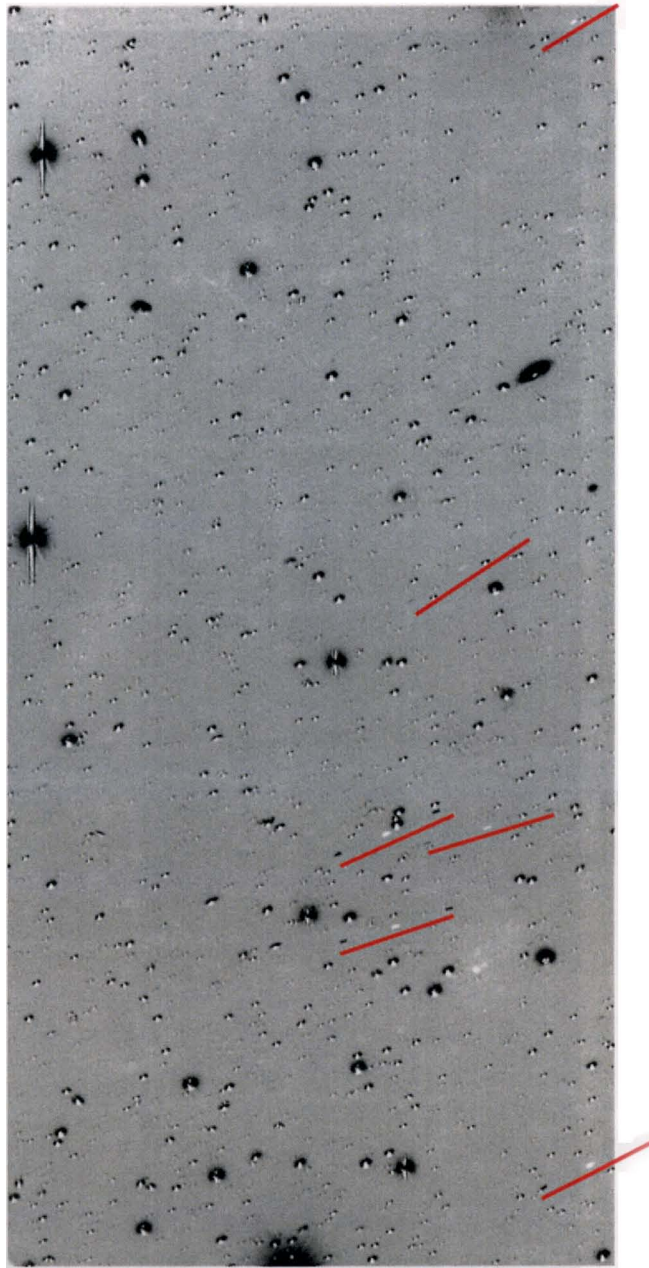


Figure 3-6

The moving objects detected on the one CCD images in the WF survey.

Some trains of black-and-white dots as asteroid images are marked by red lines for clarity. Fifteen moving objects are detected in this image altogether. Black-white-black dots appear fairly separated because of long exposure intervals (about 55 min.). Field stars and galaxies appear as slightly shifted black-white-black dots, due to the telescope guiding error during the three exposures. Up is north and left is east in this image. All moving objects moved from left side to right side (due to retrograde motions near opposition).

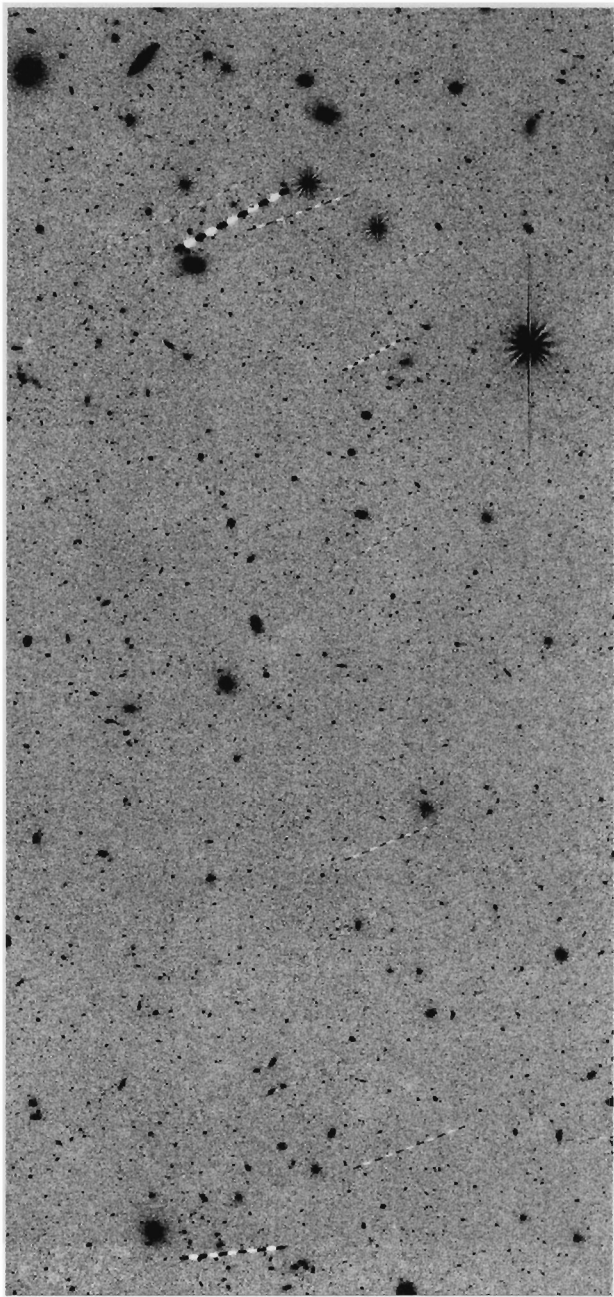


Figure 3-7

The moving objects detected on the one CCD images in the DF survey.

Twenty-three detected moving objects are included in this image. They appear as black-white straight bars because of short exposure intervals (about 11 min.). Field stars and galaxies appear as black images. Up is north and left is east in this image. All moving objects moved from left side to right side (due to retrograde motions near opposition).

This enables us to easily identify moving objects as a time sequence. For example, in the WF survey, as for white moving objects, we can surely confirm that the white dot corresponds to the image taken at the second exposure. It may also help us judge whether one elongated object is either a moving object or a galaxy. Because all galaxies are always seen as black images, we can confidently regard all white images as moving objects. This technique is also useful to confirm that a moving object is the same one even on the neighboring CCD chips.

3.2.2 (c) Number of detected moving objects

We checked by a careful eye-inspection all of the magnified images that finished the operations mentioned in Section 3.2.2 (a) and (b), and then we detected 1,194 moving objects (see **Table 3-4**). Then, after removing the same moving objects that strode over neighboring CCDs, we eventually detected 1,111 moving objects.

CHAPTRE 3 SURVEY OBSERVATIONS AND RESULTS

Table 3-4

Summary of the numbers of detected moving objects.

Date: 21 February, 2001

| Field | UT | Airmass | RA | DEC | Detected number | | | | | | | | | |
|---------------|----------|---------|----------|--------------|-----------------|----|----|---|----|---|----|----|---|-----|
| | | | | | 0 | 1 | 2 | 3 | 4 | 5 | 6 | 7 | 8 | 9 |
| WF Survey 1 | 6:42:13 | 1.704 | 10:18:00 | +10:23:00.01 | 3 | 16 | 6 | 7 | 7 | 6 | 9 | 13 | 7 | 73 |
| | 7:37:38 | 1.326 | | | | | | | | | | | | |
| | 8:33:03 | 1.135 | | | | | | | | | | | | |
| WF Survey 2 | 6:53:18 | 1.622 | 10:20:00 | +10:21:00.80 | 10 | 19 | 9 | 8 | 13 | 4 | 15 | 5 | 7 | 84 |
| | 7:48:43 | 1.289 | | | | | | | | | | | | |
| | 8:47:47 | 1.107 | | | | | | | | | | | | |
| WF Survey 3 | 7:04:23 | 1.55 | 10:21:25 | +09:52:00.17 | 11 | 7 | 7 | 8 | 12 | 9 | 8 | 11 | 9 | 80 |
| | 7:59:48 | 1.25 | | | | | | | | | | | | |
| | 8:58:53 | 1.09 | | | | | | | | | | | | |
| WF Survey 4 | 7:16:28 | 1.473 | 10:20:50 | +09:23:00.33 | 9 | 9 | 8 | 5 | 9 | 8 | 6 | 10 | 9 | 71 |
| | 8:10:53 | 1.211 | | | | | | | | | | | | |
| | 9:09:58 | 1.074 | | | | | | | | | | | | |
| | 9:32:08 | 1.044 | | | | | | | | | | | | |
| WF Survey 5 | 7:26:33 | 1.417 | 10:22:50 | +09:23:00.04 | 14 | 9 | 7 | 8 | 6 | 9 | 10 | 12 | 8 | 83 |
| | 8:21:58 | 1.183 | | | | | | | | | | | | |
| | 9:21:03 | 1.06 | | | | | | | | | | | | |
| Deep Survey 1 | 9:57:21 | 1.022 | 10:22:00 | +10:21:01.15 | 10 | 9 | 3 | 4 | 8 | 8 | 4 | 3 | 9 | 58 |
| | 10:08:27 | 1.017 | | | | | | | | | | | | |
| | 10:18:32 | 1.014 | | | | | | | | | | | | |
| | 10:30:37 | 1.014 | | | | | | | | | | | | |
| | 10:46:14 | 1.017 | | | | | | | | | | | | |
| | 10:58:19 | 1.021 | | | | | | | | | | | | |
| | 11:07:24 | 1.029 | | | | | | | | | | | | |
| | 11:18:29 | 1.038 | | | | | | | | | | | | |
| | 11:29:34 | 1.05 | | | | | | | | | | | | |
| | 11:40:39 | 1.065 | | | | | | | | | | | | |
| Deep Survey 2 | 12:20:48 | 1.138 | 10:23:05 | +10:50:00.39 | 6 | 18 | 11 | 7 | 6 | 7 | 6 | 10 | 6 | 75 |
| | 12:31:54 | 1.167 | | | | | | | | | | | | |
| | 12:42:59 | 1.201 | | | | | | | | | | | | |
| | 12:54:04 | 1.239 | | | | | | | | | | | | |
| | 13:05:09 | 1.283 | | | | | | | | | | | | |
| | 13:16:14 | 1.333 | | | | | | | | | | | | |
| | 13:27:19 | 1.39 | | | | | | | | | | | | |
| | 13:38:24 | 1.455 | | | | | | | | | | | | |
| | 13:49:29 | 1.53 | | | | | | | | | | | | |
| | 14:00:34 | 1.616 | | | | | | | | | | | | |
| | 14:11:39 | 1.717 | | | | | | | | | | | | |
| | | | | | | | | | | | | | | 624 |

Date: 24 February, 2001

| Field | UT | Airmass | RA | DEC | Detected number | | | | | | | | | | Total |
|---------------|----------|---------|----------|--------------|-----------------|----|----|----|----|----|----|----|----|------|-------|
| | | | | | 0 | 1 | 2 | 3 | 4 | 5 | 7 | 8 | 9 | | |
| WF Survey 1 | 6:25:36 | 1.752 | 10:18:00 | +10:22:59.99 | 8 | 8 | 14 | 5 | 11 | 14 | 10 | 7 | 11 | 88 | |
| | 7:21:01 | 1.35 | | | | | | | | | | | | | |
| | 8:16:28 | 1.147 | | | | | | | | | | | | | |
| WF Survey 2 | 6:36:41 | 1.664 | 10:20:00 | +10:21:00.34 | 9 | 10 | 9 | 8 | 7 | 9 | 10 | 4 | 11 | 77 | |
| | 7:32:06 | 1.307 | | | | | | | | | | | | | |
| | 8:27:33 | 1.125 | | | | | | | | | | | | | |
| WF Survey 3 | 6:47:46 | 1.587 | 10:21:26 | +09:52:00.30 | 12 | 8 | 11 | 9 | 15 | 10 | 8 | 9 | 10 | 92 | |
| | 7:43:11 | 1.269 | | | | | | | | | | | | | |
| | 8:38:38 | 1.106 | | | | | | | | | | | | | |
| WF Survey 4 | 6:58:51 | 1.505 | 10:20:50 | +09:23:00.61 | 16 | 8 | 9 | 9 | 5 | 10 | 11 | 8 | 8 | 84 | |
| | 7:54:17 | 1.228 | | | | | | | | | | | | | |
| | 8:49:43 | 1.086 | | | | | | | | | | | | | |
| WF Survey 5 | 7:09:56 | 1.446 | 10:22:50 | +09:23:00.39 | 4 | 12 | 7 | 8 | 7 | 8 | 10 | 12 | 16 | 83 | |
| | 8:05:22 | 1.197 | | | | | | | | | | | | | |
| | 9:00:48 | 1.074 | | | | | | | | | | | | | |
| Deep Survey 1 | 9:11:53 | 1.052 | 10:22:00 | +10:21:00.50 | 14 | 15 | 7 | 11 | 14 | 15 | 23 | 12 | 17 | 128 | |
| | 9:22:58 | 1.04 | | | | | | | | | | | | | |
| | 9:34:03 | 1.03 | | | | | | | | | | | | | |
| | 9:45:08 | 1.022 | | | | | | | | | | | | | |
| | 9:56:13 | 1.017 | | | | | | | | | | | | | |
| | 10:07:18 | 1.014 | | | | | | | | | | | | | |
| | 10:18:23 | 1.014 | | | | | | | | | | | | | |
| | 10:29:28 | 1.016 | | | | | | | | | | | | | |
| | 10:40:33 | 1.019 | | | | | | | | | | | | | |
| | 10:51:38 | 1.026 | | | | | | | | | | | | | |
| Deep Survey 2 | 11:02:43 | 1.034 | 10:23:06 | +10:50:00.31 | 15 | 11 | 10 | 15 | 16 | 11 | 14 | 14 | 12 | 118 | |
| | 11:27:47 | 1.06 | | | | | | | | | | | | | |
| | 11:38:53 | 1.077 | | | | | | | | | | | | | |
| | 11:49:59 | 1.097 | | | | | | | | | | | | | |
| | 12:01:04 | 1.12 | | | | | | | | | | | | | |
| | 12:12:09 | 1.146 | | | | | | | | | | | | | |
| | 12:23:15 | 1.177 | | | | | | | | | | | | | |
| | 12:34:20 | 1.211 | | | | | | | | | | | | | |
| | 12:45:26 | 1.251 | | | | | | | | | | | | | |
| | 12:56:31 | 1.296 | | | | | | | | | | | | | |
| | 13:07:36 | 1.348 | | | | | | | | | | | | | |
| | 13:18:41 | 1.407 | | | | | | | | | | | | | |
| | | | | | | | | | | | | | | 670 | |
| | | | | | | | | | | | | | | 1194 | |

3.2.3 Photometry

3.2.3 (a) Measurement of brightness

We carried out aperture photometric measurements for detected moving objects and the other objects (stars or galaxies) listed in the USNO-A2 catalogue on the same image, by using IRAF—apphot (see **Figure 3-8**). Next we added the following corrections to the measured brightness of the moving

objects:

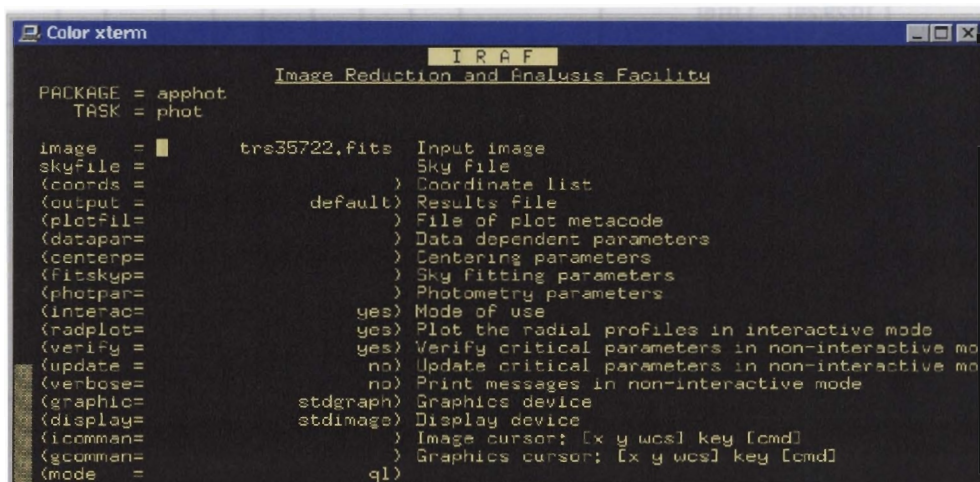
(1) The correction of difference in sensitivity between CCDs

(about this, we will mention in the Section 3.2.3 (b).)

(2) The correction of atmospheric extinction arising from the variation of airmass

(about this, we will mention in the Section 3.2.3 (c).)

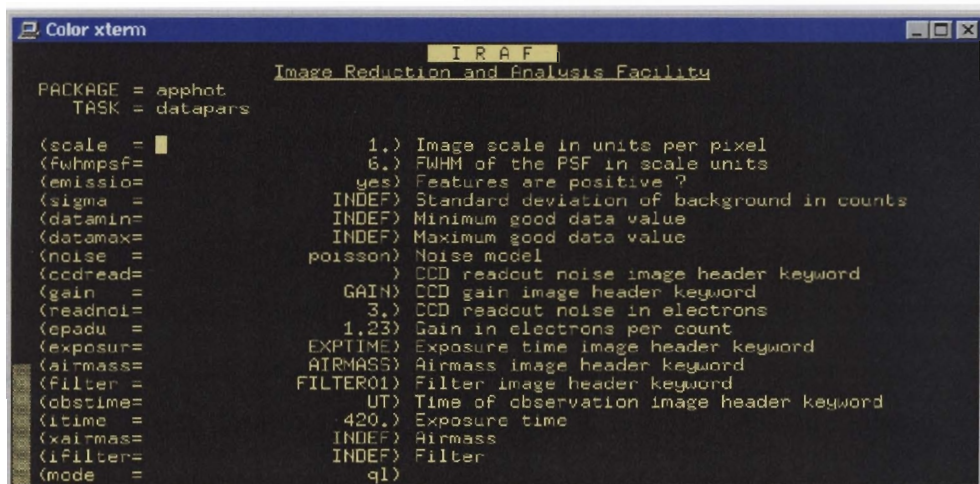
We found that a large number of moving objects detected in the DF survey showed appreciable light variations over 11 exposures (for about two hours), probably caused by rotations of asteroids. Thus we regarded here the averaged value of light variation over 11 exposed as the apparent magnitude for each object.



```

Color xterm
IRAF
Image Reduction and Analysis Facility
PACKAGE = apphot
TASK = phot

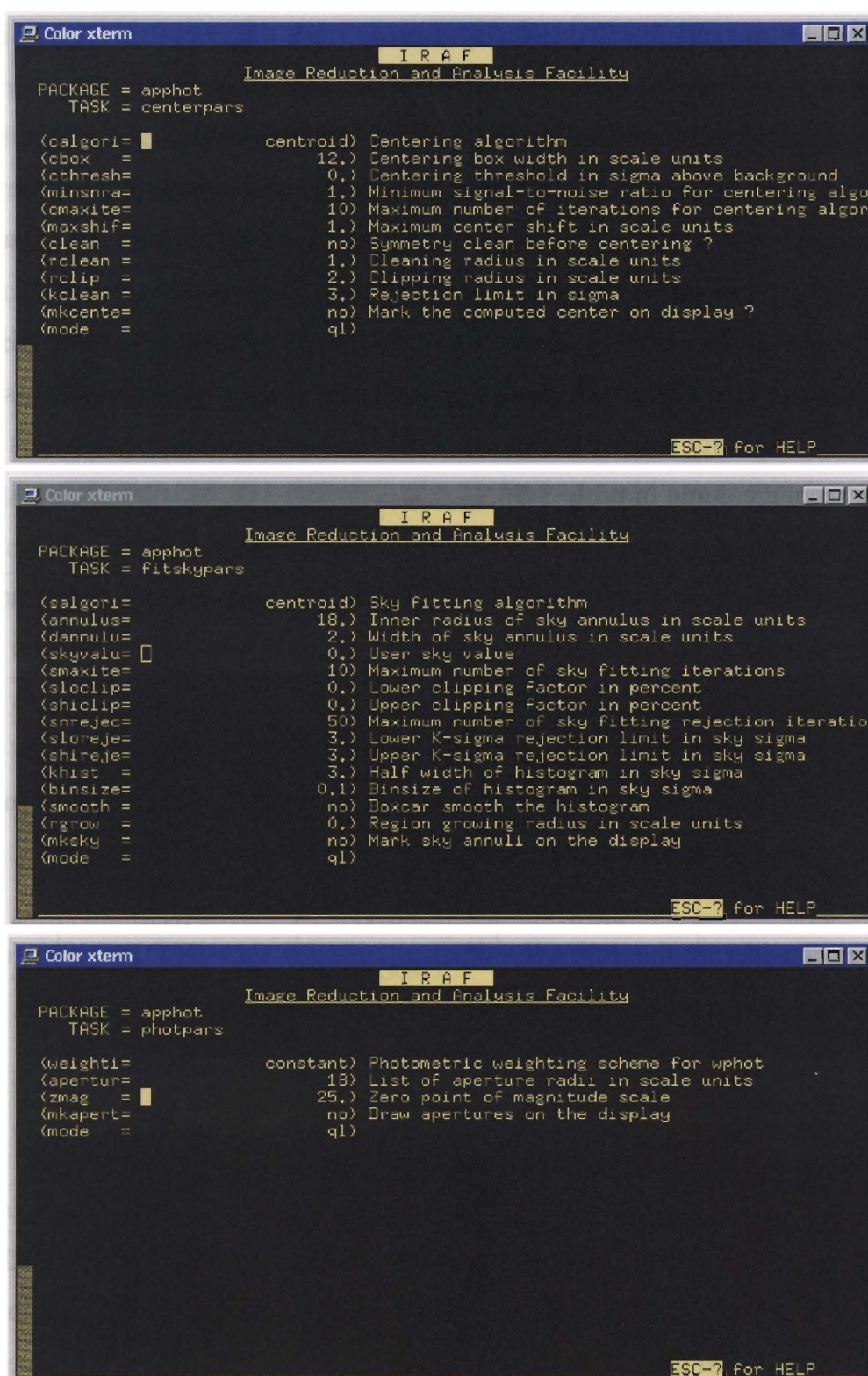
image = trs35722.fits Input image
skyfile = Sky file
(coords = ) Coordinate list
(output = default) Results file
(plotfile = ) File of plot metacode
(datapar = ) Data dependent parameters
(centerp = ) Centering parameters
(fitskyp = ) Sky fitting parameters
(photpar = ) Photometry parameters
(interac = yes) Mode of use
(radplot = yes) Plot the radial profiles in interactive mode
(verify = yes) Verify critical parameters in non-interactive mo
(update = no) Update critical parameters in non-interactive mo
(verbose = no) Print messages in non-interactive mode
(graphic = stdgraph) Graphics device
(display = stdimage) Display device
(icomman = ) Image cursor: [x y wcs] key [cmd]
(gcomman = ) Graphics cursor: [x y wcs] key [cmd]
(mode = ql)
  
```



```

Color xterm
IRAF
Image Reduction and Analysis Facility
PACKAGE = apphot
TASK = datapars

(scale = 1.) Image scale in units per pixel
(fwhmpsf = 6.) FWHM of the PSF in scale units
(emissio = yes) Features are positive ?
(sigma = INDEF) Standard deviation of background in counts
(datamin = INDEF) Minimum good data value
(datamax = INDEF) Maximum good data value
(noise = poisson) Noise model
(ccdread = ) CCD readout noise image header keyword
(gain = GAIN) CCD gain image header keyword
(readnoi = 3.) CCD readout noise in electrons
(epadu = 1.23) Gain in electrons per count
(exposur = EXPTIME) Exposure time image header keyword
(airmass = AIRMASS) Airmass image header keyword
(filter = FILTER01) Filter image header keyword
(obstime = UT) Time of observation image header keyword
(itime = 420.) Exposure time
(xairmass = INDEF) Airmass
(iFilter = INDEF) Filter
(mode = ql)
  
```

**Figure 3-8**

The parameters used in IRAF — apphot.

3.2.3 (b) Correction of sensitivity among nine CCD chips

In a mosaic CCD camera, each CCD has a slightly different sensitivity when compared with its neighbors. In order to flatten the relative response for each CCD to the incoming radiation, we need to perform the following calibrations:

1. We measure the mean value of a sky background area (e.g., $10 \times 10 \text{ pixel}^2$) where there is no star in the object frame. We compare the average signal values of several measured areas for one CCD with those in other CCDs (see the second column in **table 3-5**).
2. Practically, we calibrate the sensitivity of each CCD with respect to the No.2-CCD, for which images of the standard stars were taken (see the third column in **table 3-5**).
3. The difference of sensitivity for each CCD was translated into the difference of magnitude (see the fourth column in **table 3-5**).
4. After considering the difference of magnitude for each CCD, we can get the corrected magnitudes of moving objects.

3.2.3 (c) Correction of airmass

We observed several Landolt standard stars at some different airmasses and then measured their brightness using the IRAF—apphot (Landolt, 1992, see **Table 3-3**) . **Figure 3-9** shows an example of extinction for 24 February observations. From this figure, we got a correction of 2.8726 mag, to convert the observed magnitudes to atmosphere-less magnitudes.

We added this correction to the magnitude obtained in Section 3.2.3 (b). In this way, brightness for all moving objects was corrected. As mentioned in

Section 3.2.3 (a), since each object has a light variation, we must measure the brightness of each object for every exposure. We found that the average amplitude of the light variation is about 0.25 mag This value is about ten times larger than the measuring photometric error (about 0.03 mag) of each object. Therefore, this error of ~ 0.25 mag may affect the absolute magnitude for each object nearly by the same amount, especially for asteroids in the WF survey where only three exposures were made.

Table 3-5

The difference of sensitivity between CCDs

| Chip No. | Average value of sky background | The difference of sensitivity | The difference of magnitude | Non-uniformity within the CCD (%) |
|----------|---------------------------------|-------------------------------|-----------------------------|-----------------------------------|
| 0 | 11144.47 | 1.309691 | 0.293 | 0.96 |
| 1 | 12670.8 | 1.489065 | 0.432 | 0.38 |
| 2 | 8509.233 | 1 | 0.000 | 0.27 |
| 3 | 8216.5 | 0.965598 | -0.038 | 0.30 |
| 4 | 8861.9 | 1.041445 | 0.044 | 0.14 |
| 5 | 10471.87 | 1.230647 | 0.225 | 0.29 |
| 7 | 12970.4 | 1.524274 | 0.458 | 0.40 |
| 8 | 10712.7 | 1.25895 | 0.250 | 0.30 |
| 9 | 11111.93 | 1.305868 | 0.290 | 0.57 |

※ Note that there is no chip for No.6. It is seen that the non-uniformity within a CCD is not larger than 1 %.

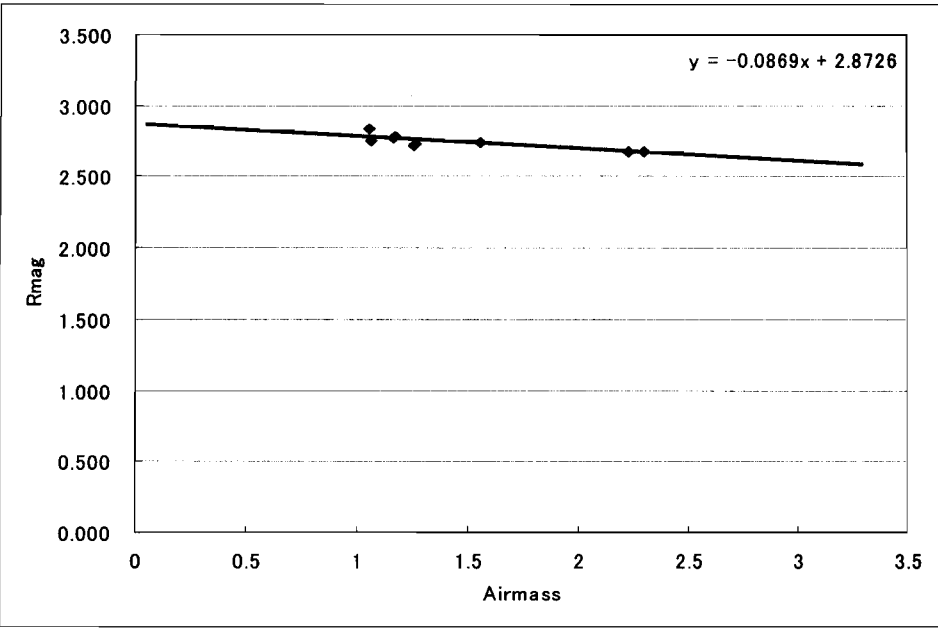


Figure 3-9

The extinction curve.

The horizontal axis shows the airmass of the observed standard stars, and the vertical axis shows the relative magnitude of the observed standard stars for the magnitude entries in the Landolt catalogue. For the data on this graph, we fitted a straight line ($y = -0.0869 x + 2.8726$) to all the data points by a least squares method.

3.2.4 Measurements of positions and velocities of moving objects

To estimate the daily motions of the detected moving objects, we picked up from each CCD about 10 stars that have entry in the USNO-A2 catalogue (<http://tdc-www.harvard.edu/software/catalogs/ua2.html>). Positional measurements of those stars were again made with IRAF—apphot. The position for each moving object was also measured relative to the catalog stars for all CCD images. The apparent velocity for the object was calculated from its positions corresponding to all of the exposure times.

3.2.5 Calculation of ecliptic components of objects' motions

In order to estimate the semi-major axis (a) and inclination (I) of the orbit for each sub-km MBA by using our method described in Chapter 2, we must calculate the ecliptic components of the moving velocity for each moving object. So we obtained their ecliptic components as follows.

1. If the field of view of a CCD is small enough ($< 1^\circ$), we can assume that the celestial sphere projected on the CCD is approximately plane, because an error between the sphere and the plane is negligible. For example, an asteroid near the center of the main-belt moves about 0.6' per hour. The difference in the hourly movements of the asteroid seen on the celestial sphere and on the plane is only 0.005". This value is much smaller than the pixel size of Suprime-Cam (0.2").
2. We determined the directions of the north pole and the equator on the CCD image by using the position (right ascension (α), declination (δ)) of stars of the USNO-A2 catalog. We used the positions (α_1, δ_1) and (α_2, δ_2) of two known stars, and calculated the scale factor (f) that relates the unit of the standard coordinate to the (x, y) pixel unit of the CCD image. The f is the number of pixels corresponding to $\{(\delta_2 - \delta_1)^2 + (\alpha_2 - \alpha_1)^2 \cos^2 \delta\}^{1/2}$, where $\delta = (\delta_2 + \delta_1) / 2$. We can translate the (α, δ) of the object to the ecliptic longitude (λ) and latitude (β) using **Equations (3.3) – (3.5)**.

$$\cos \beta \cos \lambda = \cos \delta \cos \alpha \quad (3.3)$$

$$\cos \beta \sin \lambda = \sin \delta \sin \epsilon + \cos \delta \sin \alpha \cos \epsilon \quad (3.4)$$

$$\sin \beta = \sin \delta \cos \epsilon - \cos \delta \sin \alpha \sin \epsilon, \quad (3.5)$$

where ϵ is the obliquity of the ecliptic for the observational day, and

$$\varepsilon = 23^{\circ} 26' 21'' .448 = 23^{\circ} .4392911 \quad (\text{J2000}) \quad (3.6)$$

3. When the positions of two stars in the standard coordinate system are (ξ_1, η_1) and (ξ_2, η_2) , and the positions of the two stars in the pixel coordinate system are (x_1, y_1) and (x_2, y_2) , the relation between the standard coordinate (ξ, η) and the pixel coordinate (x, y) is represented as follows.

$$\Delta x / f = A \Delta \xi + B \Delta \eta \quad (3.7)$$

$$\Delta y / f = C \Delta \xi + D \Delta \eta \quad (3.8),$$

where $\Delta \xi = (\xi_2 - \xi_1)$, $\Delta \eta = (\eta_2 - \eta_1)$, $\Delta x = x_2 - x_1$, and $\Delta y = y_2 - y_1$. The A, B, C and D are constants. We can determine these constants from the positions of two stars as shown in **Figure 3-10**.

4. By measuring the position of two known stars in the xy pixel coordinate, we obtained $\Delta x (= x_2 - x_1)$ and $\Delta y (= y_2 - y_1)$.

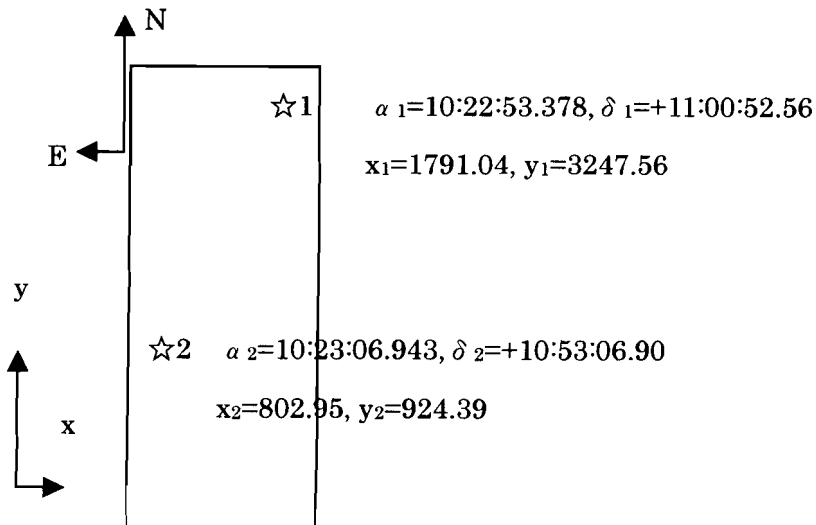


Figure 3-10

Example of the positions of USNO-A2 stars on a CCD chip.

5. We calculated the positions (λ_1, β_1) , (λ_2, β_2) of two stars in the ecliptic coordinate from the positions (α_1, δ_1) , (α_2, δ_2) of the USNO-A2 catalog using **Equations (3.3)–(3.6)**. Next, we obtained the $\Delta \xi$ and $\Delta \eta$ using the following **Equations (3.9), (3.10)** (Mueller 1969).

$$\Delta \xi = \frac{\cos \beta_1 \sin (\lambda_1 - \lambda_2)}{\sin \beta_1 \sin \beta_2 + \cos \beta_1 \cos \beta_2 \cos (\lambda_1 - \lambda_2)} \quad (3.9)$$

$$\Delta \eta = \frac{\sin \beta_1 \cos \beta_2 - \cos \beta_1 \sin \beta_2 \cos (\lambda_1 - \lambda_2)}{\sin \beta_1 \sin \beta_2 + \cos \beta_1 \cos \beta_2 \cos (\lambda_1 - \lambda_2)} \quad (3.10)$$

6. On the other hand, since the relation between the $x' y'$ coordinate and the ecliptic coordinate is shown in **Figure 3-11**, we can write the relation as follows.

$$x' = \xi \cos \theta + \eta \sin \theta \quad (3.11)$$

$$y' = \eta \cos \theta - \xi \sin \theta \quad (3.12)$$

$$x = -x' \quad (3.13)$$

$$y = y' \quad (3.14).$$

Therefore,

$$\Delta \xi = -\Delta x \cos \theta - \Delta y \sin \theta \quad (3.15)$$

$$\Delta \eta = -\Delta x \sin \theta + \Delta y \cos \theta \quad (3.16).$$

Finally we obtained $\theta = 21.445^\circ$.

Therefore we can calculate the ecliptic components of moving velocity for individual moving objects from **Equation (3.17)** and **(3.18)**, after the measurements of its $(\Delta x, \Delta y)$.

$$\Delta \xi = -\Delta x \cos (21.445^\circ) - \Delta y \sin (21.445^\circ) \quad (3.17)$$

$$\Delta \eta = -\Delta x \sin (21.445^\circ) + \Delta y \cos (21.445^\circ) \quad (3.18)$$

$\Delta \xi$ and $\Delta \eta$ correspond to λ and β in Bowell's equations, respectively. Now we can calculate the a and I of each moving object using Bowell's equations (2.1)-(2.4) from Equations (3.17), (3.18) and its position measured in the xy pixel coordinate.

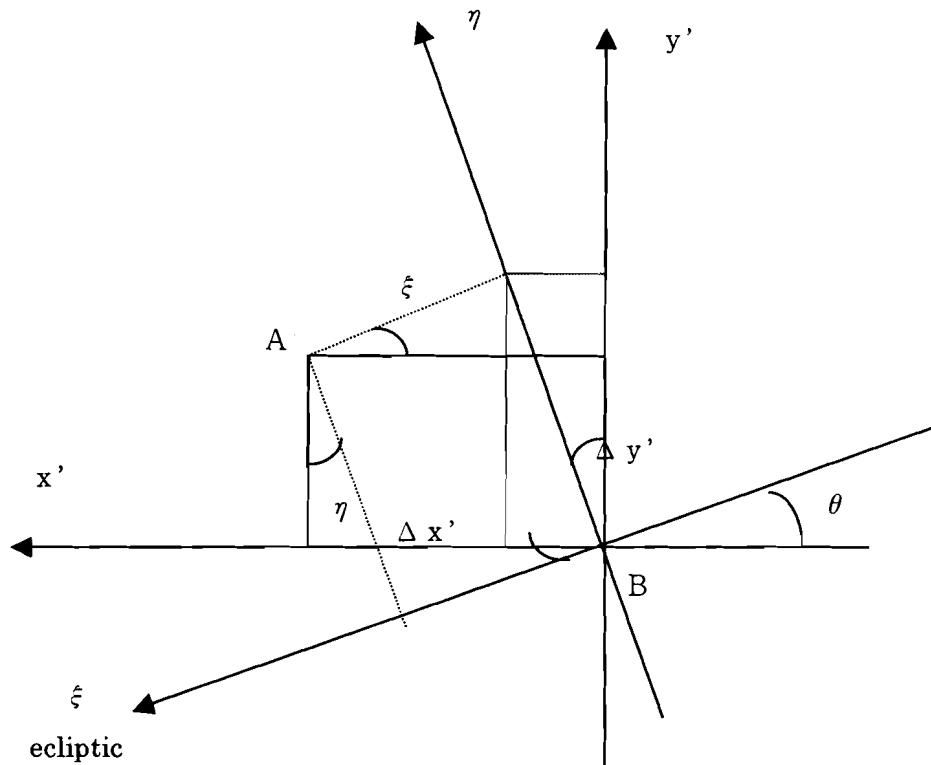


Figure 3-11

The relation between the (x', y') pixel coordinate and the (ξ, η) ecliptic coordinate.

3.2.6 Observational bias corrections

SMBAS was conducted in a very small sky area only near opposition and near the ecliptic. For such observational conditions, we must consider some observational biases. Observational biases of asteroids were already investigated by several researchers (e.g., Bendix et al., 1992, Jedicke, 1996, Jedicke & Metcalfe, 1998, Tancredi, 1998). Generally, two kinds of biases exist : 1) the absolute bias and 2) the relative bias. The absolute bias correction is necessary to estimate the H -distribution of asteroids which are in specific orbital region and are brighter than a limiting magnitude. The relative bias concerns only a relative number of asteroids normalized with the asteroid number in a specified orbital region. Any observational biases must be adjusted correctly to match observational conditions of each survey.

Nakamura & Yoshida (2001) and Yoshida (1999) have already estimated observational biases for a small area near opposition and near the ecliptic (see **Figure 3-12, 3-13**). They calculated the relative biases as functions of a and I that are major bias-affected components for the observational field of view ($5^\circ \times 4^\circ$), centered at opposition and near the ecliptic. **Figure 3-12** shows the relative bias as a function of a . The relative bias is defined here as the number ratio between near-ecliptic asteroids with $r \sim 6$ AU and those with $r = a$ (AU). Three relative bias curves are calculated for circular, near-circular, and elliptic orbits. **Figure 3-13** shows the relative bias as a function of I . The relative bias is defined here to be the number ratio between near-ecliptic asteroids ($I \sim 0$) and those with I . Three relative bias curves are calculated for the inner- (2.3 AU), middle- (2.7 AU), and outer-MBAs (3.1 AU). In this paper, we applied the bias corrections shown in **Figure 3-12** and **3-13** to SMBAS, and corrected the a -distribution and I -distribution for MBAs obtained from SMBAS.

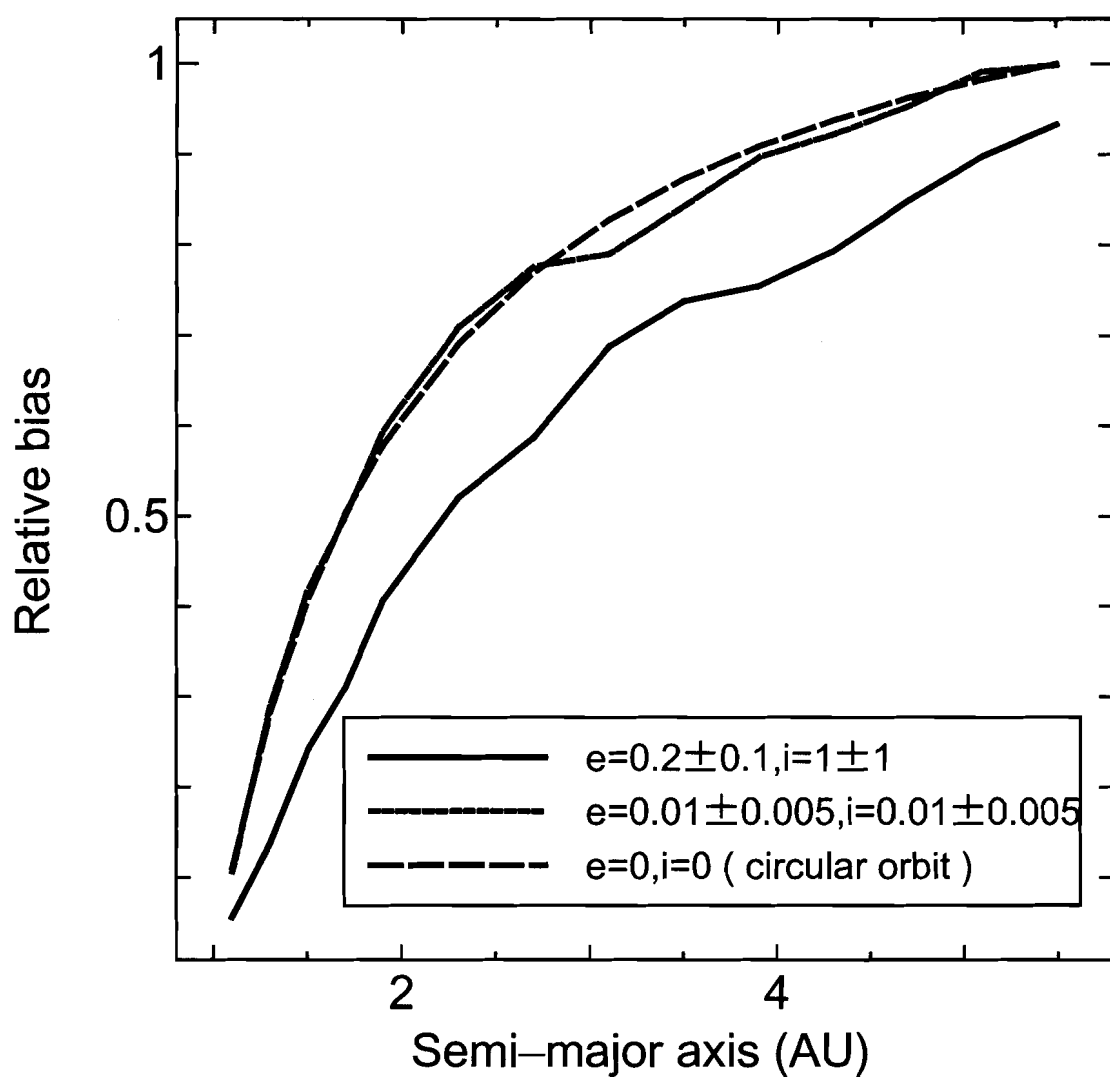


Figure 3-12

The relative bias as a function of a .

The relative bias is the number ratio between near-ecliptic asteroids with $r \sim 6$ AU and those with $r = a$ (AU). The relative bias curves are calculated for circular, near-circular and elliptic orbits.

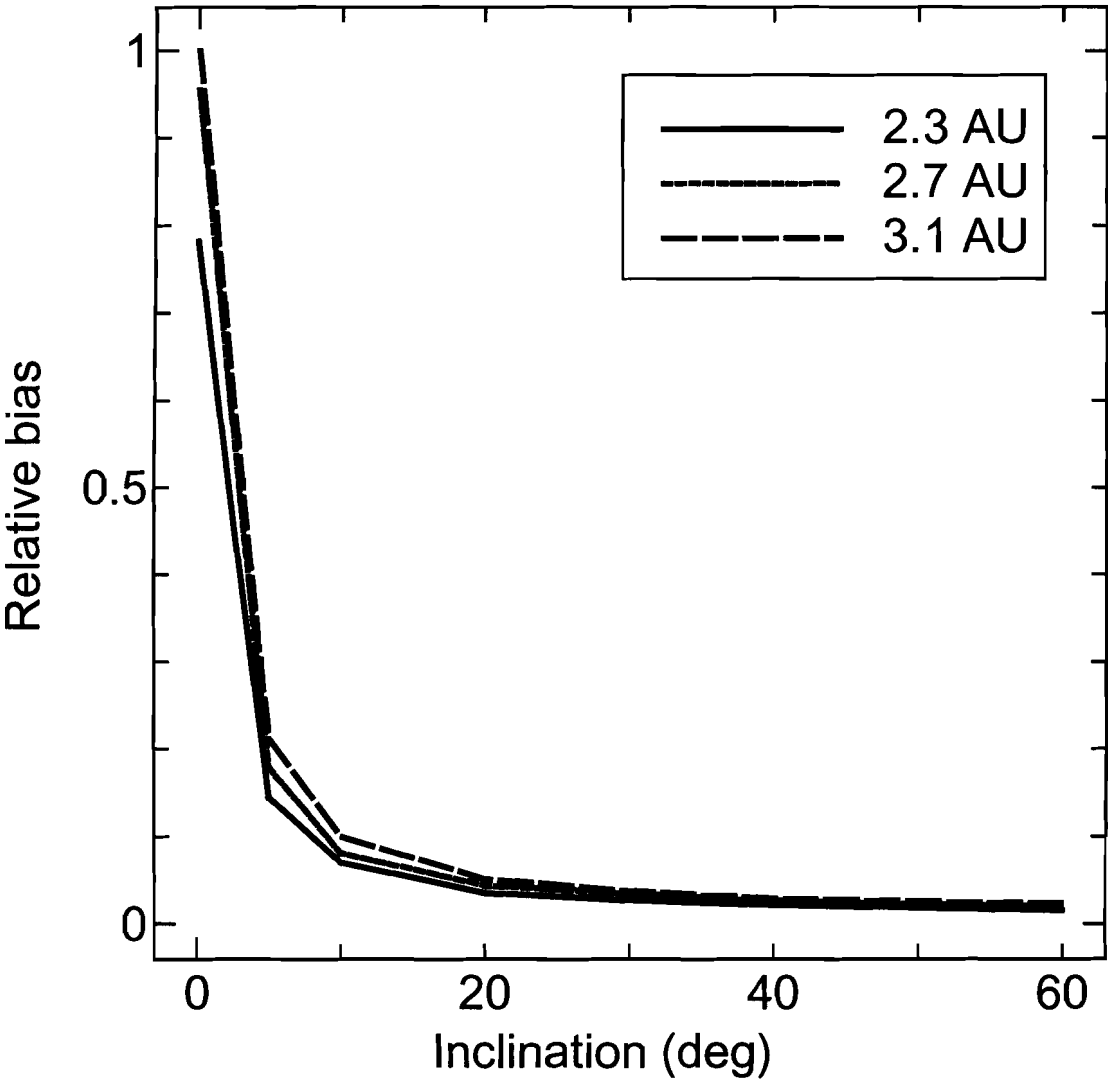


Figure 3-13

The relative bias as a function of I .

The relative bias is the number ratio between near-ecliptic asteroids ($I \sim 0$) and those with I .

Three relative bias curves are calculated for the inner-, middle-, and outer-MBAs.

3.2.7 Results

3.2.7 (a) Overview of results

We detected 1,111 moving objects down to $R = 26.5$ mag in the sky area of 3.26 deg^2 near opposition and the ecliptic. Following the methods in Chapter 2 and 3, we calculated the a and I from the measured position and brightness for each detected object using Bowell's equations. The a s of moving objects estimated from their daily motions ranged from 0.2 to 45 AU. Since we are mainly interested in the structure of the main-belt, we intended to pick up only MBAs. Here, we defined the main-belt zone as $a = 2 - 3.5$ AU according to the past surveys, and we regarded all the moving objects which fell in between 2 and 3.5 AU as MBAs. Then the detected MBAs were 861 asteroids in total. From this, we found that the sky number density of MBAs is 264 per deg^2 down to $R = 26.5$ mag near opposition and near the ecliptic. Moreover, using methods mentioned in Section 2.3.1, we found that the H 's range for MBAs from SMBAS is $13.2 < H \text{ (mag)} < 23.0$, and then also found that the D 's range for them is $0.1 < D \text{ (km)} < 10$. Of course, we applied the systematic corrections shown in Table 2-1 and 2-2 of Section 2.2 to the a and I calculated of each MBA.

Figure 3-14 (a) shows the a -distribution of 861 MBAs detected in the SMBAS. The green, yellow, and gray boxes indicate, respectively, the a -distribution of 861 MBAs from SMBAS, that of MBAs corrected by the relative bias calculated for elliptic orbits, and that of MBAs corrected by the relative bias calculated for circular orbits in Figure 3-12.

Figure 3-14 (b) shows the a -distribution of 85,150 known MBAs (<ftp://ftp.lowell.edu/pub/elgb/astorb.html>). In the a -distribution of the existing MBAs, it is well known that the diminution of asteroids near 2.1, 2.5 and 2.9 AU is reflected by the existence of the Kirkwood gaps. In order to fairly compare the result of known MBAs with that for the MBAs of our SMBAS, we drew Figure 3-14 (b) by *intentionally degrading the resolution* for the a . It is interesting to

note that, for the MBAs discovered with SMBAS, one can see the same trend in the a -distribution (depression near $a = 2.5$ AU) as that of the known MBAs. This might imply that, even for sub-km MBAs, the 3:1 Kirkwood gap still gives strong dynamical effects.

To compare with a -distribution (**Figure 3-14 (d)**) of MBAs with $3 < D$ (km) < 22 obtained from the Spacewatch survey, we rewrote the vertical axis of **Figure 3-14 (a)** by the logarithm scale and then drew **Figure 3-14 (c)**. From **Figure 3-14 (c)** and **3-14 (d)**, one can see that both of the a -distributions resemble each other. This suggests that there is no clear the size dependence in the a -distribution of MBAs for the size ranging from a few hundred m to a few 10 km. However, we can not surely understand the detail structure near the Kirkwood gaps because of a the rough resolution of about 0.1 AU in SMBAS.

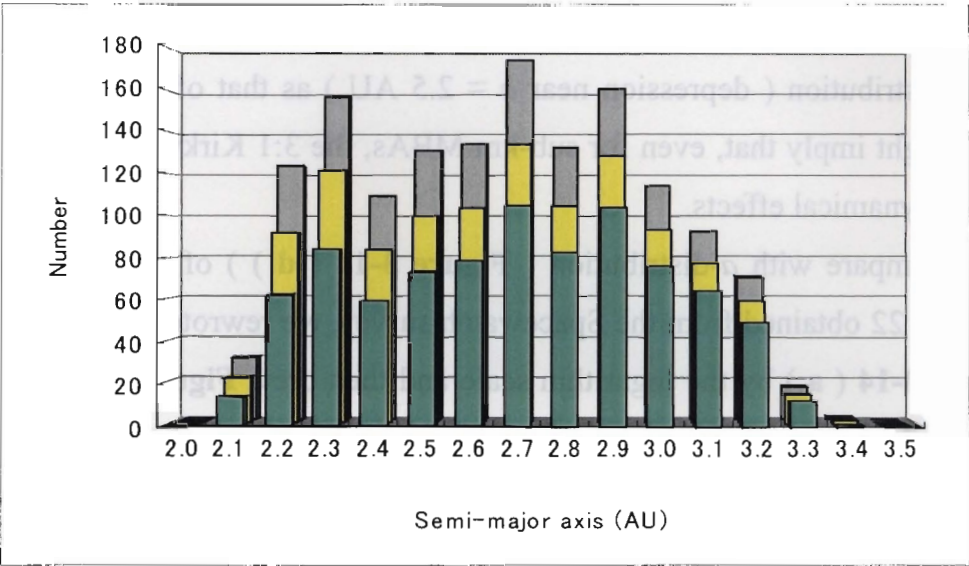


Figure 3-14 (a)

The a -distribution of MBAs ($0.1 < D \text{ (km)} < 10$) detected in our observations.

The green, yellow, and gray boxes respectively indicate the a -distribution of 861 MBAs from SMBAS, that of MBAs corrected by the relative bias calculated for ecliptic orbit, and that of MBAs corrected by the relative bias calculated for circular orbit in **Figure 3-12**.

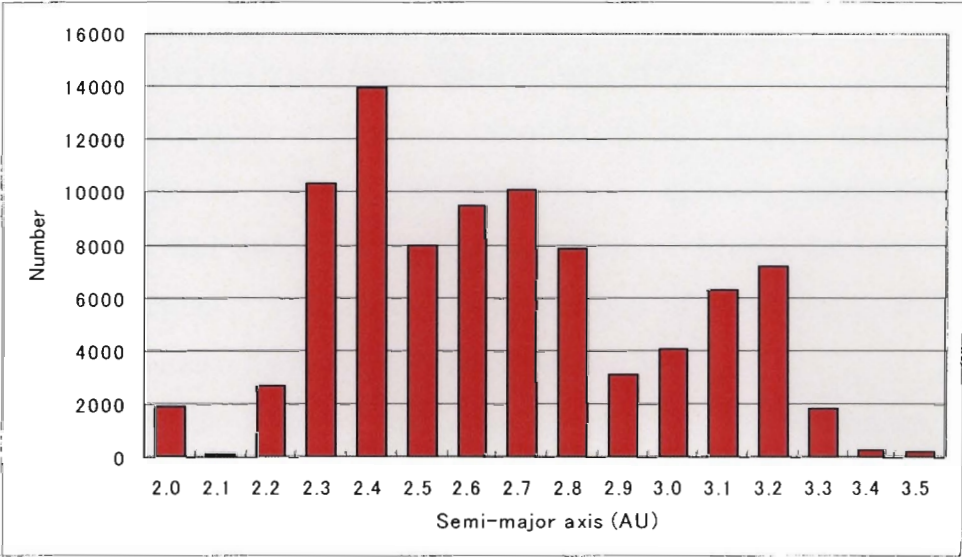


Figure 3-14 (b)

The a -distribution of known MBAs.

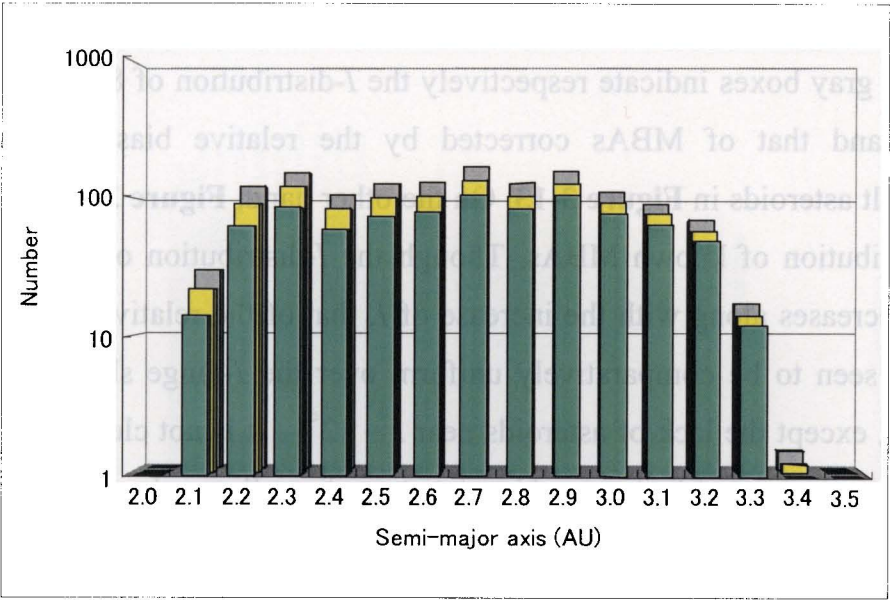


Figure 3-14 (c)
The a -distribution of MBAs detected in our observations (by the logarithm scale).

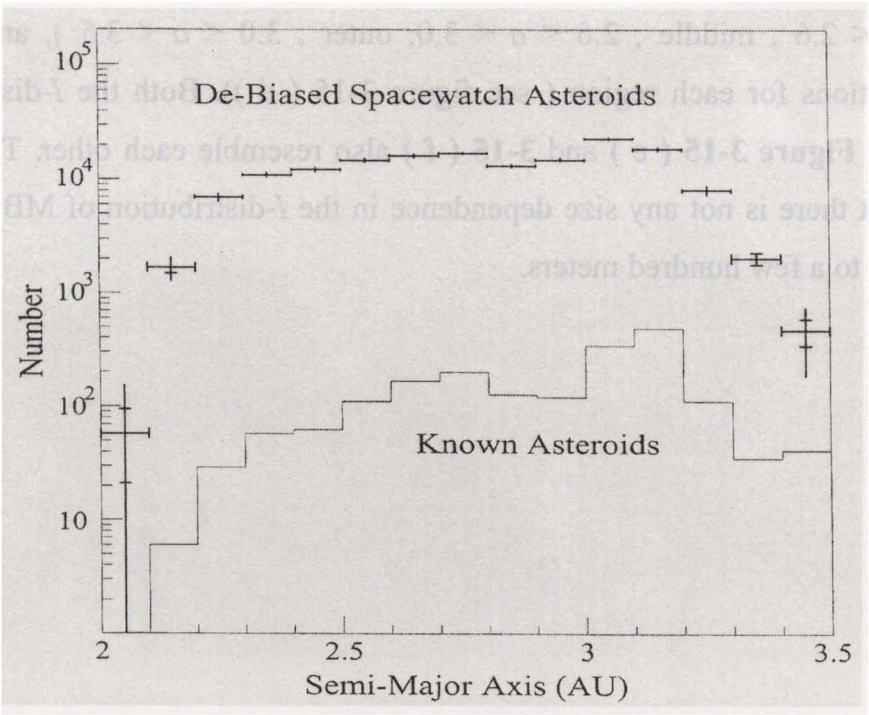


Figure 3-14 (d)
The a -distribution of MBAs ($3 < D \text{ (km)} < 22$) detected in the Spacewatch survey.

Figure 3-15 (a) shows the I -distribution of MBAs detected in SMBAS. The green and gray boxes indicate respectively the I -distribution of 861 MBAs from SMBAS and that of MBAs corrected by the relative bias calculated for middle-belt asteroids in **Figure 3-13**. On the other hand, **Figure 3-15 (b)** shows the I -distribution of known MBAs. Though the I -distribution of known MBAs steeply decreases along with the increase of I , that of the relative-bias-corrected MBAs is seen to be comparatively uniform over the I -range shown in **Figure 3-15 (a)**, except the lack of asteroids near $I \sim 12^\circ$. It is not clear now whether the lack is real or an artifact caused by statistics of small sample number.

To compare with the I -distribution (**Figure 3-15 (d)**) of MBAs with D (km) > 5 obtained from the PLS, we changed **Figure 3-15 (a)** into **Figure 3-15 (c)**. From **Figure 3-15 (c)** and **3-15 (d)**, one can see that both of the I -distributions resemble considerably. Moreover, to compare with the I -distribution (**Figure 3-15 (f)**) for three regions of the main-belt obtained from the Spacewatch survey, we divided the main-belt into three regions (inner ; $2.0 < a < 2.6$, middle ; $2.6 < a < 3.0$, outer ; $3.0 < a < 3.5$), and plotted I -distributions for each region (see figure 3-15 (d)). Both the I -distributions shown in **Figure 3-15 (e)** and **3-15 (f)** also resemble each other. These may mean that there is not any size dependence in the I -distribution of MBAs which are down to a few hundred meters.

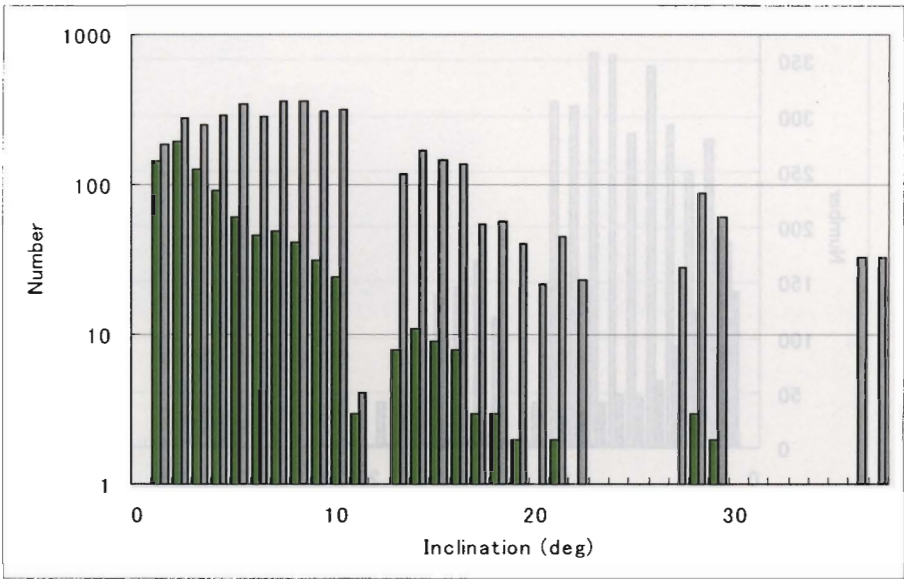


Figure 3-15 (a)

The I -distribution of MBAs detected in SMBAS.

The green and gray boxes indicate the I -distribution of 861 MBAs from SMBAS and one of MBAs corrected by the relative bias calculated for middle-belt asteroids in **Figure 3-13**. Note that there are two detected asteroids near $I = 37$ and 38 deg.

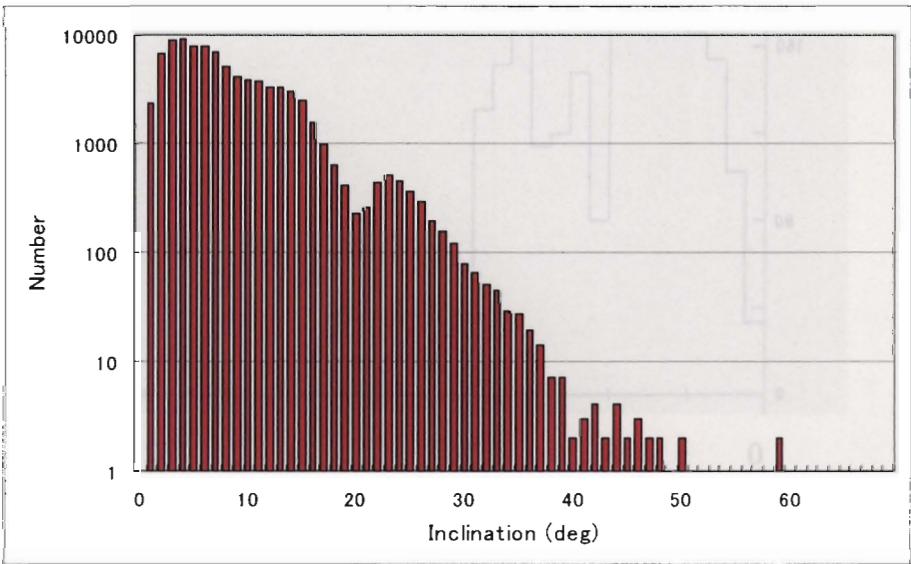


Figure 3-15 (b)

The I distribution of known MBAs.

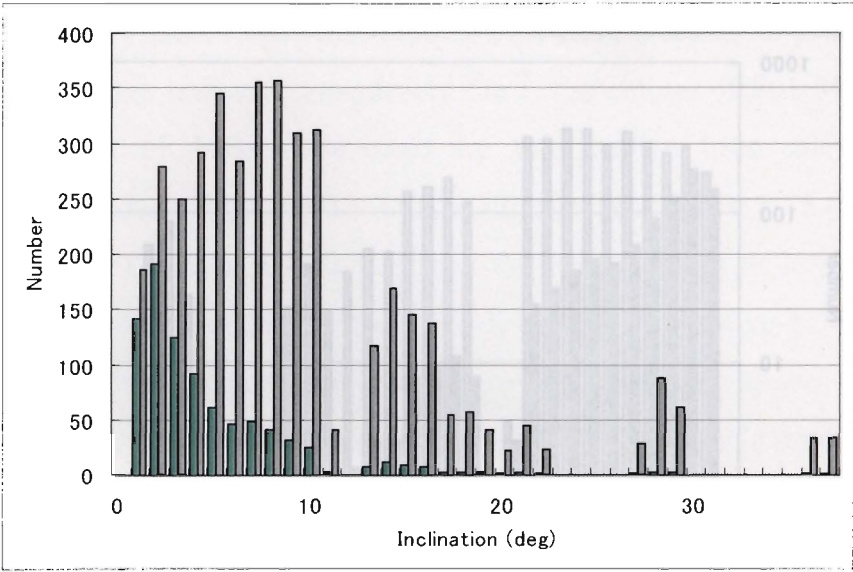


Figure 3-15 (c)
The *I*-distribution of MBAs detected in SMBAS (shown by the linear scale).

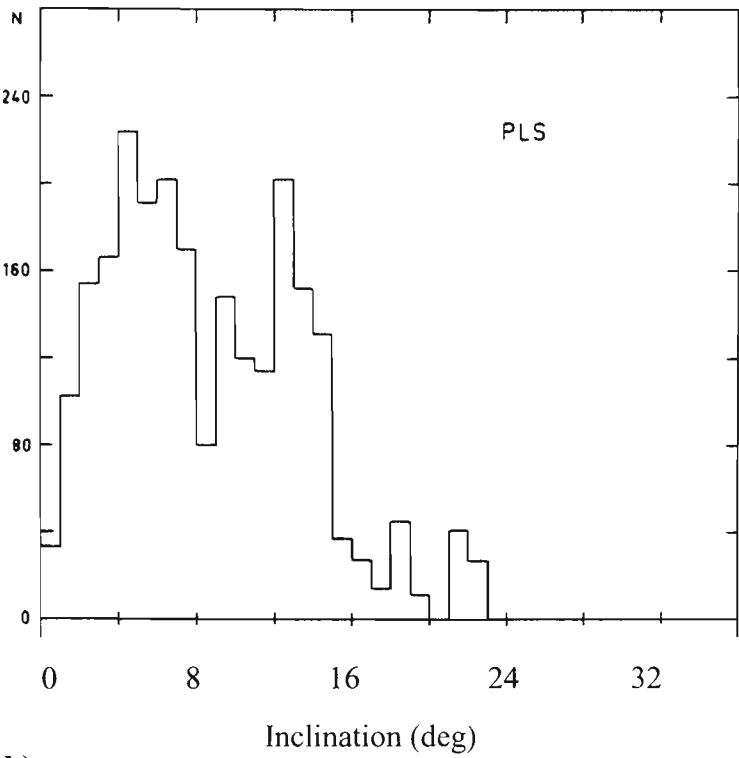


Figure 3-15 (d)
The *I*-distribution of MBAs ($D \text{ (km)} > 5$) detected in PLS.

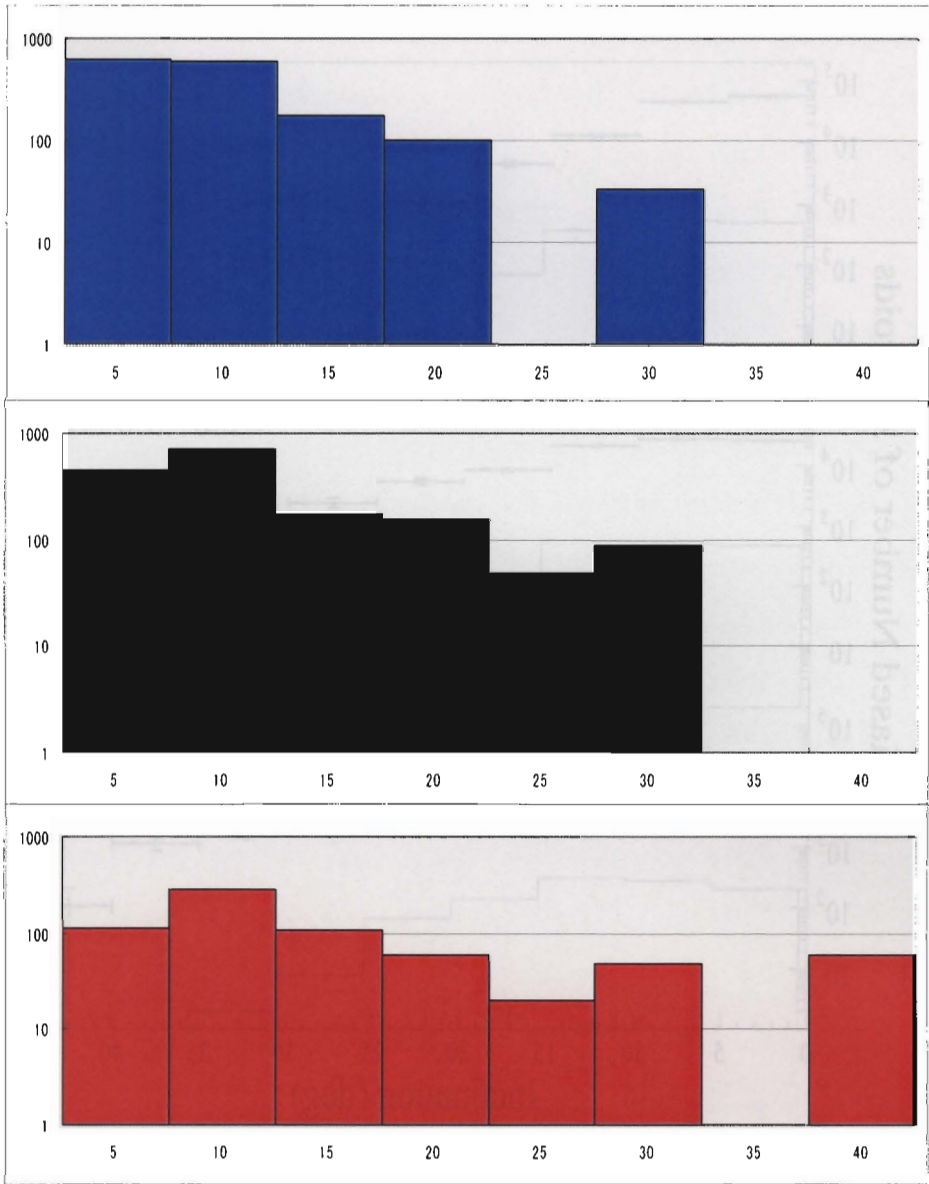


Figure 3-15 (e)

The *I*-distributions for each region for MBAs detected in SMBAS.

Blue : inner-belt ($2.0 < a < 2.6$), black : middle-belt ($2.6 < a < 3.0$), and red : outer-belt ($3.0 < a < 3.5$).

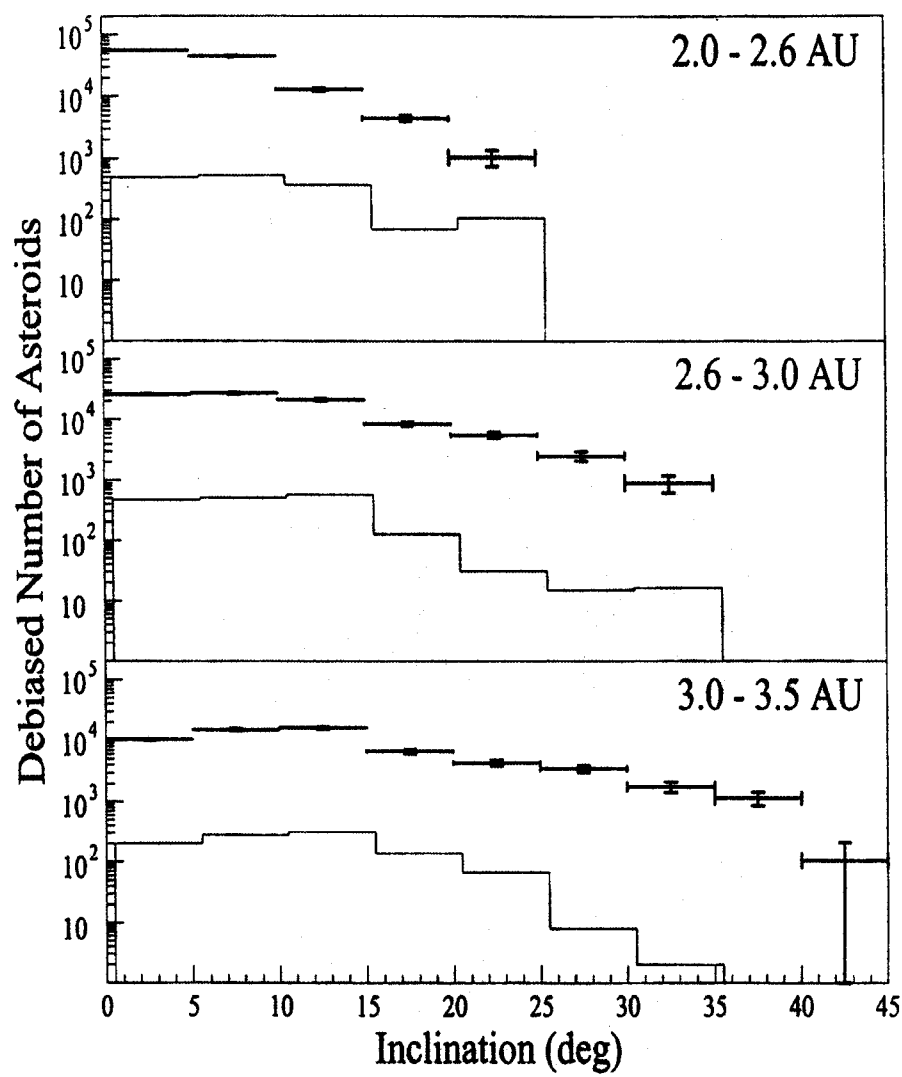


Figure 3-15 (f)
The *I*-distribution for each region for MBAs detected in the Spacewatch survey.

Figure 3-16 shows the H -distribution of MBAs detected in SMBAS and the known MBAs. In a previous Section, we said that H -mag of each asteroid in the SMBAS result can have a mean error of $\sim 0.25\text{mag}$. However, note that the magnitude error in the histogram of **Figure 3-16** is generally much better, because the statistical H -error in a H -bin is improved by the amount of $\Delta H / \sqrt{n}$ (ΔH : the mean light variation error for a single asteroid, n : data number in a H -bin), unless the data number is too small.

From **Figure 3-16**, we see that the peak of the H -distribution for known MBAs is about 15 mag (corresponding to about 4.5 km in diameter), whereas the peak for the MBAs obtained with SMBAS is about 20 mag (corresponding to about 450 m in diameter). Therefore, one can understand that our SMBAS could observe the size region of MBAs roughly by *one order of magnitude smaller* than that of known asteroids. Thus, we expect that our observational data on sub-km faint asteroids will give a new insight into the collisional evolution in the main-belt in various respects. This point is discussed more in Chapter 4.

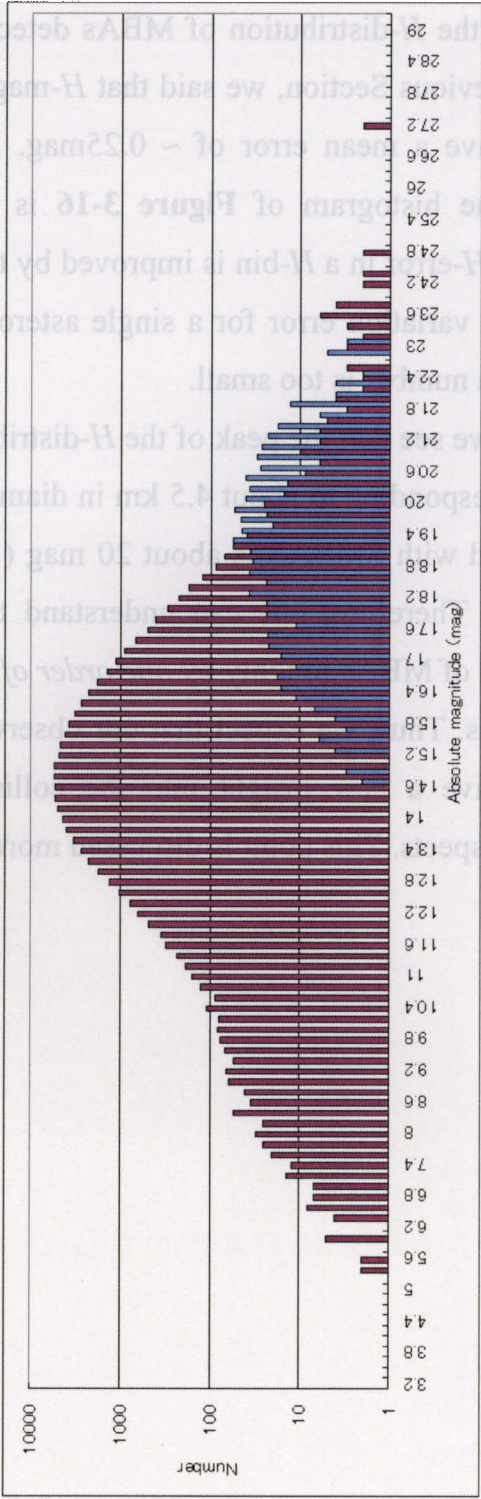


Figure 3-16

The H -distribution of the MBAs detected in our observations and that for the known MBAs (blue column: the MBAs detected in our MBAS; red column: the known MBAs.).

3.2.7 (b) Size distribution in the whole main-belt

When we discuss the CSD of sub-km MBAs, we must be aware of that to what magnitude is the statistics in question reliable. This is because some fraction of asteroids is always lost by chance near the detectable limiting magnitude, whatever measuring approach (automatic/visual) we may take.

In Section 3.2.2, we have mentioned that our black-and-white image overlapping method degrades the sky S/R to some extent. The degree of deterioration was about 2σ for three exposures and 3σ for 11 exposures, where σ represents the standard deviation of the sky-background fluctuation for a single exposure image. Statistics teaches us that a signal level higher than $2 \sim 3\sigma$ can surely be detected. Hence, we can also say that the detection of black-and-white trailed asteroids which we performed in Section 3.2.2 is least affected by accidental detection loss, to the limiting magnitude of overlapped images.

Nevertheless, for a modest estimate, we defined here, as a critical magnitude for completeness, the magnitude below which 90 % of detected MBAs is included (roughly corresponding to the level of two magnitudes brighter than the faintest magnitude, $H \sim 23$ in **Figure 3-17**). From this definition, we found that the critical magnitude is about 20.9 for *all* of the MBAs detected in SMBAS. More exactly, this critical limiting magnitude depends upon the heliocentric distance, and this will be discussed in the next Section.

Figure 3-17 shows the differential (white-box histogram) and cumulative (black dots) H -magnitude distributions for 861 MBAs detected from our SMBAS. The solid line was drawn to compare with the slope ($b \sim 1.75$) of the CSD from PLS and the Spacewatch survey. It seems that the slope of the CSD for asteroids brighter than $H \sim 16$ is a little more steep than 1.75, and that of asteroids for the H -range ~ 18 to 20.9 is much more gentle. As the Spacewatch (Jedicke & Mefcalfe, 1998) and SDSS (Ivezić *et al.*, 2001) ascertained (see Chapter 1), we could also confirm that the slope of the CSD of small MBAs is

shallower than previous estimates and cannot be represented by a single power-law.

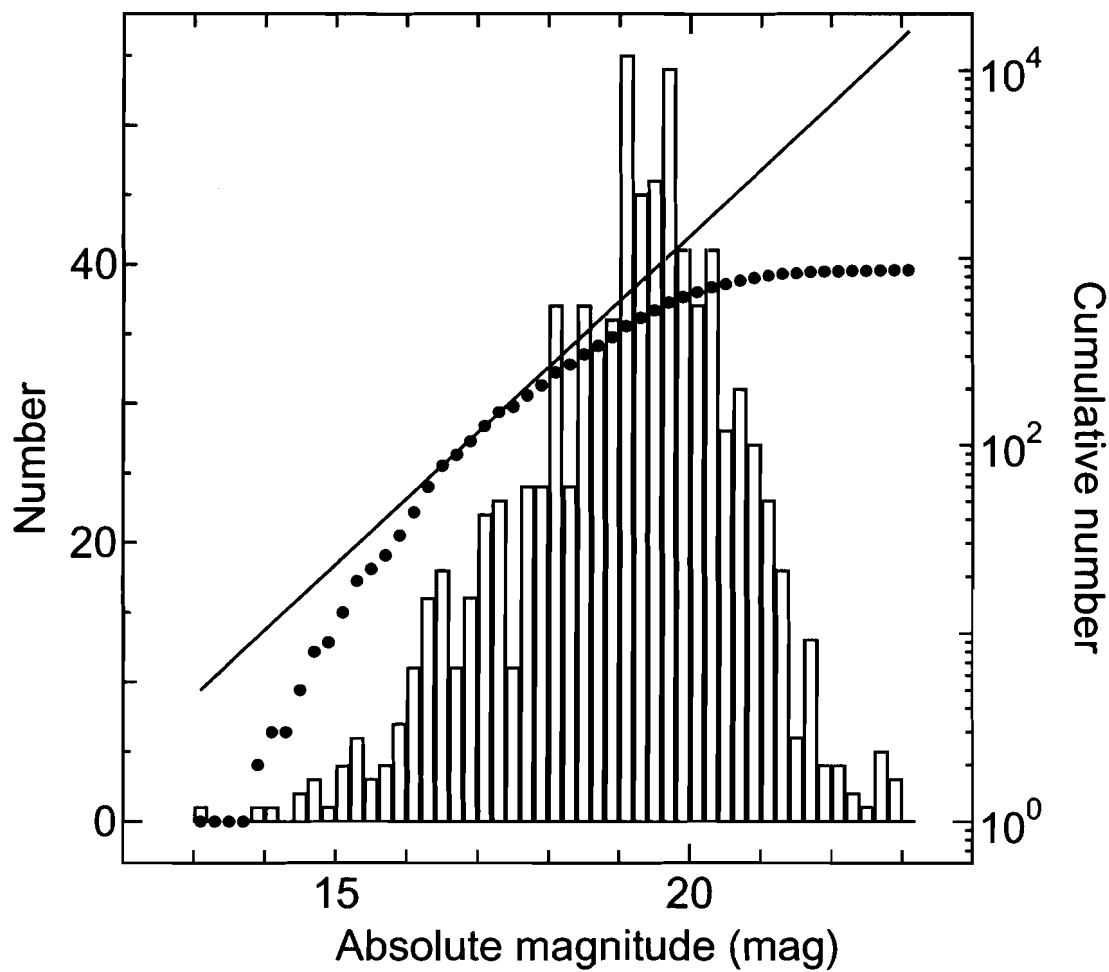


Figure 3-17
The H -distribution of MBAs detected with SMBAS in the whole main-belt.

The white-box histogram is the differential H -distribution and the H -distribution with black dots stands for the CSD. The solid line was drawn to compare with the slope ($b \sim 1.75$) of the CSD from PLS and the Spacewatch survey.

3.2.7 (c) Size distribution in three regions of the main-belt

In this section, we partitioned the main-belt into the inner, middle and outer regions defined by $2.0 < a < 2.6$, $2.6 < a < 3.0$, and $3.0 < a < 3.5$ AU, respectively. This division is conformable to the previous surveys : YMS, PLS and the Spacewatch survey. Since the limit of the detectable magnitude becomes brighter along with the increase of asteroid's heliocentric distance, it is important to take such an effect into account when we examine the CSD of MBAs for each region of the main-belt.

The H -distribution for each region of the main-belt is shown in **Figure 3-18**. One can see that the peak of the H -distribution from the inner region to outer region shifts to the left, i.e., to the brighter H -mag. Here again, just as done in the previous section, we adopted 90% limit of the detected MBAs in each region as a critical magnitude for completeness. The resulting critical magnitudes are found to be about 21.1, 20.7, and 19.7 for the three regions (see **Table 3-6**).

Table 3-6

a -, I -, and H -ranges of SMBAS asteroids for three regions and critical limiting magnitudes.

| | Inner-belt | Middle-belt | Outer-belt |
|---------------|-------------------|-------------------|-------------------|
| | $2.0 < a < 2.6$ | $2.6 < a < 3.0$ | $3.0 < a < 3.5$ |
| | $0.3 < I < 27.1$ | $0.3 < I < 28.8$ | $0.3 < I < 36.3$ |
| | $13.2 < H < 23.0$ | $14.1 < H < 22.8$ | $14.0 < H < 21.4$ |
| Critical mag. | 21.1 | 20.7 | 19.7 |

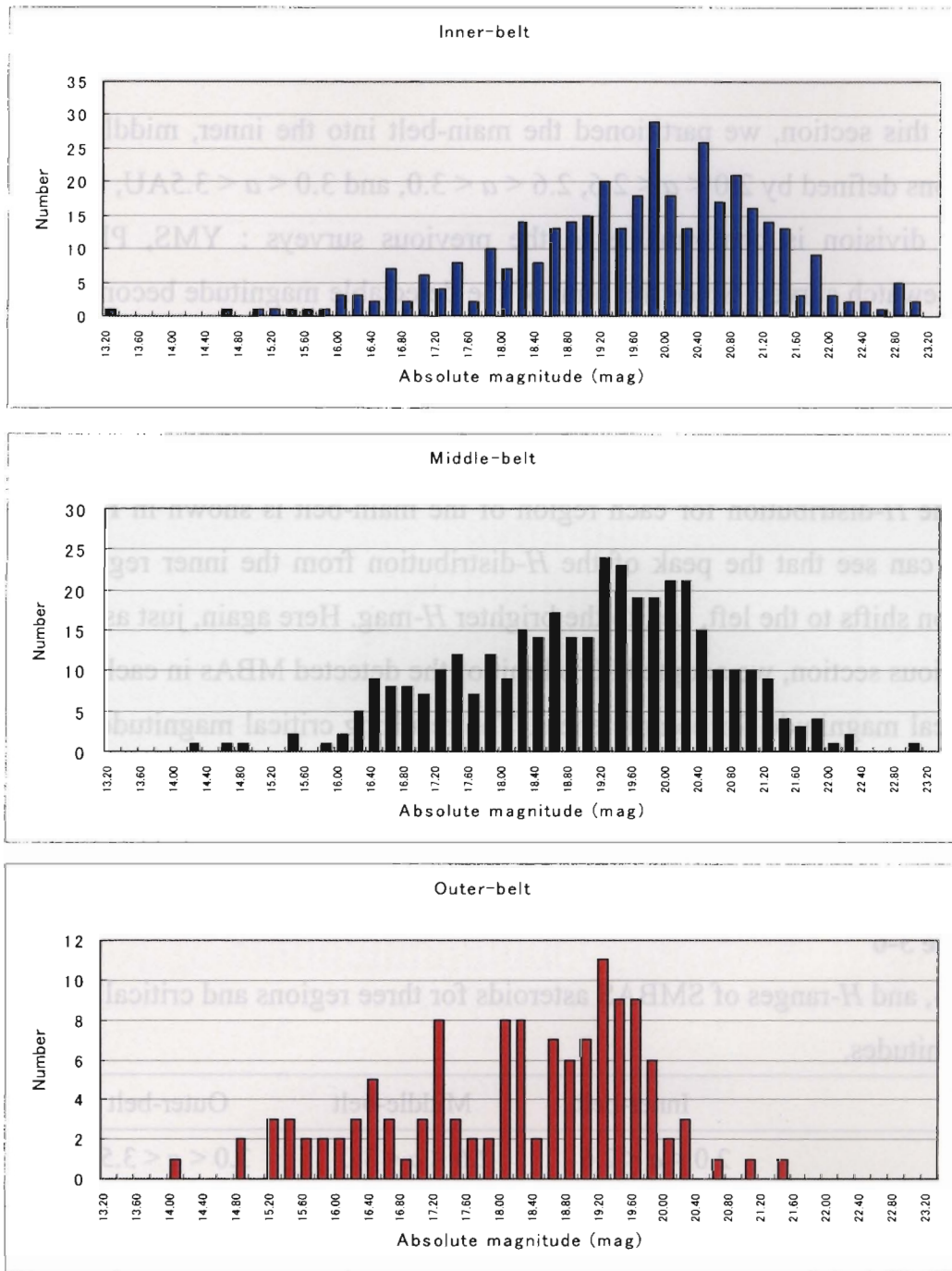


Figure 3-18

H-mag distributions of the three regions in the main-belt.

Blue : inner-belt ($2.0 < a < 2.6$), black : middle-belt ($2.6 < a < 3.0$), red : outer-belt ($3.0 < a < 3.5$).

The size distributions for each region in the belt are shown in **Figure 3-19**. It seems that, for asteroids with $H > \sim 15$, the slope of the CSD for the outer region (red dots) is gentler than that for the inner region (blue dots). However, when seen more in detail, the slope of the CSD changes continuously with the H -range for any of the three regions. So, we calculated the local slope values as a function of H , and then drew them in **Figure 3-20**. In **Figure 3-20**, the blue, black, and red curves in the figure show the changes in the CSD slope of MBAs for the inner, middle and outer main-belt, respectively. For asteroids with $H > \sim 17.5$, it is seen that the slopes of the CSDs becomes gentler in order of the inner-, middle-, and outer-belt. On the other hand, for asteroids with $H < 17.5$, the slope is steepest in the middle-belt, though it is possible that this trend may be an artifact of small sample statistics.

For the main purpose of this paper, we especially focus on the CSD slopes of sub-km MBAs (< 1 km in diameter). Assuming a mean albedo for known C- and S-type MBAs, the brightness of an asteroid with 1km in diameter is found to be $H \sim 18.3$ mag. So one can understand that the H -mag ranges where the slopes of the CSDs should be calculated are 18.3 to 21.1, 18.3 to 20.7, and 18.3 to 19.7 for respective main-belt regions (see **Table 3-6**).

Any observed slopes of the CSDs must be corrected using the results shown in **Figure 2-6**, since the size distributions here were obtained with **Bowell's** equations (see Section 2.3.2). Therefore, we calculated the corrected values of slopes based on **Figure 2-6**. The resulting mean slopes covering the above H -ranges are 1.06 ± 0.11 , 0.87 ± 0.11 , and 0.87 ± 0.12 for the inner-, middle-, and outer- regions, respectively.

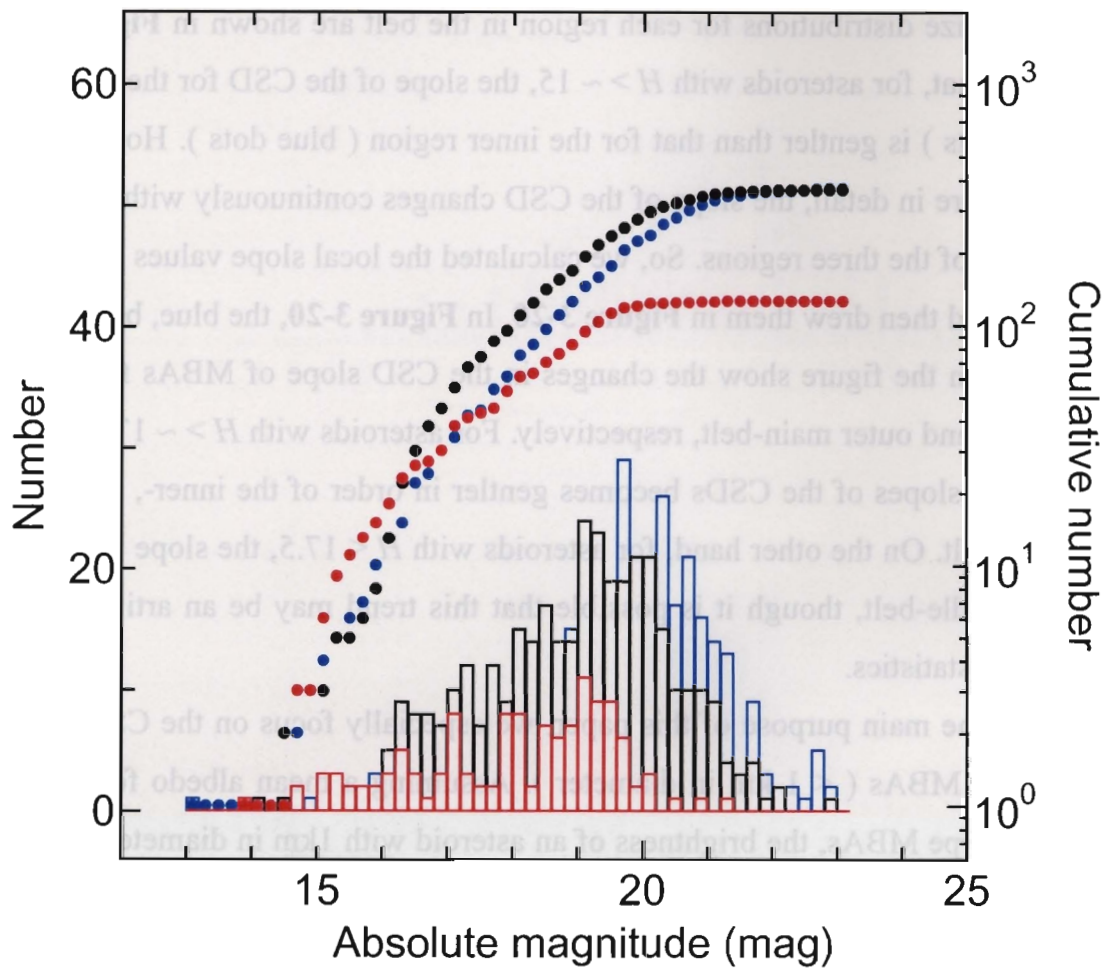


Figure 3-19
The size distribution detected with SMBAS in three regions of the main-belt.
The blue, black, and red-box histograms are the differential H -magnitude distribution of the MBAs of the inner, middle and outer main-belt, respectively. The blue, black, and red-dots show the cumulative H -magnitude distribution in the inner, middle and outer MBAs, respectively.

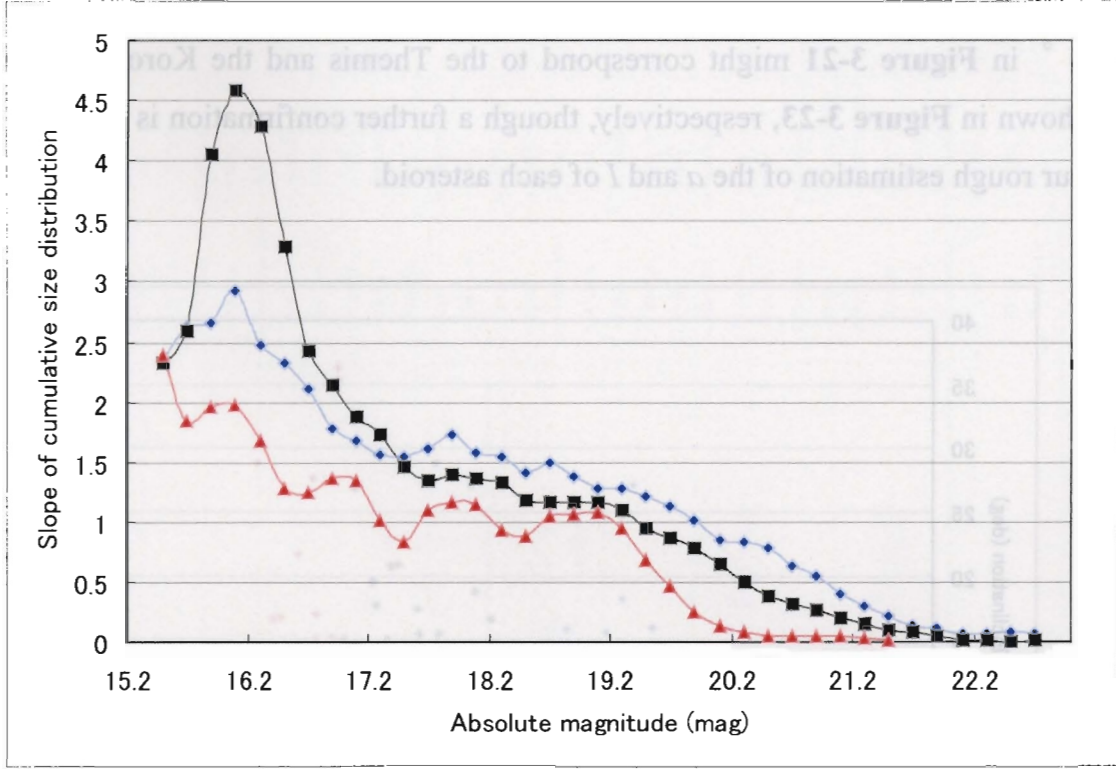


Figure 3-20

Local slopes of the CSDs shown as a function of the absolute magnitude.

The blue, black, and red lines show the change of the CSD slope of MBAs in the inner-, middle- and outer-region, respectively.

3.2.7 (d) Spatial distribution in the whole main-belt

Figure 3-21 shows the spatial distribution of MBAs detected in SMBAS. Note that each data point includes the errors for the a and I mentioned in Section 2.2 (also see **Tables 2-2, 2-3**). Probably due to these errors, one cannot confirm the well-known Kirkwood gaps in **Figure 3-21**. Instead, however, there seem to be several vague gaps near $I \sim 5$ deg in the middle and outer belts, and near $I \sim 12$ deg for all three regions. Furthermore, it seems that asteroids with a larger a show a trend to have a higher I . The situation can be seen more clearly seeing in **Figure 3-22**. Currently, 63 families are known as shown in **Figure 3-23**. The

swarm of asteroids with $a \sim 3.1$ AU and $I \sim 1^\circ$ and that with $a \sim 2.9$ AU and $I \sim 2^\circ$ in **Figure 3-21** might correspond to the Themis and the Koronis families shown in **Figure 3-23**, respectively, though a further confirmation is required for our rough estimation of the a and I of each asteroid.

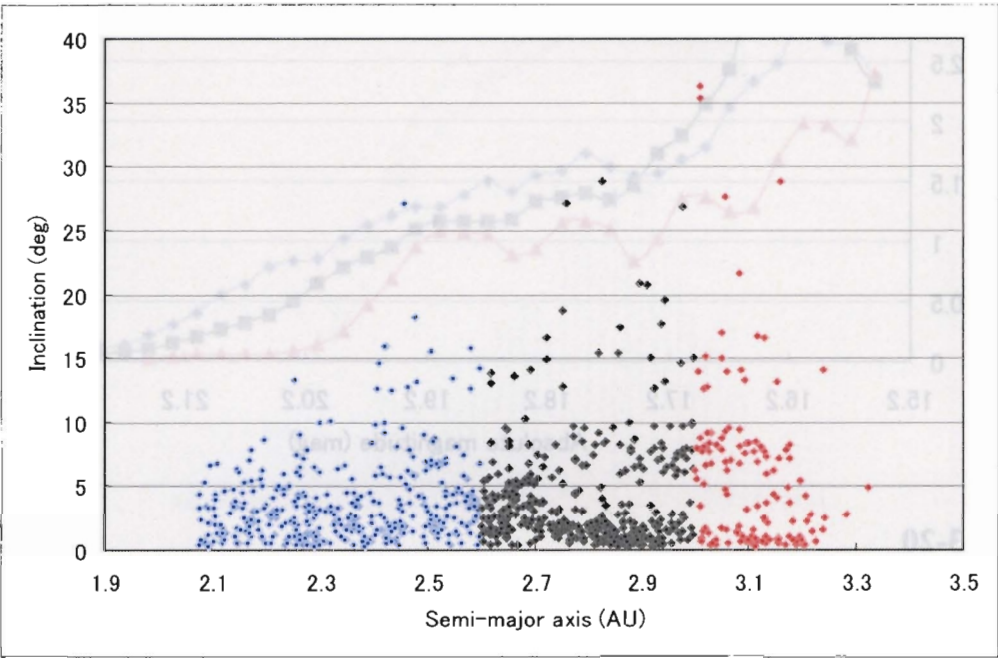


Figure 3-21
The spatial distribution of MBAs detected in the SMBAS.

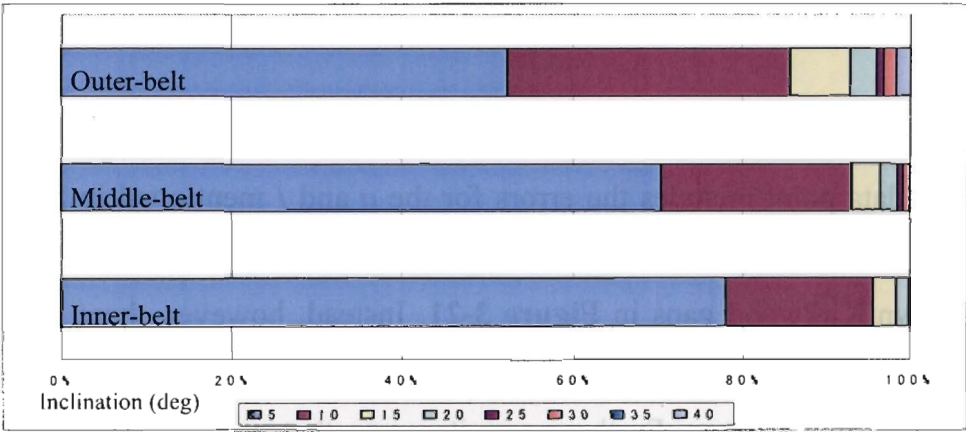


Figure 3-22
The fraction of high inclination asteroids in each belt region.

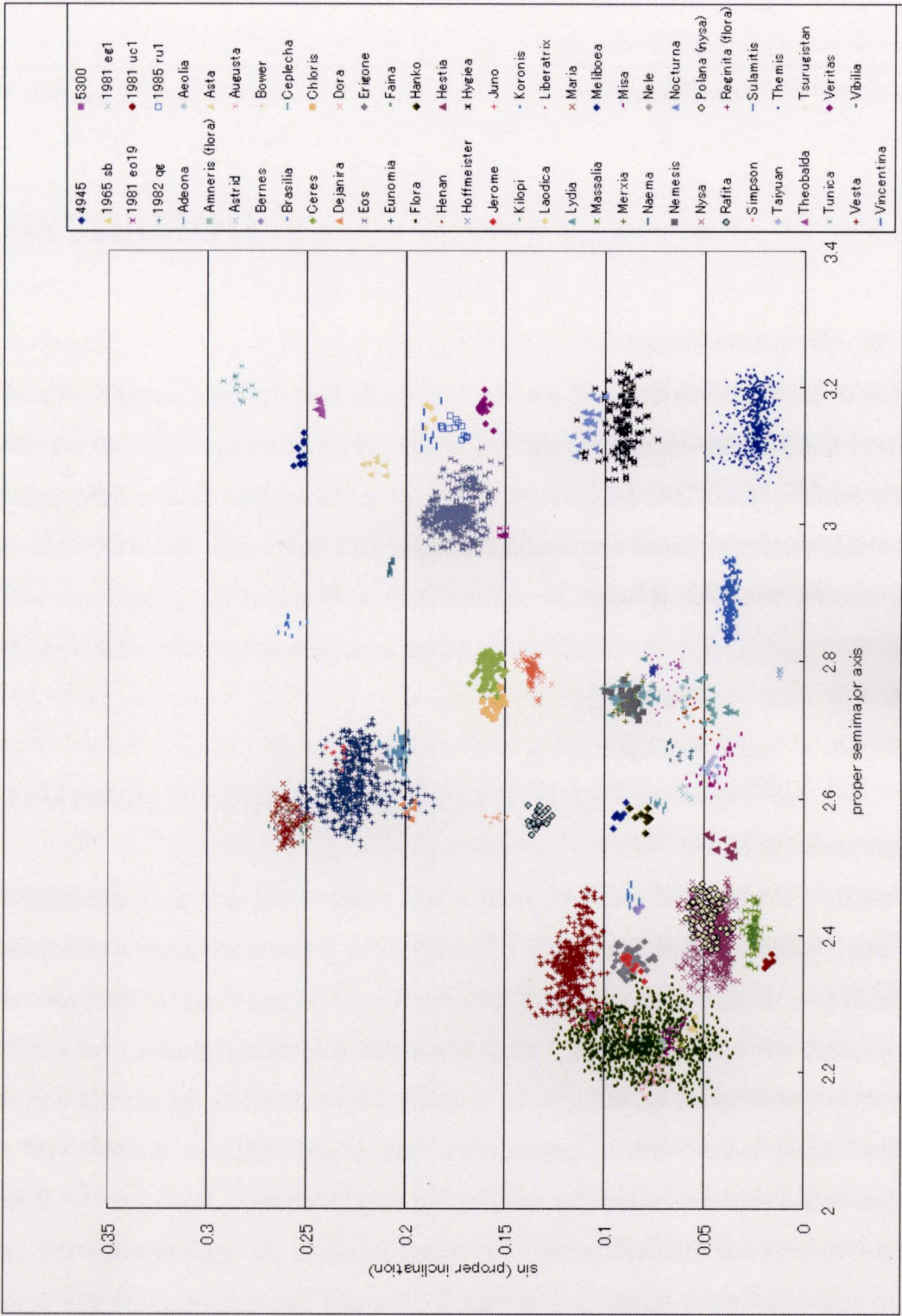


Figure 3-23
Known asteroid's families (<http://pdssbn.astro.umd.edu>).

Chapter 4

Discussion

In this chapter, we discuss the CSD of sub-km MBAs obtained from our observations. We suggest several causes for the difference of the CSD between sub-km MBAs and large MBAs in this section. The difference of the slopes between inner-belt and outer-belt was also discussed from the viewpoint of the taxonomic-type (or material) distribution of MBAs. In addition, we also examined some characteristics seen in the spatial distribution of sub-km MBAs.

4.1 Size distribution of sub-km MBAs

We found that the CSD slope for sub-km MBAs is about 1.0 from our preliminary survey mentioned in Section 3.1 (Yoshida *et al.*, 2001a) and also from our SMBAS in Section 3.2. Obviously, these slopes are shallower than that (1.75) for multi-km asteroids estimated with YMS, PLS, and the Spacewatch surveys. On the other hand, SDSS (Ivezić *et al.*, 2001) found that the slope is 1.3 for asteroids smaller than 5 km in diameter. In their paper published just recently, Ivezić *et al.* concluded that the number of smaller asteroids extrapolated from previous studies which could detect only asteroids with the size of 5 km or larger was an overestimate. Namely, it seems that small asteroids were not as plentiful as had been expected from observations of larger ones.

Our analysis of SMBAS shows that our result is consistent with that of SDSS,

and our CSD slopes are shallower than that obtained in SDSS. This implies that the number of sub-km MBAs detectable sub-km MBAs only in SMBAS is much more depleted compared with the prediction by Ivezić *et al.* (2001).

Given that our obtained slopes are true, let us consider physical implications of our finding. As possible causes of the depletion of small asteroids in the main-belt, researchers have so far proposed some physical processes as follows:

- (1) *Small asteroids may become a part of large asteroids that have the structure of strengthless “rubble-piles”.*

Possible existence of rubble-pile asteroids which consist of re-accumulated impact fragments was theoretically predicted for the first time by Weidenschilling (1981). In fact, the asteroid (253) Mathilde observed by the NEAR spacecraft (Veverka *et al.*, 1999), and (216) Kleopatra observed by radar (Ostro *et al.*, 2000) have been regarded as having the rubble pile structure, because of their observed low bulk density.

Recent collisional theories and experiments suggest that the impact energy needed to disperse an asteroid is greater than that to thoroughly shatter it, for asteroids larger than a few km to sub-km in size. This means that it is difficult to disperse collisional fragments for asteroids of such sizes. If this is the case, it is likely that a large number of known MABs observed so far should have the rubble pile structure.

- (2) *Small asteroids would have been thrown into the Kirkwood gaps by the Yarkovsky effect and then they would have been removed from the main-belt (e.g. Farinella & Vokrouhlicky, 1999).*

According to calculations by Farinella & Vokrouhlicky (1999), the semi-major axes of the asteroids with 1 – 10 km in mean radius can be moved by a few hundredths AU by the Yarkovsky effect during their collisional lifetime

(10—1000 million years). Especially, the semi-major axes of small asteroids with 10—100 m in mean radius will change more effectively. Since this size region spans a part of the size region observed with our SMBAS, the Yarkovsky effect can be another candidate for depletion of small MBAs.

(3) *Small asteroids would have been thrown out of the main-belt with high speeds acquired in a collision beyond the escape velocity.*

Seemingly, this is the simplest process to remove asteroids from the asteroid belt. However, since many collisional theories and the experiments so far have indicated that it is difficult that the release velocity of fragments in a collision far exceeds the escape velocity of the parent body, it is unlikely that impacted asteroids can be ejected from the asteroid belt only with the velocity acquired in a collision. In fact, it is generally believed that NEAs have been removed from the main-belt, *not* by the direct impacts, *but* by the subsequent strong chaotic perturbations in the Kirkwood gaps in which they were thrown in after impacts.

Presently we cannot say from only our SMBAS which process among the above three candidates is more plausible. For this purpose, more observations of NEAs are necessary. If small asteroids have been removed selectively from the parent population, their number would decrease in the parent population and the CSD of the removed population should reproduce the original CSD of the parent population. In other words, the CSD of NEAs is expected to be the same as the CSD of large MBAs. Actually, the CSD of NEAs (~ 1.6) in the range of $D = 500 \text{ m} \sim 5 \text{ km}$ seems to resemble to that of large MBAs (1.75), rather than that of sub-km MBAs (~ 1.0) (see Section 1.3). However, we must remember that since all of NEAs have not yet been discovered, the CSD of NEAs may change after more discoveries of NEAs.

Here we summarize all of the size distributions of MBAs known so far, including our investigation:

- 1) The classical CSD slope is 2.5 for a self-similar collision cascade system in equilibrium (Dohnanyi, 1969). From available observational data, on the other hand, the CSD slopes of Hirayama families which have been believed to be collisional products are $3.6 \sim 4.2$ (Klacka, 1992).
- 2) The observed CSD slope for large asteroids with $30 \text{ km} < D < 300 \text{ km}$ is ~ 2.4 (YMS : Kuiper *et al.*, 1958).
- 3) The CSD slope for asteroids with $D > 5 \text{ km}$ is 1.75 (PLS : Van Houten *et al.*, 1970, the Spacewatch : Jedicke & Metcalfe, 1998).
- 4) The CSD slope for asteroids with $1 \text{ km} < D < 5 \text{ km}$ is ~ 1.3 (SDSS : Ivezić *et al.*, 2001).
- 5) The CSD slope for asteroids with $\sim 500 \text{ m} < D < 1 \text{ km}$ is ~ 1.0 (this work, and Yoshida *et al.*, 2001).
- 6) The CSD slope for NEAs with $\sim 500 \text{ m} < D < 5 \text{ km}$ is ~ 1.6 ,
(<http://cfa-www.harvard.edu/iau/lists/Unusual.html>).

From the CSDs in several size regions as listed above, it seems that smaller asteroids are more depleted in the main-belt region. As mentioned before, from only the observations on the size distribution of MBAs, however, one cannot surely judge which is the main cause of this depletion among the above-mentioned physical processes. Possibly, all processes had occurred or are still occurring, and as a result the present distribution of the MBAs was created. The predominate process will better be determined based on the location and size of parent bodies in the main-belt, the material property (for example, strength, thermal conductivity, etc) and the relative velocity and frequency of collisions. In any case, we would say that our investigation of the CSD for

sub-km MBAs (namely NEA-sized asteroids) plays a very important role in estimating the supply rate of NEAs and the formation rate of rubble piles asteroids.

Next, we discuss the CSDs of sub-km MBAs investigated for three regions of the main-belt. As we have already seen in Section 3.2.7 (c), it is not clear whether the difference of the slopes between the middle- and the outer-belts is real or not (see also **Table 4-1**). However, it is fairly certain that there is a difference of the slopes between the inner-belt and other regions ; the slope of the inner-belt is steep (~ 1.1), while that of the outer-belt is shallow (~ 0.9). Even the slope in the inner-belt of the SMBAS data is much shallower than that of larger MBAs. However, we must remember here that transformation from the brightness (H -mag) of asteroids to the size considerably depends on their albedo. For well-observed MBAs, we know that S-type asteroids with a high albedo are abundant in the inner main-belt and C-type asteroids with a low albedo are dominant in the outer region of the main-belt. **Figure 4-1 (a)** and **(b)** show the distributions of the S-type and C-type asteroids in the whole main-belt (<http://pdssbn.astro.umd.edu>). One can see from these figures that the number ratio of the S-type and C-type asteroids varies with the heliocentric distance. Note that the size of a C-type asteroid is about twice larger than that of a S-type asteroid for the same absolute magnitude, because of the difference in albedo. Xu *et al.* (1995) showed, in the Small Main-belt Asteroid Spectroscopic Survey (SMASS), that the majority of the small main-belt asteroids ($D < 20$ km) are C- and S-type asteroids, and their distributions are similar to the one of large asteroids. Thus, assuming that the trend shown in **Figure 4-1 (a)** and **(b)** can also be applied to the sub-km MBAs detected in SMBAS, we attempted here again to re-estimate the CSD slopes for the three main-belt regions by taking the albedo effects into account. Namely, we assumed that the inner-belt consists of asteroids with the albedo of S-type asteroids, the middle-belt with a mean albedo between S-type asteroids and C-type asteroids, and the outer-belt with the albedo of C-type asteroids.

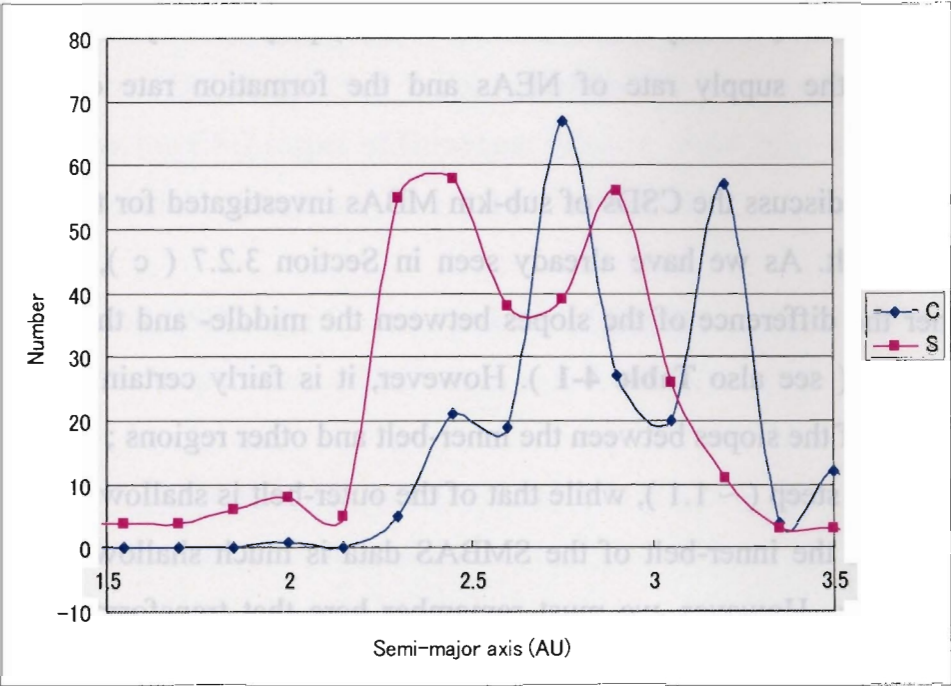


Figure 4-1 (a) The abundance of the known S-type and C-type asteroids in the main-belt.

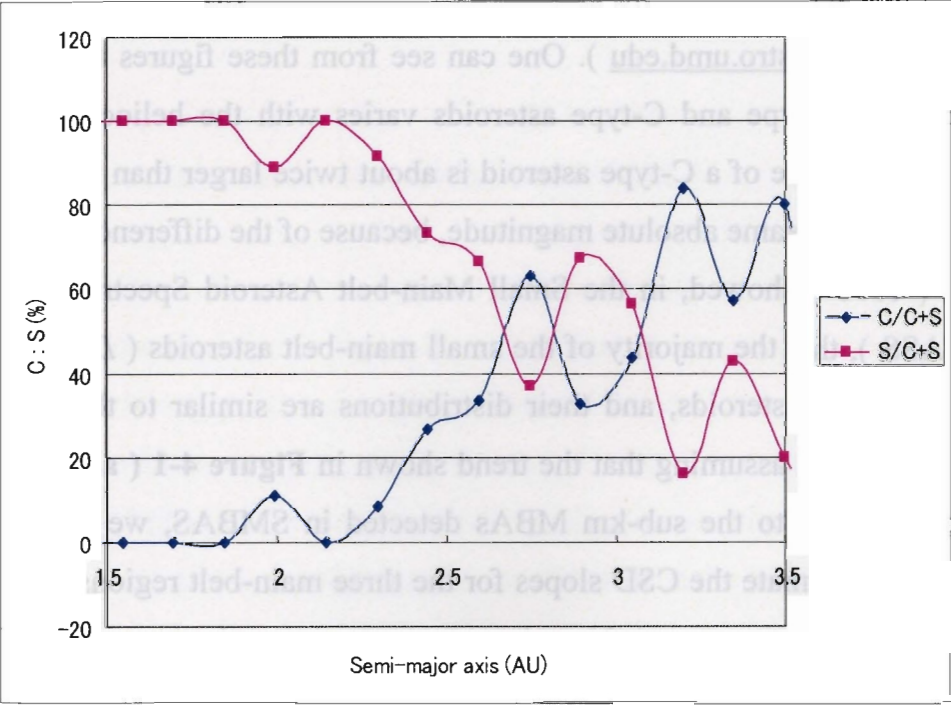


Figure 4-1 (b) The number ratio of the known S-type and C-type asteroids in the main-belt.

Table 4-1 The H ranges and the mean slopes of the CSD in each region of the main-belt.

| | Inner-belt | Middle-belt | Outer-belt |
|--------------|-------------------|-------------------|-------------------|
| | $2.0 < a < 2.6$ | $2.6 < a < 3.0$ | $3.0 < a < 3.5$ |
| | $18.3 < H < 21.1$ | $18.3 < H < 20.7$ | $18.3 < H < 19.7$ |
| mean slope 1 | 1.06 ± 0.11 | 0.87 ± 0.11 | 0.87 ± 0.12 |
| | $17.5 < H < 21.1$ | $18.3 < H < 20.7$ | $19.0 < H < 19.7$ |
| mean slope 2 | 1.19 ± 0.11 | 0.87 ± 0.11 | 0.83 ± 0.14 |

Note : mean slope 1 ; the mean slope of the CSD for asteroids of the H -range (< 1 km in diameter) estimated based on the assumption that any asteroids have the mean albedo of well-known MBAs, mean slope 2 ; the mean slope of the CSD for asteroids of the H -range (< 1 km in diameter) estimated in considering the ratio of the S-type and C-type asteroids in the main-belt.

So we found that the resulting H -mag ranges for asteroids smaller than 1km in diameter (see Section 3.2.7) are respectively 17.5 to 21.1, 18.3 to 20.7, and 19.0 to 19.7 for the inner-, the middle-, and the outer-belt regions. For each H range of each region of the main-belt, we obtained again the slope of the CSD, and then we calculated the correction values of slopes based on **Figure 2-6**. The resulting slopes (we call them mean slope 2) were 1.19 ± 0.11 , 0.87 ± 0.11 , and 0.83 ± 0.14 in each region, respectively. These results were listed in **Table 4-1**. That is, the “ mean slope 1 ” and the “mean slope 2” represent the slopes obtained in Section 3.2.7 (c) and the new slopes, respectively. From comparison of the two mean slopes in **Table 4-1**, unless the S / C number ratio for sub-km MBAs is unacceptably different from that for larger MBAs, it seems that the slope of CSD for sub-km MBAs in any part of the main-belt is certainly shallower than that for large known MBAs.

Kresak (1977) mentioned that the results of PLS contradicted the difference

between the CSD of asteroids in the inner region of the belt and that in the outer part of the belt, which had been found from previous observations. However, we again propose this difference in the size region of sub-km MBAs. Namely, as for the slope of the CSD of sub-km MBAs, it is comparatively steep ($b = 1.2$) in the inner main-belt, and shallow ($b = 0.8$) in the outer main-belt. From this, we may infer that some mechanism to remove a large number of small asteroids had existed or rubble piles asteroids have been produced in the outer belt rather than in the inner belt.

However, according to the latest taxonomic distribution of asteroids with $D > 1\text{km}$ obtained from SDSS (Ivezić, 2001), there are an overwhelming majority of S-type asteroids in the inner belt and the abundance ratio of C- and S-type asteroids reverses near 3.2 AU. It is also possible that we may be able to consider that the difference of the CSD between the inner-belt asteroids and the outer-belt asteroids is a result of the difference in the distributions between S- and C-type asteroids. For larger asteroids, Anders (1965) had suggested that the frequency of collisions is different between the inner-belt and the outer-belt: in the inner belt, impact frequency is only a few times throughout its history, while highly fragmented in the outer-belt due to the greater proximity to Jupiter. However, for sub-km asteroids, it seems that the degree of the fragmentation is more important rather than the frequency of collisions. We know that C-type asteroids and S-type asteroids are like carbonaceous chondrites and silicate rocks, respectively. Since it is likely that a C-type asteroid is more fragile than a S-type asteroid from a viewpoint of material strength, we can infer that the difference of the slopes of the CSD in the individual regions of the main-belt originates in the material strength of the asteroid. Furthermore, by recent space probe investigations, we know that the densities of (243) Ida (S-type asteroid) and (253) Mathilda (C-type asteroid) are $\sim 2.6 \text{ g/cm}^3$ and $\sim 1.3 \text{ g/cm}^3$, respectively. It is likely that the different outcomes would occur in collisions of bodies which have the different material and density.

Figure 4-2 shows the CSDs of the well-known three families. As far as we

know in the previous observation data, most members of the Themis family are C-type asteroids. In the Koronis family, all members are S-type asteroids. The Eos family consists of C-type and S-type asteroids. From **Figure 4-2**, it seems that the slope of the CSD of S-type member's family and that of C-type member's family are different.

On the other hand, Nolan *et al.* (2001) found by their numerical simulations that since a shock wave fractures an asteroid in advance of crater excavation flow, impact results are controlled by gravity ; the tensile strength is unimportant whether asteroids are initially intact or rubble-piles. This means that the dispersion of fragments after a collision is independent from the tensile strength of parent bodies.

In short, whether or not a correlation exists between the size distribution of the collisional fragments and the tensile strength of the parent bodies is not yet known. Therefore, in order to pursue the cause of the difference of slopes of the CSDs in three regions of the main-belt that we found, it is necessary to investigate separately the size distributions of C-type and S-type asteroids.

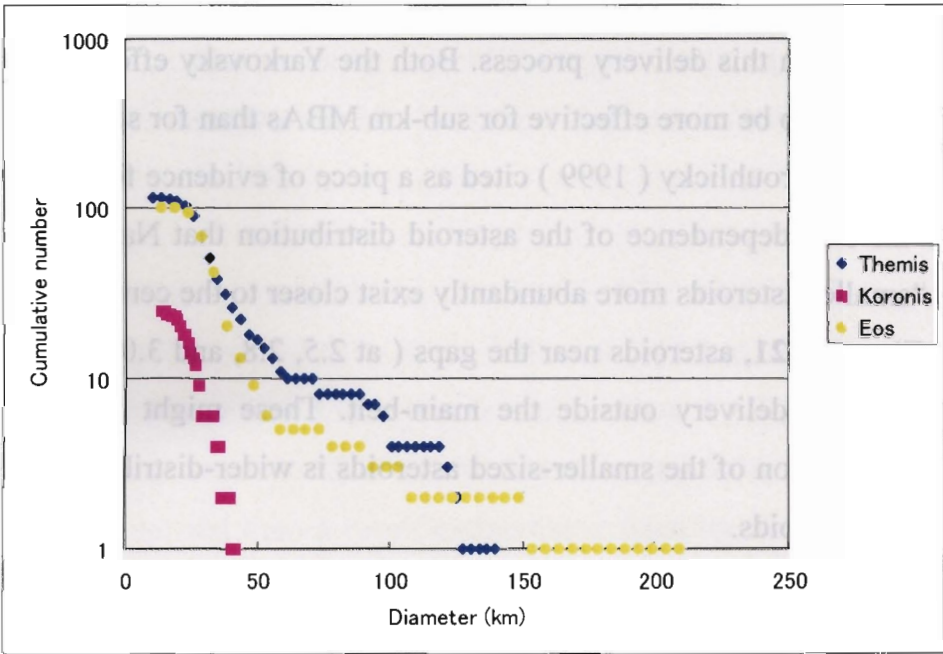


Figure 4-2 The cumulative size distributions of the well-known families.

4.2 Spatial distribution of sub-km MBAs

Finally, we shortly discuss the spatial distribution of sub-km MBAs. The spatial distribution obtained from SMBAS contains the error ~ 0.1 AU in the a and the error of 2° (for high inclination $\sim 6^\circ$) in the I for each asteroid. Since the error of the semi-major axis is larger than the width of the Kirkwood gaps, it is natural that one cannot see gaps in **Figure 3-21**. Instead of it, one can see in **Figure 3-21** a small number of asteroids with high inclination in the neighborhood of the distinct Kirkwood gaps at 2.5, 2.8, and 3.0 AU.

Generally, once an asteroid gets trapped into a gap, it will undergo a chaotic orbital transition, its eccentricity grows unexpectedly to a very high value, and finally it is delivered from the main-belt to the near-Earth region or the other regions in the solar system. In some cases where a mean-motion resonance is coupled with a secular resonance or the Kozai resonance, it is shown that the inclination also pumps up to a high level (Morbidelli and Moons 1995). So it is possible that the high-inclination asteroids near the Kirkwood gaps in **Figure 3-21** might be correspond to such chaotic asteroids.

It is also said that the Yarkovsky effect or mutual collisions will play an important part in this delivery process. Both the Yarkovsky effect and collisions are considered to be more effective for sub-km MBAs than for several-km MBAs. Farinella & Vokrouhlicky (1999) cited as a piece of evidence for the Yarkovsky effects the size dependence of the asteroid distribution that Nakamura (1994) found “smaller asteroids more abundantly exist closer to the centers of the gaps”. In the **Figure 3-21**, asteroids near the gaps (at 2.5, 2.8, and 3.0 AU) may be in the process of delivery outside the main-belt. These might indicate that the spatial distribution of the smaller-sized asteroids is wider-distributed than that of larger-size asteroids.

Chapter 5

Conclusions and future prospect

5.1 Summary and conclusions

We carried out for the first time a systematic survey observation of sub-km MBAs using the 8.2m Subaru telescope to investigate their size and spatial distributions.

We found the following results:

- (1) We detected 1,111 moving objects down to $R = 26.5$ mag in the sky area of 3.26 deg^2 near opposition and the ecliptic. Then, we identified 861 MBAs by estimating the a of each moving object by using Bowell's equations. Therefore, the sky number density of MBAs is 264 per deg^2 down to $R = 26.5$ mag near opposition and the ecliptic.
- (2) The slope of the cumulative size distribution for small MBAs ranging from a few km to sub-km seems to be fairly shallower ($\sim 0.8 - 1.2$, depending upon locations in the main-belt) than that for large MBAs (~ 1.8) obtained from the past asteroid surveys. This means that the number of sub-km MBAs is much more depleted than a result extrapolated from the size distribution for large asteroids.
- (3) The CSD slope of the inner sub-km MBAs is some steeper than that of the

outer sub-km MBAs. This may reflect the difference of the spatial distribution between S- and C-type asteroids.

- (4) The spatial distribution of sub-km MBAs resembles that of known MBAs or that obtained from past asteroid surveys. However, if investigated more detail, the I -distribution of sub-km MBAs suggests that a large number of small asteroids with high inclination may exist compared with that of larger MBAs.

From these results, we conclude that overall size and spatial distributions of very small asteroids are fairly different from those for large asteroids. However, one possible weak point of our survey described in this paper might be smallness of the survey area, only covering about $\sim 3.3 \text{ deg}^2$. In this respect, we plan to widen the survey area in near future observations, in order to make our conclusions more reliable.

5.2 Future prospect

First we must clarify and well interpret the difference of the slopes of the CSD in the individual regions of the main-belt. For the purpose, it is necessary to investigate each size distribution for C-type and S-type asteroids. Their types can be judged from ($B-V$) or ($V-R$) color observations. We performed such observations on October 20, 2001. Data reductions are now progressing. As above mentioned, since there is some correspondence between the asteroid material and taxonomic types, such a survey observation will also allow us to argue some correlation of the collisional process, orbital evolution and material distribution of MBAs.

Furthermore, for asteroids detected in the DF survey of SMBAS, we had the data of lightcurves, covering only about two hours. Although we didn't examine them yet in detail in this paper, we found that some asteroids have the large

lightcurve amplitudes, as high as about 2 mag. This finding may be related to a reported excess of fast rotators seen among small asteroids, which are regarded as monolith-like rather than rubble-piles (e.g., Harris & Burus, 1979, Donnison & Wiper, 1999). According to them, it is likely that the angular momentum distributed into the sub-km fragments in a collision is relatively larger than that given into the several-km fragments. Thus the rate of the fast rotators is expected to become high among sub-km asteroids. If the size region where fast rotators occur is determined by observations, the boundary region of the strength regime and the gravity regime in impact fragmentation of asteroids may also be established. Since SMBAS could discover about one hundred asteroids within single observational field at a time, we will be able to obtain lightcurves of several hundreds asteroids from one-night observations with the same strategy as in SMBAS. It is enough amount of sample for the subsequent statistical analysis. We hope that those observations will be put into practice in near future.

Acknowledgments

First I would like to thank my advisor, Prof. Tsuko Nakamura at the National Astronomical Observatory of Japan (NAOJ), for his tremendous support and orientation during the course of this study. I would like to especially thank my institute chairman of the Kobe University, Prof. Tadashi Mukai, who kindly sent me to the NAOJ with generous support and suggestions for this study. Without their constant backup, the completion of this thesis project would have never been achieved.

I am also grateful to Prof. M. Hirai at the Fukuoka University of Education for his continuous encouragement while I have been a graduate student of Kobe Univ. I also wish to acknowledge Prof. I. Hasegawa and K. Hurukawa for their valuable advice.

This study was mainly based on the data which was offered from the *Edgeworth-Kuiper Belt Survey* led by Prof. Jun-ichi Watanabe, at the Subaru Telescope operated by the National Astronomical Observatory of Japan. I gratefully thank Prof. J. Watanabe, the Suprime-Cam team, and the Subaru telescope supporting staff for allowing me to use it. I am also grateful to Dr. Takashi Ito and staff of the Astronomical Data Analysis Center, NAOJ whose advice in data reduction was very useful.

Finally, I acknowledge the NAOJ for providing research and financial support. I also thank many researchers and friends of the Kobe Univ. and the ISAS, whose advice and suggestions much inspired my interest in asteroids.

Bibliography

- [1] Anders, E. (1965) Fragmentation history of asteroids, *Icarus*, **4**, 398-408.

- [2] Bendix, G. K., McFadden, L. A., Morrow, E. M., and Fomenkova, M. N. (1992) Bias correction factors for Near-Earth Asteroids, in *Asteroids Comets Meteors 1991*, Harris, A. W. and Bowell, T. (eds.), Lunar and Planetary Institute, pp.65-68 .

- [3] Bowell, E., Skiff, B. A., Wasserman, L. H. and Russell, K. S. (1990) Orbital information from asteroid motion vectors, in *ACM- III*, Uppsala Univ., pp.19-24.

- [4] Bowell, E., Hapke, B., Domingue, D., Lumme, K., Peltoniemi, J., and Harris, A. W. (1989) Application of photometric models to asteroids, in *Asteroids II*, Binzel, R. P., Gehrels, T., and Matthews, M. S. (eds.), the Univ. of Arizona press, pp.524-556.

- [5] Bowell, E. and Lumme, K., (1979) Colorimetry and magnitudes of asteroids, in *Asteroids*, Gehrels, T. eds., the Univ. of Arizona press, pp.132-169.

- [6] Cellino, A., Zappala, V. and Farinella, P. (1991) The size distribution of main-belt asteroids from IRAS data, *Mon. Not. R. Astron. Soc.*, **253**, 561-574.

- [7] Donnison, J. R., and Wiper, M. P., (1999) Bayesian statistical analysis of

- asteroid rotation rates, *Mon. Not. R. Astron. Soc.*, **302**, 75-80.
- [8] Dohnanyi , J. S. (1972) Interplanetary objects in review : statistics of their masses and dynamics, *Icarus*, **17**, 1-48.
- [9] Dohnanyi , J. S. (1971) Fragmentation and distribution of asteroids, *NASA-SP-267*, in *Physical studies of minor planets*, pp. 263-295.
- [10] Dohnanyi , J. S., 1969, Collisional model of asteroids and their debris, *J. Geophys. Res.*, **74**, 2531-2554.
- [11] Durda, D.D., Greenberg, R., Jedicke, R. (1998) Collisional models and scaling laws: A new interpretation of the shape of the main-belt asteroid size distribution, *Icarus*, **135**, 431-440.
- [12] Ephemerides of Minor Planets for 2001.
- [13] Ephemerides of Minor Planets for 1998.
- [14] Farinella, P. and Vokrouhlicky, D., (1999) Semimajor axis mobility of asteroidal fragments, *Science*, **283**, 1507-1510.
- [15] Gunn, J. E., Carr, M., Rockosi, C., Sekiguchi, M., Berry, K., Elms, B., Haas, E. de., Ivezi, Z., Knapp, G., Lupton, R., Pauls, G., Simcoe, R., Hirsch, R., Sanford, D., Wang, S., York, D., Harris, F., Annis, J., Bartozek, L., Boroski, W., Bakken, J., Haldeman, M., Kent, S., Holm, S., Holmgren, D., Petravick, D., Prosapio, A., Rechenmacher, R., Doi, M., Fukugita, M., Shimasaku, K., Okada, N., Hull, C., Siegmund, W., Mannery, E., Blouke, M., Heidtman, D., Schneider, D., Lucinio, R., and Brinkman, J. (1998) The Sloan Digital Sky Survey Photometric Camera, *Astron. J.*, **116**, 3040-3081.

- [16] Harris, A. W., and Burns, J. A. (1979) Asteroid rotation I. Tabulation and analysis of rates, pole positions and shapes, *Icarus*, **40**, 115-144.
- [17] Harris, A. W. (1979) Asteroid rotation rates II. A theory for the collisional evolution of rotation rates, *Icarus*, **40**, 145-153.
- [18] Hellyer, B. (1971) The fragmentation of the asteroids—II, *Mon. Not. R. Astron. Soc.*, **154**, 279-291.
- [19] Hellyer, B. (1970) The fragmentation of the asteroids, *Mon. Not. R. Astron. Soc.*, **148**, 383-390.
- [20] Ivanov, B. A., Neukum, G., and Wagner, R. (2001) Size-frequency distributions of planetary impact craters and asteroids, *Marov, M.Ya. and Rickman, H. (eds.)*, in *Collisional Processes in the Solar System*, pp.1-34.
- [21] Ivezić, Z., Tabachnik, S., Rafikov, R., Lupton, R. H., Quinn, T., Hammergren, M., Eyer, L., Chu, J., Armstrong, J. C., Fan, X., Finlator, K., Geballe, T. R., Gunn, J. E., Hennessy, G. S., Knapp, G. R., Leggett, S. K., Munn, J. A., Pier, J. R., Rockosi, C. M., Schneider, D. P., Strauss, M. A., Yanny, B., Brinkmann, J., Csabai, I., Hindsley, R. B., Kent, S., Lamb, D. Q., Margon, B., McKay, T. A., Smith, J. A., Waddel, P., and York D. G. (for THE SDSS COLLABORATION) (2001) Solar system objects observed in the Sloan Digital Sky Survey commissioning data, *Astron. J.*, **122**, 2749-2784.
- [22] Jedicke, R. and Metcalfe, T. S. (1998) The orbital and absolute magnitude distributions of main belt asteroids, *Icarus*, **131**, 245-260.
- [23] Jedicke R. (1996) Detection of Near Earth Asteroids Based Upon Their Rates of Motion, *Astron. J.*, **111**, 970-982.

- [24] Klacka, J. (1992) Mass distribution in the asteroid belt, *Earth, Moon, and Planets*, vol. **56**, no. 1, 47-52.
- [25] Komiyama, Y., Yagi, M., Miyazaki, S., Okamura, S., Tamura, S., Fukushima, H., Doi, M., Furusawa, H., Fuse, T., Hamabe, M., Hayashi, M., Hayashino, T., Imi, K., Iye, M., Kaifu, N., Karoji, H., Kawasaki, W., Kimura, M., Kosugi, G., Nakata, F., Noumaru, J., Okada, N., Sasaki, T., Sawada, Y., Sekiguchi, M., Shelton, I., Shimasaku, K., Suzuki, K., Takata, T., Taniguchi, Y., Usuda, T., Yamashita, T., and Yasuda, N. (2000) High-resolution images of the ring nebula taken with the Subaru telescope, *Pub. Astron. Soc. Japan*, **52**, 93-98.
- [26] Kresak, L. (1977) Mass content and mass distribution of the asteroid system, *Bull. Astron. Inst. Czechoslov.*, **28**, 65-82.
- [27] Kuiper, G. P., Fujita, Y., Gehrels, I., Groeneveld, J. K., Van Biesbroeck, G., and Van Houten, C. J. (1958) Survey of asteroids, *Astrophys. J. Suppl.*, **3**, 289-427.
- [28] Landolt, A. U. (1992) UBVRI photometric standard stars in the magnitude range $11.5 < V < 16.0$ around the celestial equator, *Astron. J.*, **104**, 340-371, 436-491.
- [29] Landolt, A. U. (1983) UBVRI photometric standard stars around the celestial equator, *Astron. J.*, **88**, 853-865.
- [30] Melosh, H. J. and Ryan, E. V. (1997) Asteroids: shattered but not dispersed, *Icaurs*, **129**, 562-564.
- [31] Mermilliod, J. C., Mermilliod, M. (1994) in *Catalogue of mean UBV data on stars*, *Spribger-Verlag, New York*.

- [32] Morbidelli, A. and Moons, M. (1995) Numerical evidence on the chaotic nature of the 3/1 mean motion commensurability, *Icarus*, **115**, 60-65.

- [34] Mueller, I. I. (1969) in *Spherical and practical astronomy as applied to geodesy*, Frederick Ungar Publishing Co., New York, 187.

- [35] Nakamura, T. and Yoshida, F. (2001) Statistical method for deriving spatial and size distribution of sub-km main belt asteroids from their sky motions, submitted to *Pub. Astron. Soc. Japan*.

- [36] Nakamura, T. (1997) Statistical survey observations of faint belt asteroid with SUBARU-class telescopes, *Proc. of the 29th Sympo. on Celestial Mechanics, Tokyo*, pp.274-278 (in Japanese).

- [37] Nakamura, T. (1994) Size dependence of asteroid belt structure, *Seventy-five years of Hirayama asteroid families ASP conference series, Vol. 63*, Kozai, T., Binzel, R. P., and Hirayama, T. (eds.), pp.52-61.

- [38] Nolan, M. C., Asphaug, E., Greenberg, R., and Melosh, H. J. (2001) Impacts on asteroids : fragmentation, regolith transport, and disruption, *Icarus*, **153**, 1-15.

- [39] Ostro, Steven J.; Hudson, R. Scott; Nolan, Michael C.; Margot, Jean-Luc; Scheeres, Daniel J.; Campbell, Donald B.; Magri, Christopher; Giorgini, Jon D.; Yeomans, Donald K. (2000) Radar Observations of Asteroid 216 Kleopatra, *Science*, **288**, 836-839.

- [40] Piotrowski, S. (1953) The collisions of asteroids, *Acta Astron. Ser. A, Vol. 5*, 115-138.

- [41] Soberman, R. K., Neste, S. L. and Petty, A. F. (1971) Asteroid detection from Pioneers F and G ?, *NASA SP-267*, in *Physical studies of minor planets*, pp. 617-631.
- [42] Tancredi, G. (1998) in *Solar system formation and evolution, ASP Conf. Ser.*, vol. **149**, Lazzaro, D., et al.(eds.), 135.
- [43] Van Houten, C. J., Van Houten-Groeneveld, I., Herget, P., Gehrels, T. (1970) The Palomar-Leiden survey of faint minor planets, *Astr. Astrophys. Suppl.*, **2**, 339-448.
- [44] Veverka J., Thomas, P., Harch, A., Clark, B., Bell III, J. F., Careich, B., Joseph, J., Murchie, S., Izenberg, N., Chapman, C., Merline, W., Malin, M., McFadden, L., and Robinson, M. (1999) NEAR encounter with asteroid 253 Mathilda : overview, *Icarus*, **140**, 3-16.
- [45] Wetherill, G. W. (1989) Origin of the asteroid belt, in *Asteroids II*, Binzel, R. P., Gehrels, T., and Matthews, M. S. (eds.), the Univ. of Arizona press, pp.661-680.
- [46] Weidenschilling, S. J. (1981) How fast can an asteroid spin ?, *Icarus*, **46**, 124-126.
- [47] Wisdom, J. (1983) Chaotic behavior and the origin of the 3/1 Kirkwood gap, *Icarus*, **56**, 51-74.
- [48] Xu, S., Binzel, R. P., Burbine, T. H., Bus, S. J. (1995) Small main-belt asteroid spectroscopic survey : initial results, *Icarus*, **115**, 1-35.
- [49] York, D. G., Adelman, J., Anderson Jr., J. E., Anderson, S. F., Annis, J.,

Bahcall, N. A., Bakken, J. A., Barkhouser, R., Bastian, S., Berman, E., Boroski, W. N., Bracker, S., Briegel, C., Briggs, J. W., Brinkmann, J., Brunner, R., Burles, S., Carey, L., Carr, M. A., Castander, F. J., Chen, B., Colestock, P. L., Connolly, A. J., Crocker, J. H., Csabai, I., Czarapata, P. C., Davis, J. E., Doi, M., Dombeck, T., Eisenstein, D., Ellman, N., Elms, B. R., Evans, M. L., Fan, X., Federwitz, G. R., Fiscelli, L., Friedman, S., Frieman, J. A., Fukugita, M., Gillespie, B., Gunn, J. E., Gurbani, V. K., Haas, E. de, Haldeman, M., Harris, F. H., Hayes, J., Heckman, T. M., Hennessy, G. S., Hindsley, R. B., Holm, S., Holmgren, D. J., Huang, Chi-hao, Hull, C., Husby, D., Ichikawa, S., Ichikawa, T., Ivezić, Z., Kent, S., Kim, R. S. J., Kinney, E., Klaene, M., Kleinman, A. N., Kleinman, S., Knapp, G. R., Korienek, J., Kron, R. G., Kunszt, P. Z., Lamb, D. Q., Lee, B., Leger, R. F., Limmongkol, S., Lindenmeyer, C., Long, D. C., Loomis, C., Loveday, J., Lucinio, R., Lupton, R. H., MacKinnon, B., Mannery, E. J., Mantsch, P. M., Margon, B., McGehee, P., McKay, T. A., Meiksin, A., Merelli, A., Monet, D. G., Munn, J. A., Narayanan, V. K., Nash, T., Neilsen, E., Neswold, R., Newberg, H. J., Nichol, R. C., Nicinski, T., Nonino, M., Okada, N., Okamura, S., Ostriker, J. P., Owen, R., Pauls, A. G., Peoples, J., Peterson, R. L., Petravick, D., Pier, J. R., Pope, A., Pordes, R., Prosapio, A., Rechenmacher, R., Quinn, T. R., Richards, Gordon T. M., Richmond, W., Rivetta, C. H., Rockosi, C. M., Ruthmansdorfer, K., Sandford, D., Schlegel, D. J., Schneider, D. P., Sekiguchi, M., Sergey, G., Shimasaku, K., Siegmund, W. A., Smee, S., Smith, J. A., Snedden, S., Stone, R., Stoughton, C., Strauss, M. A., Stubbs, C., SubbaRao, M., Szalay, A. S., Szapudi, I., Szokoly, G. P., Thakar, A. R., Tremonti, C., Tucker, D. L., Uomoto, A., Berk, D. V., Vogeley, M. S., Waddell, P., Wang, Shu-I., Watanabe, M., Weinberg, D. H., Yanny, B., and Yasuda, N. (THE SDSS COLLABORATION) (2000) The Sloan Digital Sky Survey : Technical Summary, *Astron. J.*, **120**, 1579-1587.

- [50] Yoshida, F., Nakamura, T., Fuse, T., Komiyama, Y., Yagi, M., Miyazaki, S., Okamura, S., Ouchi, M., and Miyazaki, M. (2001a) First Subaru Observations

of Sub-km Main Belt Asteroids, *Pub. Astron. Soc. Japan Letter*, **53**, L13-L16.

- [51] Yoshida, F., Sato, Y., and Nakamura, T (2001b) Sub-km Main Belt Asteroid Survey (SMBAS) using SUBARU telescope —The Estimation Methods of Size Distributions —, *Proceedings of the 33rd symposium on Celestial Mechanics*, 269-276.
- [52] Yoshida, F. and Nakamura, T. (2000) SUBARU sub-km main belt asteroid survey plan —Statistical estimation of size distribution—, *Proc. of 33rd ISAS Lunar and Planetary Sympo.*, 21-24.
- [53] Yoshida, F. and Nakamura, T. (1999a) Sub-km belt asteroid survey observations with SUBARU telescopes — Estimation of the intrinsic distribution—, *Proc. of the 31th Sympo. on Celestial Mechanics, Kashima space research center communications research laboratory, Ibaraki, Japan*, pp.278-285 (in Japanese).
- [54] Yoshida, F. and Nakamura, T. (1999b) Sub-km Belt Asteroid Survey Observations with 8m-Class Wide-field Telescopes, *Asteroids, Comets, Meteors, Cornell University, July 26-30, 1999, U.S.A.* p.187
- [55] 吉田二美 (1999) (修士論文) 微小惑星の真のサイズ分布の推定—小惑星サーベイ観測の観測選択効果の見積もり—.
- [56] The data base of Near Earth Asteroids :
<http://cfa-www.harvard.edu/iau/mpc.html>
- [57] The data base of known Asteroids : <ftp://ftp.lowell.edu/pub/elgb/astorb.html>

[58] The data base of Near Earth Objects :

<http://cfa-www.harvard.edu/iau/NEO/TheNEOPage.html>

[59] USNO-A2 catalog : <http://tdc-www.harvard.edu/software/catalogs/ua2.html>

[60] The data base of Atens, Apollos, and Amors :

[*http://cfa-www.harvard.edu/iau/lists/Unusual.html*](http://cfa-www.harvard.edu/iau/lists/Unusual.html)

[61] The data base of small bodies in the solar system :

<http://pdssbn.astro.umd.edu>

Appendix 1

Proc. of 33rd ISAS Lunar and Planetary Sympo., 21-24.

SUBARU Sub-km Main Belt Asteroids Survey Plan –Statistical Estimation of Size Distribution–

Fumi Yoshida¹ and Tsuko Nakamura²

¹*Kobe Univ./National Astronomical Observatory*

fumiy@komadori.planet.sci.kobe-u.ac.jp

²*National Astronomical Observatory*

tsuko@cc.nao.ac.jp

Abstract

Although theory and experiments point to the importance of sub-km-sized bodies in the collisional history of the asteroid belt, it is difficult to estimate the global distributions of the sub-km asteroids from traditional approaches such as orbit determination of individual asteroids. Therefore here, we propose instead a statistical method to deduce the spatial and size distribution of sub-km main belt asteroids (MBAs), only from their apparent motion vectors on the sky.

By using the Bowell's scheme, we estimate statistically semi-major axis(a) and inclination(I) of each asteroid from its apparent motion vector. The estimated error of a and I determined by our method are about 0.1AU and about 0.8 degree (near the ecliptic plane), respectively. When the estimated a is adopted as the heliocentric distance, the original size distributions generated by simulations are well reproduced. The slope(b) of cumulative size distribution reproduced has error of about 0.1. If there is a difference in b larger than 0.1 for the size distribution of sub-km MBAs and for km-sized MBAs, then it will be detectable in our proposed SUBARU sub-km MBAs survey.

Keywords: faint main belt asteroid, size distribution

1. Introduction

The collision plays a very important part in the origin and the evolution of the MBAs, and the size distributions caused by the mutual collisions reflect a direct result. The size distribution of the MBAs down to 1km in diameter has been determined from the Palomar-Leiden survey (PLS : van Houten et al. 1970), and the Spacewatch survey (Jedicke and Metcalfe 1998). On the other hand, sub-km asteroids have never been observed systematically because of their faintness.

The observation of the sub-km asteroids is especially important from the following two viewpoints.

- 1) Theory and laboratory experiments suggest that the structure of asteroids changes from rubble-pile to monolith in the sub-km size region (e.g. Melosh & Ryan 1997).
- 2) It is predicted that there is no regolith on the surface of small asteroids ($D < 1\text{km}$) due to their low gravity.

With the background in mind, we have planned to deduce the global size, space and taxonomic type distributions of sub-km asteroids which anybody has never known, with the SUBARU telescope + Suprime-cam (wide-field mosaic camera). Asteroids with 150-300m in diameter are detected at the center of main belt ($a \approx 2.7\text{AU}$) by using the Suprime-cam. We estimate that the number of detectable asteroid is 2,000-4,000 for three nights. The number of this sample is enough for the subsequent statistical interpretation.

Our approach is unique in that we estimate the spatial distribution of sub-km MBAs *statistically*, rather than determine orbits of individual asteroids. Traditionally, orbit's determination has been done, based on a few follow-up observations. But it is practically impossible to follow-up the asteroids detected by SUBARU with other 8-10m large telescopes. So we introduced a method to estimate statistically a and I of each asteroid from its motion vector on the sky without follow-up observations (Nakamura 1997, Yoshida 1999 master thesis).

In this paper, our goal is to estimate quantitatively the size distribution of asteroids, using the above-obtained a and I .

2. Procedure for estimation of size distribution

Figure 1 represents a correlation diagram between a and daily motion on the sky for existing asteroids, observed in a near-opposition window. Similarly, Figure 2 stands for a correlation between I and the position angle of the sky motion vector for the same asteroids. From these figures, it is understood that approximate a and I for each asteroids can be obtained from only apparent motion vectors, without making exact orbit determination. However, for quantitative analysis, we need a more mathematical procedure.

In 1990, *Bowell et al.* proposed a method to derive approximate a and I from the sky motion vector. They showed that if the eccentricity (e) of an asteroid's orbit is zero, its semi-major axis (a') and inclination (I') of the asteroid are represented by the next equations from the apparent motion vector of the asteroid:

$$a' = \frac{1}{2\gamma} (\gamma - 2k\lambda \pm \sqrt{\kappa})$$

$$\gamma = \lambda^2 + \beta^2$$

$$\tan I' = \frac{|\beta|}{\lambda + \frac{k}{a'-1}}$$

$$\kappa = \gamma^2 - 4k\lambda\gamma - 4k^2\beta^2,$$

in which λ is the component in longitude of motion vector, β is the latitude component and k is Gauss constant. Note that these equations are valid only for near-opposition and near-ecliptic observations. We call these “Bowell's equations” in this paper.

What is most important in applying Bowell's equations is that the averaged a' over many asteroids has no systematic deviation from the true a ; as seen in Figure 3, each a' can be considerably different from the corresponding true a . To check the requirement, we made some Monte Carlo simulations in a computer by generating hypothetical a and I from some model population of asteroids. And we calculate the sky motion vector from the a and I with a two-body ephemeris generator. Then we estimate a' from Bowell's equations based on λ and β of an asteroid obtained from this model observation.

It is found that the averaged difference between the generated a in Monte Carlo simulations and the a' from Bowell's equation based on the motion vector is nearly equal to or less than 0.1AU over the main belt (2.1-3.3AU) (See Fig.3 and Table 1). Therefore, we can regard the averaged a' approximately equal to the average of the original a , without appreciable systematic deviation. Since we will be able to detect many new asteroids in SUBARU survey, the averaging procedure mentioned above is feasible in practice.

Next we will discuss the estimation of size distribution for SUBARU asteroids. Lets us assume that the above-estimated a' of an asteroid is equal to its heliocentric distance (R), and then we calculate the absolute magnitude (H') of the asteroid from the next equation,

$$H' = V - 5 \log\{r(r-1)\}. \dots\dots\dots (1)$$

in which V is apparent magnitude and $(r-1)$ is the geocentric distance of the asteroid.

Although the assumption adopted here that the e for each asteroid is zero may seem to be unacceptably crude one, it is shown in the following that the assumption works reasonably well. A similar but rougher approach than ours was adopted by Jewitt et al.(2000) to estimate of the size distribution of several ten new Trojan asteroids.

The asteroid size (R) is calculated from absolute magnitude using the following

relation,

$$H \propto -2.5 \log(AR^2), \dots\dots\dots (2)$$

where H is absolute magnitude and A is albedo.

Our simulations proceed along the procedure summarized in the next paragraph.

Procedure

1. Generate likely orbit distributions with Monte Carlo simulation. The produced parent population has various a , I , and e .
The slope (b) of cumulative size distribution of generated population is taken to be equal to 1.75, which is the value from the PLS.
2. Pick up asteroids in the observational window assumed for observations by SUBARU.
3. Calculate apparent motion velocities in longitude and in latitude, for each asteroid.
4. Estimate a' and I' of the asteroid using Bowell's equations from the apparent motion vector of the asteroid (Bowell et al. 1990).
5. Assume that $r=a'$, and calculate the H' of the asteroid with equation (1).
6. Assume an albedo of the asteroid, translate H' to the radius (R) of the asteroid with equation (2).
7. Produce the size distribution from various R of asteroids and get the slope (b') of cumulative size distribution by a least squares method.
8. Compare the b generated by simulations with the b' estimated from a' .

3. Reproduction of the original size distribution

Now we describe the simulation results.

3.1 Parent populations of asteroids

It is essential that the size distribution slope calculated from Bowell's orbits is independent from or weakly dependent upon the assumed parent populations of asteroids in the simulations, since we have no information at all on orbital distribution for the sub-km MBAs in question. In other words, we cannot help assuming that the orbital distributions for sub-km MBAs are similar to those for currently known faintest MBAs (namely 1-2km in diameter). Among those distributions, we selected in Table 2 three typically likely combinations of a , I , and e -range. For those likely three kinds of populations generated in the simulations, we calculated the slopes of the cumulative size distribution in each case, following the procedure mentioned before.

3.2 Results

Fig.4-6 show $\log N$ vs. H plot for each of the three cases, where N is the cumulative number of asteroids and H is calculated from equation (1) with $r=a'$. The solid line represents the H -slope (α), 0.35, corresponding to the b of the PLS, 1.75. Because the H and the R is connected by the equation (2), we can have the following relation, $b=5\alpha$.

For Fig.4-6, open circles show the cumulative H -distribution generated by the simulations and filled circles show the cumulative H -distribution based on a' . The open circles and filled circles are linearly fitted by a least squares method, representatively.

Thus obtained b' for each case listed in Table 3, along with α s.

4. Discussion

As Table 1 shows, the estimated error of a' determined by our method is about 0.1AU. This error is small enough to grasp roughly the global spatial distribution

of sub-km MBAs. It has been shown in Table 3 of the previous section that, by applying the correction Δb to the b obtained from a' and the assumption $r=a'$, we can recover the original slope with errors less than 0.1 for each of three cases. This therefore means that if there is a difference in b larger than 0.1 for the size distribution of sub-km MBAs and for km-sized MBAs, our proposed SUBARU survey will easily detect such a difference. Considering the first viewpoint in section 1, it actually seems likely that the size distribution for sub-km MBAs is appreciably different from that for larger ones.

5. Future Work

For likely different slopes of cumulative size distribution, for example 1.5 or 2.0, we will repeat the former procedure, and estimate the correct factor Δb .

References

- Bowell, E., Skiff, B. A., Wasserman, L. H. and Russell, K. S. (1990): Orbital information from asteroid motion vectors, ACM- III, Uppsala Univ. pp.19-24.
- Bowell, E.,(1998): Internet asteroid database of Lowell Observatory.
- Jedicke, R. and Metcalfe, T.S. (1998): *Icarus* **131**, pp.245-260.
- Jewitt, D. C., Trujillo, C. A. and Luu, J. X. (2000): *Astron. J.* (in press).
- Melosh, H. J. and Ryan, E. V. (1997): *Icaurs* **129**, pp.562-564.
- Nakamura, T. (1997): Statistical survey observations of faint belt asteriud with SUBARU-class telescopes, Proc. of the 29th Sympo. “ Celestial Mechanics”, Tokyo, pp.274-278 (in Japanese).
- Van Houten, C. J., Van Houten-Groeneveld, I., Herget, P., Gehrels, T., (1970): *Astr. Astrophys. Suppl.* **2**, pp.339-448.
- Yoshida, F. (1999): Master Thesis (in Japanese), Fukuoka Univ. of Education.

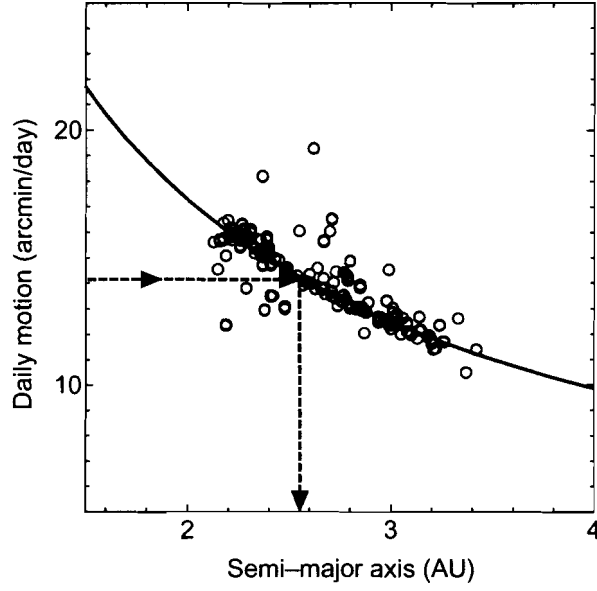


Fig 1. a vs. daily motion correlation.

Calculations were made for an assumed opposition window on September 23, 1999 for about 40,000 asteroids (Bowell 1998). The solid curve is for circular ecliptic orbits. This relationship means that the value of a can be approximately determined from observational daily motion of asteroids.

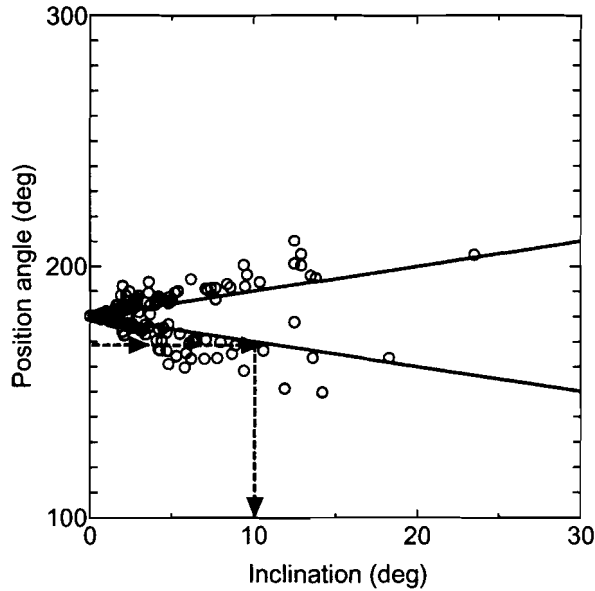


Fig 2. I vs. position angle of motion correlation.

The solid line correspond to the case that the position angle motion is $180^\circ \pm I$. For other details on conditions of calculation, see Fig.1. Based on this relation, it is expected that the value of I can roughly inferred from observational position angle of asteroids.

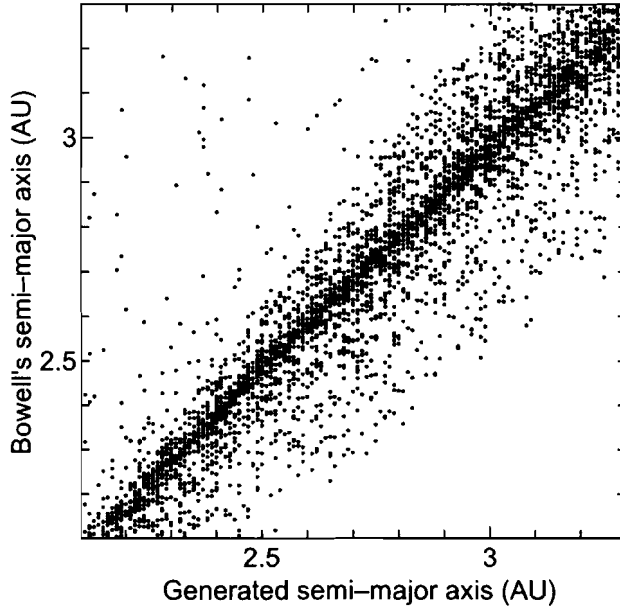


Fig 3. Generated a vs. Bowell's a' plot.

The horizontal axis: the value of a generated in a computer run. The vertical axis: the value of a' from Bowell's equation. Table 1 shows error in a obtained from Bowell's equation.

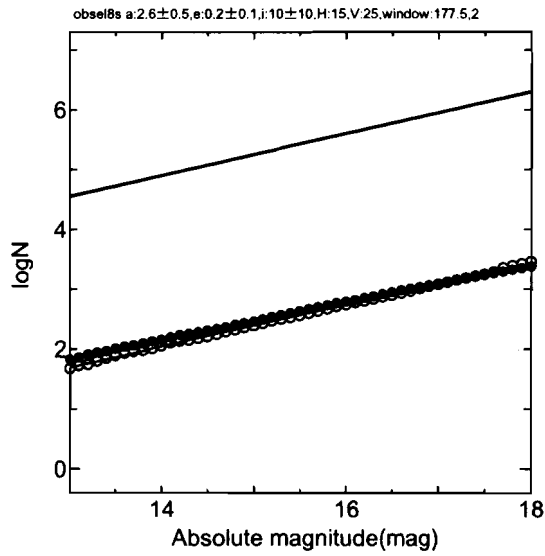


Fig.4 (left) logN vs. H based on Case I

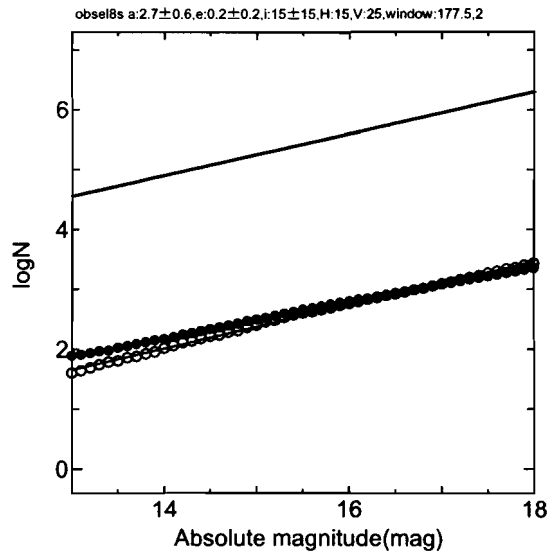


Fig.5 (middle) logN vs. H based on Case II

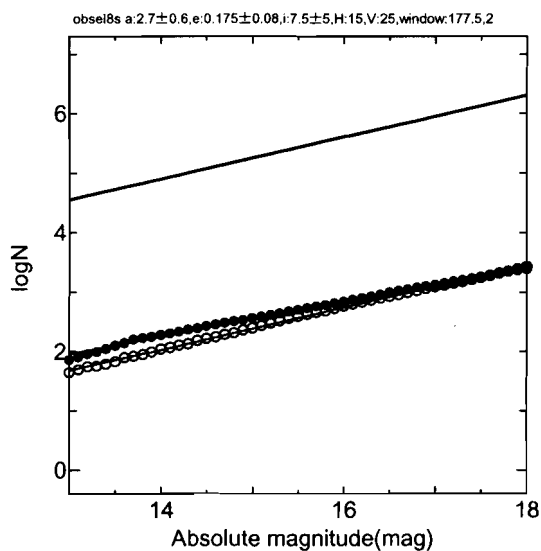


Fig.6 (right) logN vs. H based on Case III

Table 1 Errors in a obtained from Bowell's orbit

| a | ave($a-a'$) |
|-----------------------|---------------|
| $2.1 \leq a \leq 2.5$ | 0.094 |
| $2.5 < a \leq 2.9$ | 0.102 |
| $2.9 < a \leq 3.3$ | 0.113 |

Table 2 Adopted orbital populations

| Case | I | II | III |
|--------------|---------------|---------------|------------------|
| a | 2.6 ± 0.5 | 2.7 ± 0.6 | 2.7 ± 0.6 |
| i | 10 ± 10 | 15 ± 15 | 7.5 ± 5 |
| e | 0.2 ± 0.1 | 0.2 ± 0.2 | 0.175 ± 0.08 |
| limiting mag | 25mag | 25mag | 25mag |

Table 3 The slopes of the size distributions

| | I | II | III |
|-----------------------------------|--------|-------|-------|
| Generated α | 0.347 | 0.361 | 0.353 |
| Bowell's α' | 0.309 | 0.297 | 0.292 |
| Generated b | 1.735 | 1.805 | 1.765 |
| Bowell's b' | 1.545 | 1.485 | 1.460 |
| $\Delta b = b - b'$ | 0.190 | 0.320 | 0.305 |
| Δb -average of Δb | -0.082 | 0.048 | 0.033 |

Appendix 2

Proceedings of the 33rd symposium on Celestial Mechanics (in press).

Sub-km Main Belt Asteroids Survey (SMBAS) using SUBARU telescope -The Estimation Methods of Size Distributions-

Fumi Yoshida

National Astronomical Observatory of Japan,

Mitaka, Tokyo, 181-8588 Japan

Graduate School of Science and Technology, Kobe University,

Nada, Kobe 657-8501, Japan

E-mail fumiy@komadori.planet.sci.kobe-u.ac.jp

Tsuko Nakamura

National Astronomical Observatory of Japan,

Mitaka, Tokyo, 181-8588 Japan

E-mail tsuko@cc.nao.ac.jp

Abstract

We have attempted to estimate the size distribution of the sub-km Main Belt Asteroids (MBAs), using large telescopes such as SUBARU telescope, for study of the collisional process among MBAs. However we cannot make the precise orbit determination by the successive follow-up observations, because of the limited observing times of large telescopes. So we are interested in estimating the orbital elements of the asteroids with the short observational arc (e.g. one day).

We have shown that the semimajor axis (a) and inclination (I) of MBAs can be statistically estimated from apparent motion vectors projected on the celestial

sphere. However it is impossible to determine actually the eccentricity (e) of the asteroid without follow-up observations. The uncertainty of the e influences the estimation of the a for each asteroid and it also affects the size distribution of MBAs through translating the brightness of the asteroid into the size. So it is necessary to evaluate the error of a caused by the uncertainty of e and the resulting error on the size distribution of MBAs.

In this paper we used various orbital distributions of asteroids generated by the Monte Carlo simulations to evaluate the error of the a estimated from an apparent motion vector for individual asteroids. The simulations produced for three sets of orbital distributions, nine cases of size distributions respectively. Each case includes 5000 asteroids. In order to estimate quantitatively the error of a , we calculated the motion vectors of asteroids from orbits generated in the above simulations, by Bowell's equations which assumed $e = 0$, and estimated the a' for each asteroid (hereafter we express the semimajor axis calculated by Bowell's equations; a'). And the a' of the asteroid was compared with the true a . The difference between the a' and a corresponds to the error of the a which includes the uncertainty of its e .

Next in all orbital distributions, we constructed the size distributions based on the a' and the a respectively. Then we obtained the corresponding two slopes of the cumulative size distribution for each orbital distribution.

Finally we found that the differences of the two slopes was less than ± 0.1 in all. This means that if there is a difference in the observed cases slope larger than 0.1 for sub-km MBAs and km-sized MBAs, the difference will be detected by the method mentioned above. A preliminary analysis of our Sub-km Main Belt Asteroids Survey (SMBAS), which was performed on Feb. 21 and 24, 2001, seems to suggest that the size distribution for sub-km MBAs is appreciably different from that for larger ones.

1 Introduction

In the origin of the solar system, the study on the origin and the evolution of the MBAs is a very important issue. Especially, it is worth knowing their collisional process to estimate the relative velocities or the material strength of MBAs. The size distribution of the current MBAs reflects direct results caused by the mutual collisions among the MBAs. The size distribution of the MBAs down to a few km in diameter has been determined from the Palomar-Leiden survey (PLS : van Houten et al. 1970), and the Spacewatch survey (Jedicke and Metcalfe 1998). On the other hand, sub-km asteroids have never been observed systematically in the past because of their faintness.

However, the Suprime-cam, which is a wide-field mosaic CCD camera, attached to the prime focus of the 8.2m SUBARU telescope, allows us to detect the MBAs with about 150-300m in diameter at the center of main belt ($a = 2.7\text{AU}$). Now we can examine the size distribution of sub-km MBAs which anybody has never explored before.

Even if the motion of an asteroid was observed only one night, the orbit can be determined in principle from the three measured positions of the asteroid. However the orbit determined with this method can include large errors. The IAU has adopted currently the rule that if a new asteroid was observed more than three nights, the asteroid is given a temporary number and after a few more observations at opposition, it can be numbered. Practically it is impossible to follow-up the faint asteroids discovered by SUBARU on other days or with other 8-10m large telescopes, because of the restriction of the telescope's allocated times. So it is probably impossible to determine the precise orbital elements for those faint asteroids. But we noticed that the approximate a and I of an MBA can be statistically estimated from its motion vector without follow-up observations (Nakamura 1997, Yoshida 1999 master thesis), thanks to the special geometry in near-opposition observations. Moreover, the inferred a and I of many asteroids allow us to calculate the statistical errors of their a and I . Fortunately it is

expected to detect a large number of sub-km MBAs in the SMBAS using SUBARU telescope (Yoshida and Nakamura 2000).

The goal of our paper is to determine the difference between the simulated size distribution of MBAs and that calculated from the a based on the apparent motion vector of each asteroid. This is to infer the true size distribution of the MBAs from SMBAS with the short observational arcs. We argue the difference between the true a and the a' calculated by Bowell's equations for individual asteroids (section 2). In section 3 we investigate the influence of the error of the a' on the size distribution of the MBAs. Finally we refer to the correct values on the slope of the cumulative size distribution for sub-km MBAs.

2 a and I estimated from motion vector

First, by generating various orbital elements with the Monte Carlo simulations, we made the orbital distributions of various objects in the solar system and calculated their daily motions using a two-body ephemeris generator, under the condition that they locate at oppositions. Fig.1 represents a correlation diagram between a and daily motion for various objects in the solar system. From this figure, it seems that we can distinguish the a estimated from their motion vector for inner MBAs from ones for outer MBAs. However, for quantitative analysis, we need a more mathematical procedure.

In 1990, Bowell et al. proposed a method to derive an approximate a and I of an asteroid from the sky motion vector, assuming that its $e = 0$. They showed that a and I of the asteroid are represented by the following equations from the apparent motion vector of the asteroid:

$$\begin{aligned}
a' &= \frac{1}{2\gamma} \left(\gamma - 2k\lambda \pm \sqrt{|\kappa|} \right) \\
\tan I' &= \frac{|\beta|}{\lambda + \frac{k}{a'-1}} \\
\gamma &= \lambda^2 + \beta^2 \\
\kappa &= \gamma^2 - 4k\lambda\gamma - 4k^2\beta^2,
\end{aligned}$$

where λ is the component in longitude of motion vector, β is the latitude component and k is Gauss constant. Note that these equations are valid only for near-opposition and near-ecliptic observations. We call these “Bowell’s equations” and express the semimajor axis calculated by Bowell’s equations as “ a' ” to distinguish from true a determined by traditional orbit determination in our paper. What must be careful in applying Bowell’s equations is that the value of a' are calculated as $e = 0$. Generally, it is difficult to determine the e of an asteroid without the follow-up observations. It is the same in our SMBAS because of the short observational arc. So we must assume $e = 0$ and estimate the a from the motion vector only. However, actually the e distribution of MBAs ranges from 0 to 0.4. Therefore the a' of one asteroid includes the uncertainty of its e .

In an orbital distribution of asteroids generated by the Monte Carlo simulation, we compared the a for each asteroid, which we defined as the true a , with the a' calculated by Bowell’s equations from the motion vector of the asteroid. As seen in fig.2, individual a' can considerably be different from the corresponding true a . However one can see that the averaged a' over many asteroids has no systematic deviation from the true a . We divided the main belt into three regions, i.e. inner, middle and outer regions and examined the difference between the a' and a (see table 1). It is found that the averaged difference is nearly equal to or less than 0.1AU over the main belt (2.1-3.3AU). Therefore, we can regard that the error of the a' derived from the uncertainty of its e is about 0.1 AU for each region.

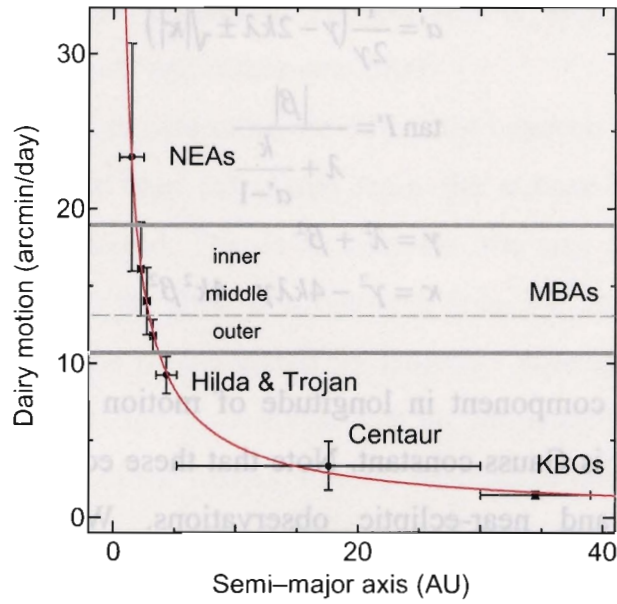


Fig.1 a vs. daily motion for various objects in the solar system.

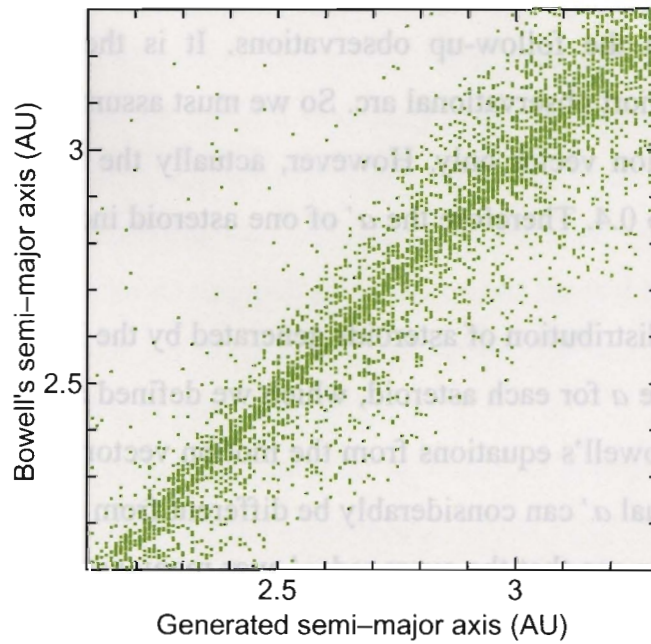


Fig.2 Generated a vs. Bowell's a' plot for members of an orbital distribution generated by the simulation.

The horizontal axis: the value of a generated in a computer run. The vertical axis: the value of a' from Bowell orbit. The a' of each asteroid is considerably averaged different from it's a . The difference between a' and a is about 0.1 AU.

Table 1 The differences between the a' and a in three belt regions.

| a | $\text{ave}(a-a')$ |
|----------------------------------|--------------------|
| inner belt $2.1 \leq a \leq 2.5$ | 0.094 |
| middle belt $2.5 < a \leq 2.9$ | 0.102 |
| outer belt $2.9 < a \leq 3.3$ | 0.113 |

3 Estimation of size distribution based on a'

We found out in section 2 that the error of the a' estimated from the apparent motion vector only is about 0.1 AU. We now examine in this section how the a' error affects the size distribution inferred from our SMBAS. For this purpose, we carried out simulations by the following procedure.

1. Generate three likely orbital distributions with Monte Carlo simulation (see table 2). We produced nine parent populations with different size distribution slopes, each population with 5000 members of asteroids. Individual asteroids of each parent population have various a , I and e within the range designated in table 2. Therefore, we made 27 orbital distributions in total.
2. Pick up asteroids in an observational window assumed for observations by our SMBAS, for each distribution.
3. Calculate apparent motion velocities in longitude and in latitude, with a two-body ephemeris generator, for each asteroid picked up.
4. Calculate a' and I' of each asteroid using Bowell's equations from the apparent motion vector of the asteroid.
5. Assume that the heliocentric distance (r) of each asteroid is equal to its a' , and calculate the absolute magnitude (H) of the asteroid by the following

equation,

$$H = V - 5 \log \{a'(a' - 1)\} \dots\dots\dots(1),$$

where V is apparent magnitude of the asteroid.

6. Assume an albedo of the asteroid, and translate the H to the radius (R) of the asteroid with the following equation,

$$H \propto -2.5 \log (AR^2) \dots\dots\dots(2),$$

where A is the albedo.

7. Produce the size distribution from various R of asteroids for every population and get the slope (b') of the cumulative size distribution by a least squares method.
8. Compare the slope (b) of the original cumulative size distribution generated in simulations with the b' estimated from a' .

Since we have no information at all on orbital distribution for the sub-km MBAs, we assumed that the orbital distributions for sub-km MBAs are similar to those for currently known MBAs. Among those distributions, we selected in table 2 three typically likely combinations of a , I , and e -range. For those likely three kinds of the populations generated in the simulations, we calculated the slopes of the cumulative size distribution in each case, following the procedure mentioned before.

Next we investigated whether or not the b' inferred from a' using Bowell's equations can reproduce properly the original b , in comparison of the b' with the b for each population. We adopted the nine kinds of $b = 1.0, 1.5, 1.6, 1.7, 1.75,$

1.8, 1.9, 2.0 and 2.5, for each original orbital distribution. Fig.4(a)-(c) show $\log N$ vs. H plot for the three cases (I , II and III in table 2) with $b = 1.75$ whose value was determined by the PLS. N is the cumulative number of asteroids as a function of their H . The solid line represents the slope (α) as a function of H , namely 0.35. Because H and the size (or R) are connected by the equation (2), we can find immediately the following relation, $b = 5 \alpha$. In fig.4(a)-(c), open circles show the original cumulative H -distribution generated by the simulations and filled circles show the cumulative H -distribution derived from Bowell's equations. The open circles and filled circles are linearly fitted by a least squares method, respectively. The obtained b 's for each case are listed in table 3, along with α 's. Due to the observational bias that the field observed by our SMBAS is very small compared with the whole sky, the slope of the H -distribution represented by open circles is different slightly from the original one ($\alpha = 0.35$) generated by the simulation.

The true size distribution of asteroids that will be detected in the SMBAS is regarded as that (b) expressed by open circles in fig.4 (a)-(c), on the other hand, the size distribution that we will obtain from the analysis of SMBAS data corresponds to the distribution (b') expressed by filled circles in fig. 4(a)-(c), which is estimated from the apparent motion vector for each asteroid. Therefore, we attempt to determine the correction value for the b' by calculating the difference between b' and b . When the correction value is applied to the size distribution derived from a 's, we will obtain the true size distribution of MBAs.

Fig.5 shows the correction values calculated for each parent orbital distribution with the various b 's. For the data points on this graph, we draw a straight line coming as close as possible to all the data points in a least-squares sense. The error bars for each data point correspond to the standard deviation of the b' (error bar of x) and $b - b'$ (error bar of y), both of which are derived from the three variations of the parent orbital distributions. Note that all the correction values are less than ± 0.1 in all cases.

Table 2 Adopted orbital populations

- I : It is most similar to the orbital distribution of currently known MBAs.
- II : It is slightly wider in range than the orbital distribution of currently known MBAs.
- III : It corresponds to the FWHM of the orbital distribution for currently known MBAs.

| Case | I | II | III |
|--------------|-------------|-------------|----------------|
| <i>a</i> | 26 ± 0.5 | 27 ± 0.6 | 27 ± 0.6 |
| <i>i</i> | 10 ± 10 | 15 ± 15 | 7.5 ± 5 |
| <i>e</i> | 0.2 ± 0.1 | 0.2 ± 0.2 | 0.175 ± 0.08 |
| limiting mag | 25mag | 25mag | 25mag |

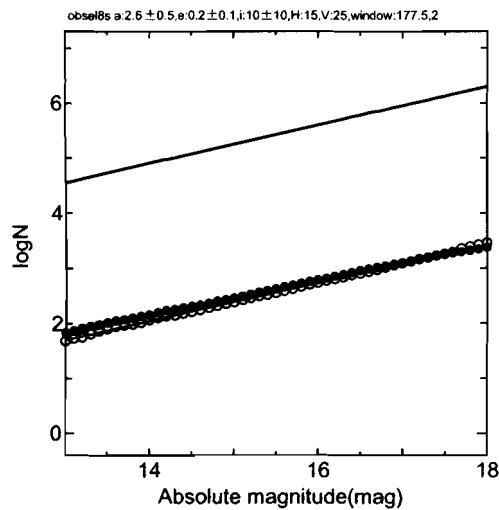


Fig.4 (a) $\log N$ vs. H based on Case I .

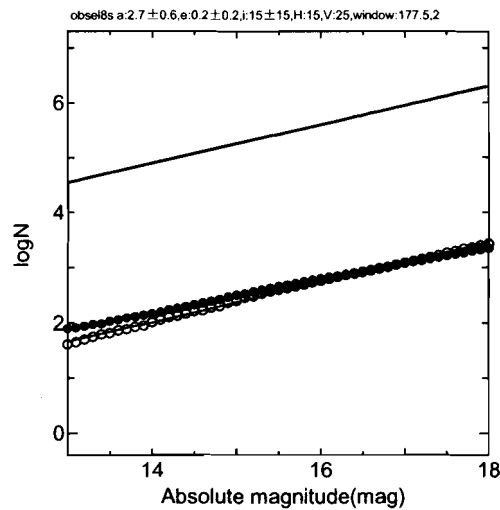


Fig.4 (b) $\log N$ vs. H based on Case II .

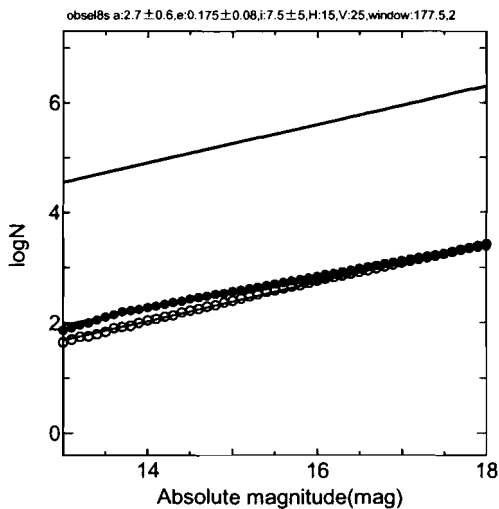


Fig.4 (c) $\log N$ vs. H based on Case III .

Table 3 The slopes of the size distributions

| | I | II | III |
|-----------------------------------|--------|-------|-------|
| Generated α | 0.347 | 0.361 | 0.353 |
| Bowell's α' | 0.309 | 0.297 | 0.292 |
| Generated b | 1.735 | 1.805 | 1.765 |
| Bowell's b' | 1.545 | 1.485 | 1.460 |
| $\Delta b=b-b'$ | 0.190 | 0.320 | 0.305 |
| Δb -average of Δb | -0.082 | 0.048 | 0.033 |

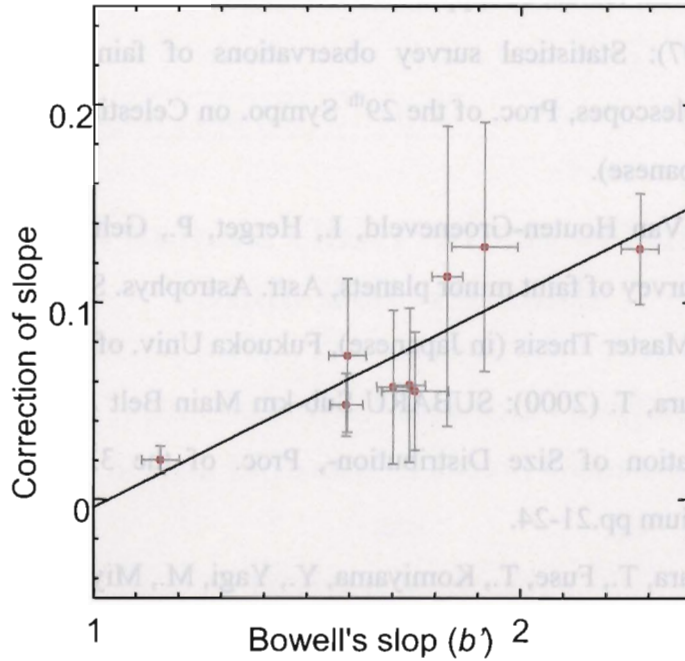


Fig.5 The correction value of b' .

This means that if there is a difference of slope larger than 0.1 between the size distribution for sub-km MBAs and that for km-sized MBAs, one can expect that the difference will be detected using our statistical method as mentioned above. Our SMBAS was performed on Feb. 21 and 24, 2001. According to the preliminary analysis, it actually seems likely that the size distribution for sub-km MBAs is appreciably different from that for larger ones. Furthermore, a more simplified analysis of only several tens of sub-km MBAs observed with SUBARU on June 12, 2000 also seems to support the conclusion discussed above (Yoshida et al. 2001).

References

- Bowell, E., Skiff, B. A., Wasserman, L. H. and Russell, K. S. (1990): Orbital information from asteroid motion vectors, ACM-III, Uppsala Univ. pp.19-24.
- Jedicke, R. and Metcalfe, T. S. (1998): The orbital and absolute magnitude distributions

- of main belt asteroids, *Icarus*, **131**, pp.245-260.
- Nakamura, T. (1997): Statistical survey observations of faint belt asteroid with SUBARU-class telescopes, *Proc. of the 29th Sympo. on Celestial Mechanics*, Tokyo, pp.274-278 (in Japanese).
- Van Houten, C. J., Van Houten-Groeneveld, I., Herget, P., Gehrels, T., (1970): The Palomar-Leiden survey of faint minor planets, *Astr. Astrophys. Suppl.* **2**, pp.339-448.
- Yoshida, F. (1999): Master Thesis (in Japanese), Fukuoka Univ. of Education.
- Yoshida, F., Nakamura, T. (2000): SUBARU Sub-km Main Belt Asteroid Survey Plan -Statistical Estimation of Size Distribution-, *Proc. of the 33rd ISAS Lunar and Planetary Symposium* pp.21-24.
- Yoshida, F., Nakamura, T., Fuse, T., Komiyama, Y., Yagi, M., Miyazaki, S., Okamura, S., Ouchi, M. and Miyazaki, M.: First Subaru Observations of Sub-km Main Belt Asteroids (submitted to PASJ).

Appendix 3

Pub. Astron. Soc. Japan Letter, **53**, L13-L16.

First Subaru Observations of Sub-km Main Belt Asteroids

Fumi Yoshida,^{1,2} Tsuko Nakamura,¹ Tetsuharu Fuse,³ Yutaka Komiyama,³
Masafumi Yagi,¹ Satoshi Miyazaki,¹ Sadanori Okamura,⁴ Masami Ouchi,⁴
and
Masayuki Miyazaki,⁴

¹ *National Astronomical Observatory, Osawa, Mitaka, Tokyo 181-8588*

E-mail: yoshdafm@cc.nao.ac.jp

² *Graduate School of Science and Technology, Kobe University, Kobe 657-8501*

³ *Subaru Telescope, National Astronomical Observatory, 650 North Aohoku Place,
Hilo, Hawaii, HI 96720, USA*

⁴ *Department of Astronomy, The University of Tokyo, Hongo, Bunkyo-ku,
Tokyo 113-0033*

Abstract

We report first observations of sub-km main belt asteroids (MBAs) obtained with the prime-focus mosaic CCD camera for the Subaru telescope. We have detected 27 moving objects in a single image of the sky (field of view: $27' \times 27'$), whose location was 41° off opposition. From their positions and projected motions on the sky, all the detected objects were found to be new and consistent with the characteristic of MBAs. The V -magnitudes of the discovered asteroids range approximately from 19 to 24. Under some simple but reasonable assumptions, we estimated the cumulative size distribution for the asteroids. This

is the first statistics for sub-km MBAs (the minimum diameter corresponds to about 0.6km). It is found that the slope of the cumulative size distribution for the observed asteroids is 1.0 with an error of about 0.3. We note that our slope is fairly smaller than that obtained in the past survey observations for asteroids larger than a few kilometers(~ 1.75).

Key words: Asteroids, Size distribution, Rubble piles, Main belt

1. Introduction

Sub-km objects in the main asteroid belt had never been observed before due to their faintness, at least except for serendipitous detections. The recent advent of 8-10m gigantic telescopes with the wide field-of-view like Subaru, however, enabled us to access sub-km main belt asteroids (MBAs) systematically for the first time. The study of sub-km MBAs is important mainly from the following two viewpoints: 1) the majority ($\sim 70\%$) of near-Earth asteroids (NEAs) which are supposed to originate from the main asteroid belt are sub-km-sized (CBAT: Central Bureau for Astronomical Telegrams for IAU, <http://cfa-www.harvard.edu/iau/mpc.html>), and 2) this size region lies near the border-line size separating the two catastrophic impact mechanisms, namely those in the strength regime and the gravity regime (e.g., Melosh and Ryan 1997, Durda et al. 1998).

This is a report on the first attempt to obtain the size distribution of sub-km MBAs by a statistical analysis of their Subaru images. In the following, we describe the image reduction method, the resulting size distribution, a preliminary comparison of it with the size distribution for asteroids larger than a few kilometers deduced from the past survey observations, and discuss implications for our obtained size distribution.

2. Observation and Data reduction

Observations were made on 2000 June 12 at 14h 26m (UT) at the prime focus of the 8.2m Subaru telescope atop Mauna Kea, Hawaii. We used the wide-field mosaic camera called the Subaru Prime-Focus Camera (Suprime-Cam), which covers the field of view of $27' \times 27'$ with eight chips (2048×4096 pixels each). Since our observations were performed as a part of a Suprime-Cam testing run, we could not help pointing the telescope to the sky with the elongation angle (Sun-Earth-object angle) of 139° off opposition (RA=20h 10.0m and Dec= $-16^\circ 45'$) near the ecliptic plane, to avoid both the moon and the Milky Way. The exposure time was 5 min with *V*-filter. We took two images of the same field in succession with a time interval of 9 min, to detect moving objects. The mean seeing sizes for the two images were 0.8'' and 0.9'' respectively.

Image reduction was carried out using IRAF on a chip-by-chip basis. First, the overscan region was trimmed, and then an average dark level corresponding to each chip was subtracted. In order to correct the difference in pixel sensitivity, the flat-field calibration must be done. For the purpose, we took several images of the twilight sky with the field-center offset slightly each other. And from them a median flat-field image was constructed, with which each observed image was divided. Finally, a cosmic-ray removal procedure was applied for each chip.

Because of the short exposure time and the not-so-good seeing, asteroids could not be identified in a single image. So, we subtracted the second image from the first one, in an attempt to easily recognize moving objects. Fig. 1 shows a part of the differenced image, where one can see moving objects as pairs of separated black-and-white dots. By careful eye-inspection of segmented and enlarged images, we could eventually detect 27 moving objects in total over all the eight chips.

3. Daily motion and photometry

To estimate daily motions of the detected moving objects, we picked up from each chip about 10 stars that have entry in the USNO-A2 catalog (<http://tdc-www.harvard.edu/software/catalogs/ua2.html>).

Positional measurements of those stars were made with the APPHOT task in IRAF. The position for each moving object was also measured relative to the catalog stars for both the first image and the second one, and the apparent velocity for the object was calculated. The centroiding error of each object was much smaller than the seeing size.

We made a simulation using a two-body ephemeris generator, to deduce a statistical relation between the semi-major axis (a) of asteroids and their apparent daily motions. It was found that the motions of all the detected moving objects were consistent with those for MBAs, though it was difficult to surely distinguish MBAs from NEAs.

However, considering that the number of discovered yet MBAs (approximately one hundred thousand) is almost a hundred times larger than the total number of other small bodies including NEAs (nearly a thousand) (<http://cfa-www.harvard.edu/iau/lists/Unusual.html>), it is very unlikely that our detected moving objects include considerable number of objects other than MBAs by chance. In fact, given an expected number of non-MBA objects in our observations ($\sim 27/100=0.27$), the Poisson statistics teaches us that probabilities for our result to include one or two of non-MBAs by chance respectively are 0.20 or 0.03. This means that 27 objects detected in these observations are substantially all MBAs. We have also confirmed that those moving objects are all new by referring to the asteroid database of the CBAT's Miner Planet Service.

Then, we describe here photometric reduction of our observations. Again the APPHOT in IRAF was used to do aperture photometric measurements. For some reasons, we needed to follow the reduction procedures mentioned below. First, we could not have chances to observe photometric standard stars separately but

instead had to use background stars in the asteroid images for photometric calibration, because the observations were performed as a part of a Suprime-Cam test run. For the magnitude range of the detected asteroids ($V \sim 19\text{--}24$ mag), the only available star catalog was USNO-A2. Moreover, this catalog gives B- and R-magnitudes only, whereas our observations were made with V-band. Because of this band mismatch, we assumed, as an inevitable compromise, an average ($V-R$) for the background stars, whose average value was derived from populations of stars with known spectral types. Namely, we adopted an averaged value ($V-R$) $\sim +0.37$, which was calculated from the color frequency distribution for photometric standard stars observed over the whole sky (Landolt 1983, Mermilliod and Mermilliod 1994). By applying this color correction, we suppose that the observed V -mag for each asteroid can be tied to the R -mag of USNO-A2 catalog at least approximately. In this way, the magnitudes of the detected asteroids were found to range from 18.8 through 23.8 in V -band (see Table 1). It is inferred that thus obtained V -magnitudes of the asteroids can bear an error (σ_c) of ~ 0.27 , which is the standard deviation of ($V-R$)s for various spectral types from the above mean ($V-R$). In addition, the USNO-A2 catalog notifies us that each catalog star has a magnitude error (σ_m) of 0.25 on the average.

Next, we make estimation of absolute magnitudes (H) or equivalently the sizes for the observed asteroids. In order to calculate H -mag of an asteroid, we need to know its distances, since H -mag and the apparent V -mag are connected by the relation:

$$H = V - 5 \log(\Delta \cdot r) - p(\alpha) - \delta V, \quad (1)$$

where Δ and r stand for the geocentric and heliocentric distances (in AU) respectively, $p(\alpha)$ is the phase function (α : phase angle, namely Earth-asteroid-Sun angle), and δV light variation.

To calculate r or Δ , we must know the semi-major axis (a) and eccentricity (e) of each asteroid. However, it is surely impossible to obtain e from such a

short time arc as in this observation, though a can be estimated with an error of $\sim 0.1\text{AU}$ from the apparent daily motions, if asteroids are near opposition (Yoshida and Nakamura 2000). They also showed through extensive model calculations that, under the assumption of $e=0$ (or $r=a$) for all the asteroids, the slope of the cumulative size distribution can be determined with an error of 0.1 or so. Hence, the assumption of $r=a$ was also taken in this work. Practically, we hypothesized here as if all the detected asteroids were located in the middle of the main belt ($\sim 2.7\text{AU}$). This is because, for our observations (41° off opposition), the correlation between the daily motion and a was not so good as near opposition. How this seemingly crude assumption placed here on the a of the observed asteroids affects the resulting size distribution will be discussed later.

4. Results

Table 1 summarizes the measured daily motions, V -magnitudes and H -magnitudes of the 27 moving objects. In conversion of V -mag to H -mag using the equation (1), we adopted the phase function (with $\alpha = 14^\circ$ for the observation date) corresponding to the photometric slope parameter $G=0.15$, which is the widely used value for the majority of asteroids (Ephemerides of Minor Planets for 2001). From these H -magnitudes, one can calculate the corresponding diameters by assuming an appropriate albedo. Before doing this, however, let us estimate the overall error (σ) contained in the H -magnitude.

The σ consists of several component errors discussed in the previous section, and the error breakdown will be expressed by the equation:

$$\sigma^2 = \sigma_o^2 + \sigma_c^2 + \sigma_m^2 + \sigma_v^2. \quad (2)$$

where σ_o is the error caused by the assumptions that $a=2.7\text{AU}$ and $e=0$ for all the observed asteroids. We found out $\sigma_o \sim 0.63$ by an orbital simulation for an ensemble of the main belt asteroids with realistic ranges of a and e .

As for the light variation error (σ_v), nothing can be known for our asteroids, since the observation time was only 10 minutes. Therefore, we inferred it by regarding as σ_v as a mode value for the distribution of the peak-to-bottom light variation amplitude of asteroids (Yoshida 1999). The resulting σ_v is 0.25.

Since other errors like σ_c and σ_m have already been estimated in Section 3, we can obtain the σ from the equation (1) as $(0.63^2 + 0.27^2 + 0.25^2 + 0.25^2)^{1/2} = 0.77$. It is noted that the value is for a single asteroid. If there are n asteroids in a H -bin of Fig. 2, the error for this bin should be σ/\sqrt{n} .

Fig. 2 shows the differential (shaded histogram) and cumulative (black and white dots) H -mag distributions, drawn based on Table 1. The two asteroids whose measured magnitudes are fairly uncertain because of partial overlapping with stars are omitted in Fig. 2. The error bar attached to each dot is σ/\sqrt{n} for the above $\sigma = 0.77$. The diameter (D) scale in the upper abscissa was calculated from the lower H -mag scale for the averaged albedo of C- and S-type asteroids, that is, using an empirical formula $\log D = 3.65 - 0.2H$. One can see from the formula that the faintest asteroid in Table 1 corresponds to the diameter of about 550m.

Next, we will examine the slope of the cumulative size distribution in Fig. 2. Near the limiting magnitude, it is possible that some fraction of very faint asteroids escaped visual detection. To take into account this possible detection failure, a straight line slope was fitted by a least-squares method only for the asteroids indicated by filled (black) dots, which are 1.5 magnitude brighter than the detectable limiting magnitude. The slope of the fitted line was then found to be 1.0.

Although the least-squares error for the slope was calculated to be 0.1, this value should be taken as a formal error rather than a practical one, since the H -mag error attached to each data point in Fig. 2 is as large as 0.40--0.77. Hence, in order to estimate the realistic error of the slope, we produced in a computer a hundred sets of synthetic data points by generating random values that obey a Gaussian distribution with the standard deviation of σ/\sqrt{n} , and with them a

hundred slopes were calculated. The mean deviation of these slopes from 1.0 was about 0.3. We consider, therefore, this value as a realistic error for our observed slope.

The dashed line in Fig. 2 represents the slope (~ 1.75) estimated from the past systematic observations such as the Palomar-Leiden (1970) and Spacewatch (1998) surveys, which covered the size range of $D >$ a few kilometers. As this line is intended to only show its slope for comparison, the zero point is arbitrary. One can see from Fig. 2 that our slope for the size range of 6--1km is gentler than the Palomar-Leiden and Spacewatch slope. This suggests that, for a specified size range, the sky number density of sub-km MBAs is fairly more depleted than that extrapolated from the slope of the past surveys.

5. Discussion

One may consider the slope of 1.0 obtained in this work to be somewhat premature because this is an outcome from small number statistics, and a confirmation observation with an enlarged sample number is necessary. Concerning this, we mention that a preliminary analysis of recent Subaru observations with many more asteroids also seems to support the depletion of sub-km MBAs. Furthermore, it is pointed out that a similar statistical analysis of small Jovian Trojans with a small sample number (several tens) by Jewitt et al. (2000) gave a meaningful result.

Given the slope of 1.0 being real for sub-km MBAs, let us consider its physical implications. Recent collisional theories and experiments show that the impact energy needed to disperse an asteroid is greater than that to thoroughly shatter it, for asteroids larger than sub-km size. Thus, asteroids larger than the sub-km size range should probably be considered to be strengthless “rubble piles” (e.g., Melosh and Ryan 1997). The considerably low bulk density (~ 1.3) of the asteroid Mathilde measured by the NEAR spacecraft (Veeverka et al., 1999) also seems to evidence the existence of rubble-pile asteroids.

If the above discussion is correct, it is expected that the number of small asteroids (say, less than 1km in diameter) is much smaller than the number from the classical collisional theory (Dohnanyi 1969). Our work's result (Fig. 2) is therefore consistent with the formation of rubble piles. In other words, considering common occurrence of rubble piles among the MBAs shown in impact simulations (e.g., Campo Bagatin et al. 2001), our gentle slope in the size distribution for sub-km MBAs could be interpreted as substantial depletion of sub-km fragments in the main belt caused by their incorporation into rubble piles as building blocks.

We thank The Suprime-Cam team for allowing us to use it, and the Subaru telescope supporting staff for our observations. We are also grateful to Dr. T. Ito and the staff of the Astronomical Data Center, National Astronomical Observatory, whose advice in data reduction was very helpful.

References

- Campo Bagatin et al., 2001, How many rubble piles are in the asteroid belt?, *Icarus*, 149, 198.
- Dohnanyi , J. S., 1969, Collisional model of asteroids and their debris, *J. Geophys. Res.* 74, 2531.
- Durda, D.D., Greenberg, R., Jedicke, R., 1998, Collisional models and scaling laws: A new interpretation of the shape of the main-belt asteroid size distribution, *Icarus* 135, 431.
- Jedicke, R. and Metcalfe, T.S., 1998, The orbital and absolute magnitude distributions of main belt asteroids, *Icarus* 131, 245.
- Jewitt, D.C., Trajillo, C.A., Luu, J.X., 2000, Population and size distribution of small Jovian Trojan asteroids, *Astron. J.*, 120, 1140.
- Landolt, A. U., 1983, UBVRI photometric standard stars around the celestial equator, *Astron. J.*, 88, 439.

- Melosh, H. J. and Ryan, E. V., 1997, Asteroids: shattered but not dispersed, *Icaurs* 129, 562.
- Mermilliod, J. C., Mermilliod, M., 1994, Catalogue of mean UBV data on stars (Spribger-Verlag, New York).
- Van Houten, C. J., et al., 1970, The Palomar-Leiden survey of faint minor planets, *Astr. Astrophys. Suppl.* 2, 339.
- Veverka J., et al., 1999, NEAR encounter with asteroid 253 Mathilda : overview, *Icarus* 140, 3
- Yoshida, F., 1999, Master Thesis (in Japanese), Fukuoka Univ. of Education.
- Yoshida, F., Nakamura, T., 2000, SUBARU sub-km main belt asteroid survey plan -- Statistical estimation of size distribution, *Proc. of 33rd ISAS Lunar and Planetary Sympo.*, 21.

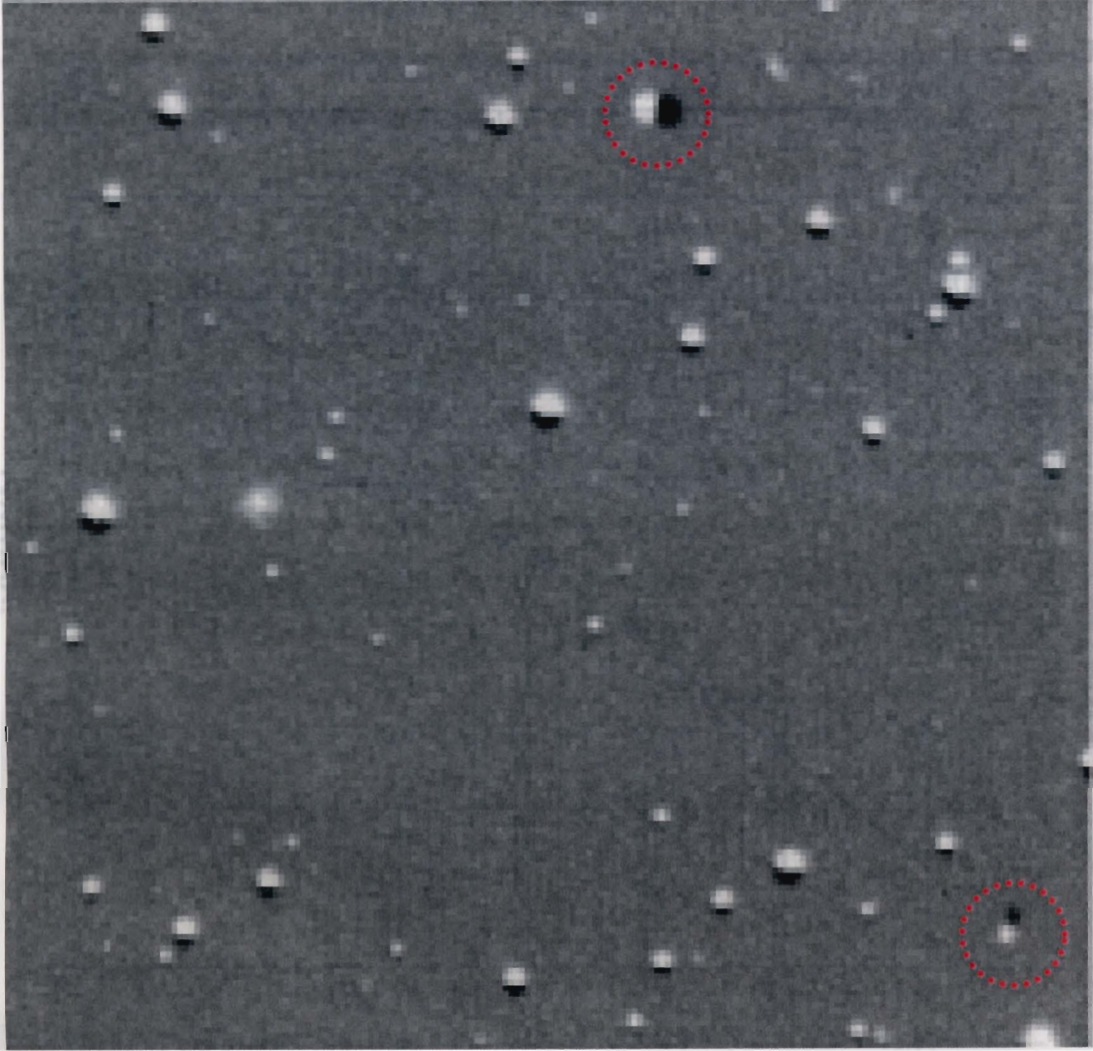


Figure 1: Two detected asteroids from Subaru Suprime-cam observations.

Moving objects appear as pairs of black-and-whites dots, since the second image was subtracted from the first one. A black rim attached to each star was caused by the telescope guiding error during the two exposures. The field-of-view of this figure is $2.5' \times 2.5'$.

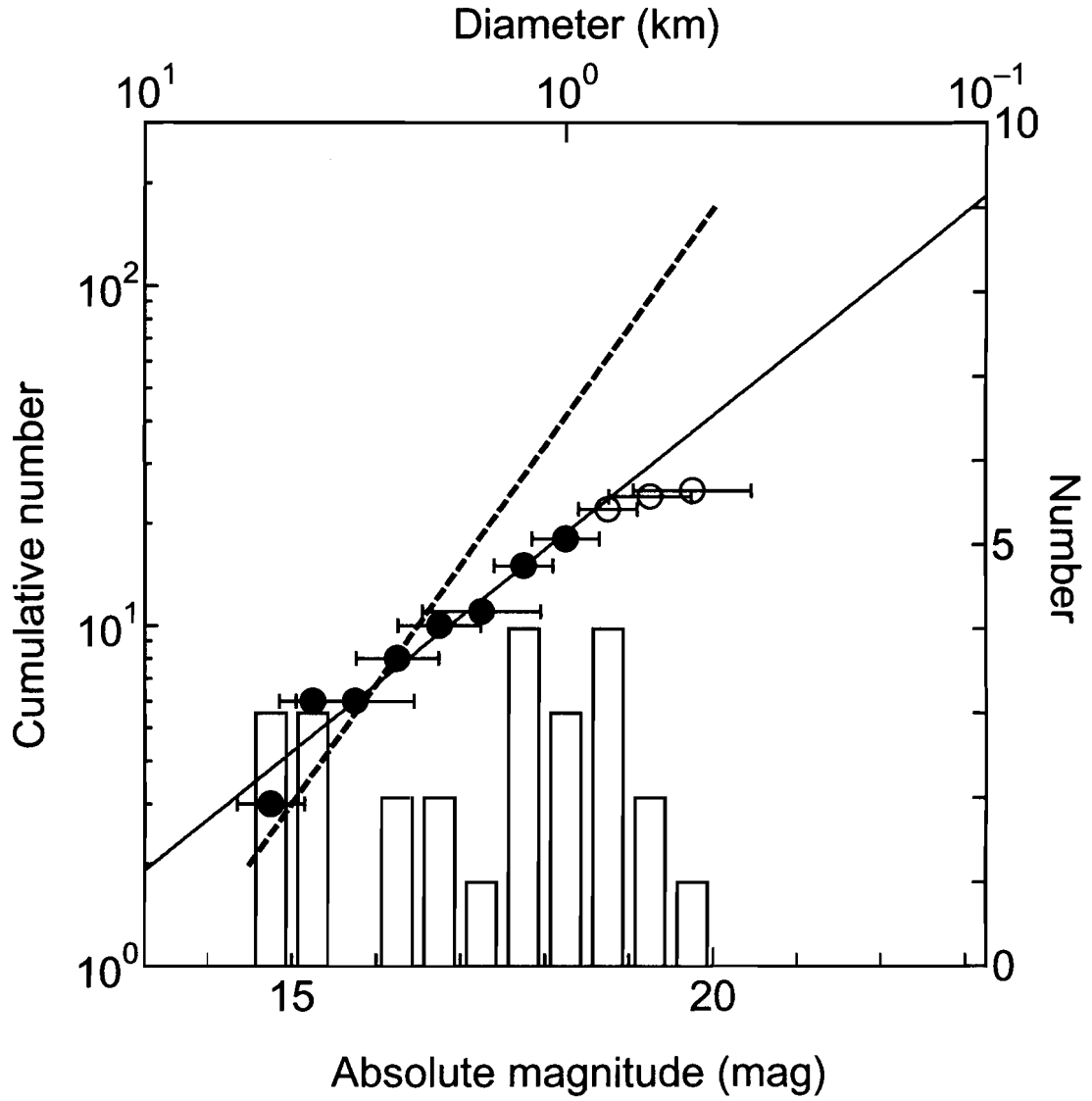


Figure 2: The differential (white-box histogram) and cumulative (black and white dots) H-mag distributions for our observed asteroids.

The diameter (logarithmic) scale in the upper abscissa is calculated from an empirical relation: $\log D = 3.65 - 0.2H$. The solid line is least-squares-fitted to the black dot points. As for the error bars, see text. The dashed line is drawn only to represent the slope for the past systematic surveys (the Palomar-Leiden and Spacewatch).

Table 1: Summary of the asteroids detected in this observation.

| Asteroid number | chip No. | Apparent motion (arcmin/day) | Apparent magnitude (mag) | Absolute magnitude (mag) |
|--------------------|-------------|---------------------------------|--------------------------------|--------------------------------|
| 1 | 2 | 5.93 | 23.13 | 18.86 |
| 2 | 2 | 9.21 | 21.40 | 17.13 |
| 3 | 3 | (7.0) | (23.5) | (19.2) |
| 4 | 3 | 7.03 | 22.96 | 18.69 |
| 5 | 3 | 3.15 | 20.84 | 16.57 |
| 6 | 3 | 3.66 | 19.02 | 14.75 |
| 7 | 3 | 4.51 | 22.64 | 18.37 |
| 8 | 3 | 6.55 | 23.19 | 18.92 |
| 9 | 4 | 5.38 | 22.24 | 17.97 |
| 10 | 4 | 3.38 | 21.98 | 17.71 |
| 11 | 4 | (5.5) | 22.75 | 18.48 |
| 12 | 4 | (6.8) | (24.0) | (19.7) |
| 13 | 5 | 4.86 | 19.30 | 15.03 |
| 14 | 5 | 7.18 | 23.06 | 18.79 |
| 15 | 5 | 6.10 | 22.27 | 18.00 |
| 16 | 5 | 6.04 | 19.76 | 15.49 |
| 17 | 5 | 1.29 | 21.08 | 16.81 |
| 18 | 6 | 7.08 | 23.80 | 19.53 |
| 19 | 7 | 7.86 | 23.37 | 19.10 |
| 20 | 7 | 4.60 | 19.38 | 15.11 |
| 21 | 7 | 8.05 | 20.74 | 16.47 |
| 22 | 8 | 6.11 | 23.69 | 19.42 |
| 23 | 8 | 4.64 | 18.77 | 14.50 |
| 24 | 8 | 5.55 | 21.91 | 17.64 |
| 25 | 8 | (6.2) | 21.98 | 17.71 |
| 26 | 8 | (3.6) | 18.95 | 14.68 |
| 27 | 8 | 6.75 | 20.72 | 16.45 |